Saint-Petersburg University

DORONIN GRIGORIY GENNADIEVICH

Mathematical modeling of two-demensional emission systems based on field electron cathodes.

Scientific specialization 1.2.2.
Mathematical modeling, numerical methods and software packages

Dissertation for candidate of science degree
in physics and mathematics

Translation from Russian

Scientific supervisor:
doctor of physics and mathematics,
Vinogradova Ekaterina Mikhailovna

Saint-Petersburg
2023

Contents

Introduction

Field emission is a fundamental method for generating electron beams in vacuum and plays a crucial role in various practical and research applications, including electron vacuum devices, light sources, and electron microscopy [48, 49]. With the growing demand for electron sources in applications such as flat-panel displays, compact microwave amplifiers, nanolithography, electron beam microscopy, and portable X-ray tubes, global research efforts have focused on alternative electron sources that are smaller in size and highly efficient. Cold cathodes utilizing field emission are promising candidates for such electron sources.

Field emission electron sources, renowned for their outstanding characteristics such as a wide temperature range, low radiation, and high spatial resolution, find applications in vacuum electronic devices such as pressure sensors, electron guns, and microwave amplifiers [73, 81]. Electron emission materials are the key to developing field emission emitters. Extensive studies have been conducted on various cathode materials, including metal oxides, metals, silicon and its carbide, carbon-based materials, and various composites [34, 66, 110].

In the past two decades, researchers have shown significant interest in studying the field emission properties of different materials used for field emission cathodes. For an effective field emitter, the material should exhibit sufficient emission current with high stability, long lifetime, high brightness, low work function, chemical inertness, high melting temperature, and mechanical strength [20, 109].

Among numerous nanomaterials, carbon allotropes (carbon nanostructures) such as carbon nanotubes, diamond-like carbon films, graphene, etc., possess similar structures and exhibit excellent thermal conductivity, electrical conductivity, and mechanical properties. They also exhibit higher and more stable current densities at minimal electric fields [29, 60, 62, 72, 92]. Recently investigated two-dimensional layered materials are expected to find wide applications in the development of new nanoscale devices [23]. The high aspect ratio of carbon nanotubes and the sharp edges of graphene make them ideal for achieving high-performance field emission. The field emission characteristics of such emitters, including volt-ampere characteristics, current stability, and emission center distribution, have been investigated both experimentally and theoretically. Carbon nanotubes are unique due to their exceptional

physicochemical properties and potential applications in various fields, including biomedical applications, energy conversion, supercapacitors, gas sensing, and field emission [21, 48, 75, 96, 111].

In addition to carbon-based nanostructures, various compounds, particularly semiconductors, are actively being explored as efficient field emitters [51]. Also numerous experiments are being conducted to create effective field emitters based on metals and various composites [52, 76, 82, 84, 107].

A field emitter can consist of either a single tip or an array of tips. Single-tip field emitters, acting as point electron sources, are the main components of electron beam control and measurement instruments and microfabrication equipment, such as scanning electron microscopy, transmission electron microscopy, and electron beam lithography [24, 67]. As an alternative to the traditional single-emitter structure, arrays with multiple emitters, such as vertically aligned carbon nanotubes, are widely used to achieve improved electron cathode configurations, high efficiency, and long-term stability [59, 63, 74].

Relevance of the investigation topic

Field emitters have attracted researchers' attention due to their unique emission properties and potential technological applications. The main characteristics of devices utilizing field emission cathodes are their small geometric dimensions and low power consumption for efficient operation. All of these factors make such devices highly promising for the development of various compact devices [48, 49].

However, the design of field emitters involves complex processes in field electron emission. While simple pointed structures with a high aspect ratio provide the best field enhancement, they are less mechanically stable than structures with lower aspect ratios, which offer a compromise between electrostatic field enhancement and other practical considerations such as mechanical stability. Additionally, some emitter formation processes naturally create structures with complex shapes [81]-[111].

Moreover, single emitters systems typically yield low emission current values. Depending on the device's purpose, there are several methods to achieve the desired total current in a field emission system. Firstly, multi-tip systems allow for increased current. Numerous experimental studies have been conducted with arrays of field cathodes of various shapes. However, due to the mutual influence of multiple emitters

on each other, known as the shielding effect, it is necessary to investigate such influence and determine the optimal set of geometric parameters for the system, such as packing density, where packing density refers to the ratio of the distance between adjacent emitters to the length of the emitter itself.

Therefore, the second method involves increasing the emission area of the field cathode itself. Blade-shaped field cathodes have a significantly larger emission area compared to single-pointed emitters, allowing for an increased overall current in the emission system. The edges of two-dimensional semiconductor nano-material layers, such as graphene, also exhibit high emission efficiency and can be considered as field emitters.

The goal of the work — is to perform mathematical modeling of axially symmetric and planar symmetric diode emission systems based on field emission electron cathodes

Tasks set to achieve the goal:

1)   To construct a mathematical model of an axially symmetric diode system with a single field emission cathode of a specific shape in a cylindrical coordinate system.

2)   To develop mathematical models for planar symmetric diode systems with single blade-shaped field emission cathodes and multi-emitter systems in a Cartesian coordinate system.

3)   To construct a mathematical model of a blade-shaped field emitter with a dielectric coating at the apex in a polar coordinate system.

4)   To determine the distribution of electrostatic potential throughout the system domain for each of the presented field cathode models, taking into account the influence of dielectrics.

5)   To develop a suite of computational programs that implement the proposed mathematical models for emission systems with field emission cathodes.

Compliance with the passport of the specialty 1.2.2. The objectives of the dissertation research align with the following research directions of specialization 1.2.2 "Mathematical modeling, numerical methods, and software packages ":

Development of new mathematical methods for modeling objects and phenomena correspond to the tasks 1) - 3);

Qualitative or analytical methods for studying mathematical models corresponds to the task 4);

Implementation of efficient numerical methods and algorithms in the form complexes of problem-oriented programs for computational experiment corresponds to the task 5).

Scientific novelty of the work.

In order to assess the effectiveness of a particular modeling method, it is necessary to calculate the distribution of the electrostatic potential throughout the system. The zero equipotential contour obtained from the potential calculation visualizes the shape of the cathode. This allows for control over the cathode surface shape by varying the parameters of the considered problem, thus determining whether the corresponding method is suitable for modeling within the required range of geometric parameter measurements.

For the first time, analytical formulas are presented for calculating the distribution of the electrostatic potential:

— in axially symmetric diode systems based on a single hollow-shaped field emitter in cylindrical coordinates, taking into account the dielectric layer;

— in plane symmetric diode systems, both with single blade-shaped field cathodes and multi-emitter systems in Cartesian and polar coordinate systems, considering dielectric layers.

Research methods.

The main research methods employed in this study include mathematical physics methods, differential equations, mathematical modeling, and applied programming.

Practicle significance.

The advantage of mathematical modeling of field emission systems lies in facilitating the study of key parameters of the system itself, such as emitter height, apex radius, and array geometry, while assuming conceptual simplicity. These models allow for the calculation of potential distribution and electric field, both for single emitters and arrays, by providing simple analytical expressions instead of solving three-dimensional problems with complex boundary conditions.

The results, presented for the defence:

— physical and mathematical models of field emission systems with single cathodes in cylindrical, polar, and Cartesian coordinate systems, considering both with and without dielectric layers,

— physical and mathematical models of field emission systems with multiple emitters in a Cartesian coordinate system, considering both with and without dielectric layers,

— methods for calculating the electrostatic potential throughout the domain of each of the presented emission systems,

— analytical formulas for the distribution of the electrostatic potential,

— a software complex for calculating the distribution of the electrostatic potential, implementing the proposed mathematical models of emission systems with field cathodes.

Reliability of the obtained results.

All the results of modeling field emission systems presented in the dissertation were obtained through properly formulated problem statements, rigorous mathematical methods in analytical derivations, and validated through numerical experiments. All these results have been reported at several international conferences and published in three Russian peer-reviewed journals listed in the Higher Attestation Commission (VAK) and indexed in the SCOPUS database.

Approbation of work.

The results of the dissertation work were presented at scientific seminars of the Department of Modeling of Electromechanical and Computer Systems at the Faculty of Applied Mathematics and Control Processes of Saint Petersburg State University, as well as at the following international conferences:

- Young Researchers in Vacuum Micro/Nano Electronics, VMNE-YR 2016, St. Petersburg, Russia;

- 14th International Baltic Conference on Atomic Layer Deposition, BALD 2016, St. Petersburg, Russia;

- Young Researchers in Vacuum Micro/Nano Electronics, VMNE-YR 2017, St. Petersburg, Russia;

- XLIX International Conference "Control Processes and Stability"(CPS'18), April 2-5, 2018, St. Petersburg, Russia.

- L International Conference "Control Processes and Stability"(CPS'19), April 8-11, 2019, St. Petersburg, Russia.

- LI International Conference "Control Processes and Stability"(CPS'20), April 20-24, 2020, St. Petersburg, Russia.

- IV International Conference "Stability and Control Processes"dedicated to the 90th anniversary of Professor V.I. Zubov, corresponding member of the Russian Academy of Sciences (SCP), October 5-9, 2020, St. Petersburg, Russia.

- 7th ITG International Vacuum Electronics Workshop (IVEW) 2020 and 13th International Vacuum Electron Sources Conference (IVeSC) 2020, Bad Honnef, Germany.

- LII International Conference "Control Processes and Stability"(CPS'21), April 5-9, 2021, St. Petersburg, Russia.

Personal contribution.

The dissertation represents a completed independent work that possesses all the characteristics of relevance, scientific novelty, and practical significance. The problem formulation was provided by Vinogradova E.M. Consultations on the methodology for solving the formulated problems were conducted by Vinogradova E.M. and Egorov N.V.

The author's personal contribution consists of direct and active participation in all stages of the research, including problem formulation and development of modeling methods.

The author of the dissertation implemented the methods for solving the formulated problems and wrote computer programs in accordance with the analytical solutions obtained by them.

All the results presented in the dissertation were personally obtained by the author.

Publications.

The main results on the topic of the dissertation are presented in 12 scientific publications [5, 6, 11, 12, 13, 14, 32, 33, 35, 43, 97, 99], three of which are published in journals listed in the VAK list [5, 6, 43], six in publications indexed in SCOPUS and Web of Science [5, 6, 32, 97, 99, 43], and in the author's final graduate work [15].

The structure of the dissertation.

The structure of the dissertation consists of an introduction, four chapters, and a conclusion. The complete volume of the dissertation is ... pages and ... figures. The list of references contains ... entries.

The **introduction** provides justification for the relevance of the study's topic, its scientific and practical significance. It formulates the aim and objectives of the research, describes the research methods, and presents the main propositions to be defended.

Chapter I is devoted to the modeling of diode and triode electron-optical systems based on a field emitter with a sharp edge in cylindrical coordinate system. Since any equipotential surface can be considered as the cathode surface, the influence of the cathode on the field distribution is replaced by a system of circular charged wires to calculate the electrostatic potential.

As a result of modeling an axially symmetric diode system based on a field emitter with a sharp edge, with two different dielectrics filling its internal region, the distribution of electrostatic potential is obtained explicitly.

When modeling an electron gun with a hollow cathode in the form of a triode system with a modulator and two dielectric layers, the solution of the initial problem is reduced to solving a system of linear algebraic equations for the coefficients of series that appear in the potential expansion using eigenfunctions.

Chapter II presents a method for modeling planar symmetric diode emission systems with single field emitters of blade shape placed on a flat substrate. The anode is a plane parallel to the substrate. Models of diode field systems without and with dielectric layers on the emitter substrate and lateral surfaces are presented.

To calculate the distribution of electrostatic potential in the entire system domain, the method of separation of variables in Cartesian coordinates is used, and the influence of the emitter is replaced by the influence of charged wires and planes. The distribution of electrostatic potential for each of the studied models is analytically

obtained in series form using eigenfunctions, and the coefficients of the series are computed explicitly.

Chapter III presents a method for modeling planar symmetric periodic systems of blade-shaped field emitters on a flat substrate using an arbitrary number of charged planes in Cartesian coordinates. The anode is a plane parallel to the substrate. The distribution of electrostatic potential is analytically obtained for periodic emitter systems with and without dielectric layers in the system region and represented in series form using eigenfunctions, with the coefficients of the series computed explicitly.

Chapter IV is dedicated to the modeling of a diode system based on a field emitter with a blade-shaped apex and a given radius of curvature at the tip, considering the presence of a dielectric coating. The solution of the boundary problem in polar coordinate system is reduced to solving a system of linear algebraic equations for the coefficients in the potential expansion using eigenfunctions.

In the **Conclusion**, the general results of the work are formulated.

I Modeling of axisymmetric field emission systems with a single emitter of special shape in a cylindrical coordinate system

In writing Chapter I, the following sources were used: [1, 11, 32, 33, 35, 99].

This chapter is devoted to modeling the field cathode in a cylindrical coordinate system. Field emitters of axisymmetric shape are widely used in electron-vacuum devices [25, 28]. Mathematical modeling of such systems is challenging due to the fact that the geometric parameters of the system can vary by several orders of magnitude [47, 68, 78]. To calculate the potential, we replace the influence of the cathode on the field distribution with a system of circular charged wires, assuming that any equipotential surface can be taken as the cathode surface [3, 4, 8, 16, 36, 37, 38, 39, 40, 41, 47, 93, 94, 95, 100, 101, 102, 103, 104, 105]. The electrostatic potential is determined using the method of separation of variables in the cylindrical coordinate system (r, z, ϕ).

I.1 Modeling of the field cathode with a circular charged wire

Physical formulation of the potential calculation created by a circular charged wire

Let's consider a diode emission system with a field cathode of a hollow shape on a planar substrate, where the cathode is modeled as a circular charged wire. The considered system is axisymmetric, so the problem can be reduced from the three-dimensional case to the two-dimensional case. Fig. 1 shows a schematic representation of the diode system on the plane, where Ω is the surface of the field cathode.

System parameters:

$z = z_1$ - cathode substrate;

$z = z_2$ - anode surface;

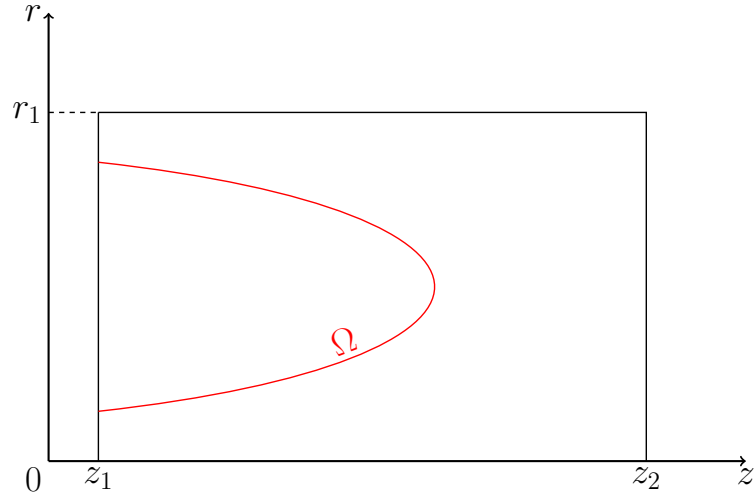$r = r_1$ - boundary surface of the system in the variable r.

Fig. 1: Schematic representation of the electron-optical system on the plane.

Mathematical model of the cathode with a circular charged wire in a bounded area

To find the distribution of the electrostatic potential $U(r, z)$ throughout the diode system, it is necessary to solve the Laplace equation:

$$\frac{1}{r}\frac{\partial}{\partial r}\left(r\frac{\partial U}{\partial r}\right) + \frac{\partial^2 U}{\partial z^2} = 0,$$
$$U(r, z)|_\Omega = 0,$$
$$\Omega - \text{apex surface.} \tag{I.1}$$

with the first-type boundary conditions:

$$U(r_1, z) = f_1(z), \ z_1 \le z \le z_2;$$
$$U(r, z_1) = f_2(r), \ 0 \le r \le r_1;$$
$$U(r, z_2) = f_3(r), \ 0 \le r \le r_1.$$

To determine the distribution of the electrostatic potential throughout the system, the influence of the cathode is replaced by the influence of a charged filament with linear charge density τ, where the coordinates of the charged filament are (r_q, z_q) as shown in Figure 2.

Let's represent the solution of Equation I.1 as:
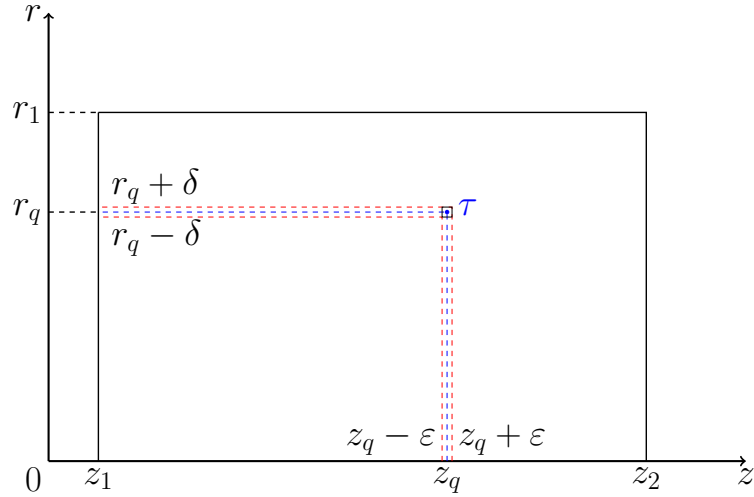
$$U(r, z) = U_1(r, z) + U_2(r, z),$$

Fig. 2: Schematic representation of the charge position in the system on the plane.

where $U_1(r, z)$ is the potential distribution created by the charged filament under homogeneous boundary conditions, and $U_2(r, z)$ is the potential distribution specified by the boundary conditions in Equation I.1.

The function $U_2(r, z)$, as a solution of the Laplace equation with first-type boundary conditions, is presented in work [42].

The problem of determining the field distribution in the system with a single charged filament and homogeneous boundary conditions is reduced to solving the Poisson equation [6]:

$$\triangle U_1 = \frac{1}{r}\left(\frac{\partial}{\partial r}r\frac{\partial U_1}{\partial r}\right) + \frac{\partial^2 U_1}{\partial z^2} = -\frac{\rho(r, z)}{\varepsilon_0}, \tag{I.2}$$

with boundary conditions:

$$\begin{aligned} U_1(r_1, z) &= 0, \\ U_1(r, z_1) &= 0, \\ U_1(r, z_2) &= 0. \end{aligned} \tag{I.3}$$

The linear charge density τ is determined by the formulas:

$$\tau = \frac{q}{2\pi r_q},$$

then the volume charge density is determined by the equation:

$$\tau = \lim_{\varepsilon \to, \delta \to 0} 4\varepsilon\delta\rho,$$

where

$$q = 2\rho\varepsilon\pi((r_q + \delta)^2 - (r_q - \delta)^2) = 8\rho\varepsilon\pi r_q\delta.$$

The charge q is located in a small volume $|r - r_q| \leqslant \delta$, $|z - z_q| \leqslant \varepsilon$.

Calculation of the potential distribution in the system with a circular charged filament in a bounded area

The potential distribution in the system with a single circular charged filament is determined using the method of variable separation in the form of Fourier-Bessel series expansions. The function $\rho(r, z)$ in the right-hand side of Equation I.2 has the form:

$$\rho(r, z) = \begin{cases} \rho, & |r - r_q| \leqslant \delta \,\&\, |z - z_q| \leqslant \varepsilon, \\ 0, & |r - r_q| > \delta \,\vee\, |z - z_q| > \varepsilon. \end{cases} \tag{I.4}$$

The solution of the boundary problem for the Poisson equation I.2-I.4 is represented as a series:

$$U_1(r, z) = \sum_{n=1}^{\infty} \nu_n(z) J_0(\gamma_n \frac{r}{r_1}), \tag{I.5}$$

where γ_n denotes the roots of the equation:

$$J_0(\gamma_n) = 0.$$

To express $\nu_n(z)$ in terms of $U_1(r, z)$, multiply both sides of this equation by $r J_0(\gamma_n \frac{r}{r_1})$ and integrate over r from 0 to r_1. Using the orthogonality property of Bessel functions, we obtain a differential equation for the function ν_n [66]:

$$\frac{r_1^2 J_1^2(\gamma_n)}{2}[\nu_n''(z) - \frac{\gamma_n^2}{r_1^2}\nu_n(z)] = \begin{cases} -\frac{\rho}{\varepsilon_0}\int\limits_{(r_q-\delta)}^{(r_q+\delta)} r J_0(\gamma_n \frac{r}{r_1})dr, & |z - z_q| \leqslant \varepsilon, \\ 0, & |z - z_q| > \varepsilon. \end{cases} \tag{I.6}$$

Let's calculate the integral appearing in the right-hand side of Equation I.6:

$$I = \int\limits_{r_q-\delta}^{r_q+\delta} r J_0(\gamma_n \frac{r}{r_1})dr = \frac{r_1^2}{\gamma_n^2}\int\limits_{\frac{r_q-\delta}{r_1}}^{\frac{r_q+\delta}{r_1}} t J_0(t)dt,$$

where $t = \gamma_n \dfrac{r}{r_1}$.

Using the limits, we obtain (reference [8]):

$$\lim_{\rho \to 0} \int_{\frac{r_q - \delta}{r_1}\gamma_n}^{\frac{r_q + \delta}{r_1}\gamma_n} t J_0(t) dt = 2\delta \frac{\gamma_n}{r_1}\frac{\gamma_n}{r_1} r_q J_0(\frac{r_q}{r_1}\gamma_n) = 2\delta \frac{\gamma_n^2}{r_1^2} r_q J_0(\gamma_n \frac{r_q}{r_1})$$

Then:

$$I = 2\delta r_q J_0(\gamma_n \frac{r_q}{r_1}). \tag{I.7}$$

The differential equation for the functions $\nu_n(x)$ with respect to equation I.7 can be written as:

$$\nu_n''(z) - \frac{\gamma_n^2}{r_1^2}\nu_n(z) = \phi(z), \tag{I.8}$$

where the right part of the equation I.8:

$$\phi(z) = \begin{cases} -\dfrac{\rho}{\varepsilon_0}\dfrac{2}{r_1^2 J_1^2(\gamma_n)} 2\delta J_0(\gamma_n \dfrac{r_q}{r_1}) = -\dfrac{\rho}{\varepsilon_0}\dfrac{4\delta J_0(\gamma_n \frac{r_q}{r_1})r_q}{r_1^2 J_1^2(\gamma_n)\gamma_n}, & |z - z_q| \leqslant \varepsilon, \\ 0, & |z - z_q| > \varepsilon. \end{cases}$$

The solution of equation I.8:

$$\nu_n(z) = C\, \mathrm{sh}(\frac{\gamma_n}{r_1}(z - z_1)) + \frac{r_1}{\gamma_n}\int_{z_1}^{z} \phi(\eta)\, \mathrm{sh}(\frac{\gamma_n}{r_1}(z_2 - \eta))d\eta,$$

where C is the integration constant, which can be found using the equation:

$$v_n(z_2) = 0.$$

Since:

$$C\, \mathrm{sh}(\frac{\gamma_n}{r_1}(z_2 - z_1)) + \frac{r_1}{\gamma_n}\int_{z_q - \varepsilon}^{z_q + \varepsilon} \phi(\eta)\, \mathrm{sh}(\frac{\gamma_n}{r_1}(z_2 - \eta))d\eta = 0,$$

evaluating the integral as $\varepsilon \to 0$, we obtain:

$$\nu_n(z_2) = C \operatorname{sh}(\frac{\gamma_n}{r_1}(z_2 - z_1)) - \frac{r_1}{\gamma_n}\frac{\rho}{\varepsilon_0}4\delta J_0(\gamma_n\frac{r_q}{r_1})\frac{r_q}{r_1^2 J_1^2(\gamma_n)}2\varepsilon \operatorname{sh}(\frac{\gamma_n}{r_1}(z_2 - z_q)) = 0.$$

Thus,

$$C = \tau\frac{2J_0(\gamma_n\frac{r_q}{r_1})\operatorname{sh}(\frac{\gamma_n}{r_1}(z_2 - z_q))r_q}{\varepsilon_0\gamma_n J_1^2(\gamma_n)\operatorname{sh}(\frac{\gamma_n}{r_1}(z_2 - z_1))r_1}.$$

Then functions $\nu_n(z)$:

$$\nu_n(z) = \tau\frac{2J_0(\gamma_n\frac{r_q}{r_1})\operatorname{sh}(\frac{\gamma_n}{r_1}(z_2 - z_q))\operatorname{sh}(\frac{\gamma_n}{r_1}(z - z_1))r_q}{\varepsilon_0\gamma_n J_1^2(\gamma_n)\operatorname{sh}(\frac{\gamma_n}{r_1}(z_2 - z_1))r_1}+$$
$$+\frac{r_1}{\gamma_n}\int_{z_1}^{z}\phi(\eta)\operatorname{sh}(\frac{\gamma_n}{r_1}(z_2 - \eta))d\eta,$$

or

$$\nu_n(z) = \tau\frac{2J_0(\gamma_n\frac{r_q}{r_1})\operatorname{sh}(\frac{\gamma_n}{r_1}(z_2 - z_q))\operatorname{sh}(\frac{\gamma_n}{r_1}(z - z_1))r_q}{\varepsilon_0\gamma_n J_1^2(\gamma_n)\operatorname{sh}(\frac{\gamma_n}{r_1}(z_2 - z_1))r_1}+$$
$$+\frac{r_1}{\gamma_n}\int_{z_q-\varepsilon}^{z_q+\varepsilon}\phi(\eta)\operatorname{sh}(\frac{\gamma_n}{r_1}(z_2 - \eta))d\eta.$$

Therefore, the solution of equation I.8 can be represented as:

$$\nu_n(z) = \tau\frac{2J_0(\gamma_n\frac{r_q}{r_1})\operatorname{sh}(\frac{\gamma_n}{r_1}(z_2 - z_q))\operatorname{sh}(\frac{\gamma_n}{r_1}(z - z_1))r_q}{\varepsilon_0\gamma_n J_1^2(\gamma_n)\operatorname{sh}(\frac{\gamma_n}{r_1}(z_2 - z_1))r_1}+ \qquad (\text{I.9})$$
$$+\tau\frac{2J_0(\gamma_n\frac{r_q}{r_1})}{\varepsilon_0 J_1^2(\gamma_n)\gamma_n}\operatorname{sh}(\frac{\gamma_n}{r_1}(z - z_q))\frac{r_q}{r_1},$$

for $z_q < z \leqslant z_2$.

Hence, the solution of equation (Poisson's equation) with respect to equations I.5 and I.9:

$$U(r, z) = \sum_{n=1}^{\infty}\tau\frac{2r_q J_0(\gamma_n\frac{r_q}{r_1})}{\varepsilon_0 J_1^2(\gamma_n)\gamma_n}\frac{\operatorname{sh}(\frac{\gamma_n}{r_1}(z_2 - z_q))\operatorname{sh}(\frac{\gamma_n}{r_1}(z - z_1))}{r_1\operatorname{sh}(\frac{\gamma_n}{r_1}(z_2 - z_1))}J_0(\gamma_n\frac{r}{r_1}), \qquad (\text{I.10})$$

for $z_1 < z \leqslant z_q$,

$$U(r,z) = \sum_{n=1}^{\infty} \tau \frac{2r_q J_0(\gamma_n \frac{r_q}{r_1})}{\varepsilon_0 J_1^2(\gamma_n)\gamma_n} \frac{\operatorname{sh}(\frac{\gamma_n}{r_1}(z_2 - z))\operatorname{sh}(\frac{\gamma_n}{r_1}(z_q - z_1))}{r_1 \operatorname{sh}(\frac{\gamma_n}{r_1}(z_2 - z_1))} J_0(\gamma_n \frac{r}{r_1}), \qquad (\text{I.11})$$

for $z_q \leqslant z \leqslant z_2$.

The distribution of the electrostatic potential $U_1(r,z)$ in the entire diode system can be calculated using equations I.10 and I.11.

**Numerical calculation results of potential with a circular charged wire**

Based on the obtained results from equations I.10 to I.11, graphs of the potential distribution in the entire system were constructed for $U_2(r, z) = U_0 \dfrac{z - z_1}{z_2 - z_1}$.

The values of all parameters are given in dimensionless units.

The potential values at the boundaries of the system are:

$$f_1(z) = U_0 \frac{z - z_1}{z_2 - z_1}, f_2(r) = 0, f_3(r) = U_0.$$

Based on the provided graphs, the shape of the simulated cathode can be determined, which plays a crucial role in understanding the adequacy of the model. The shape of the emitter is defined by the zero equipotential. The values of all parameters are presented in dimensionless units.
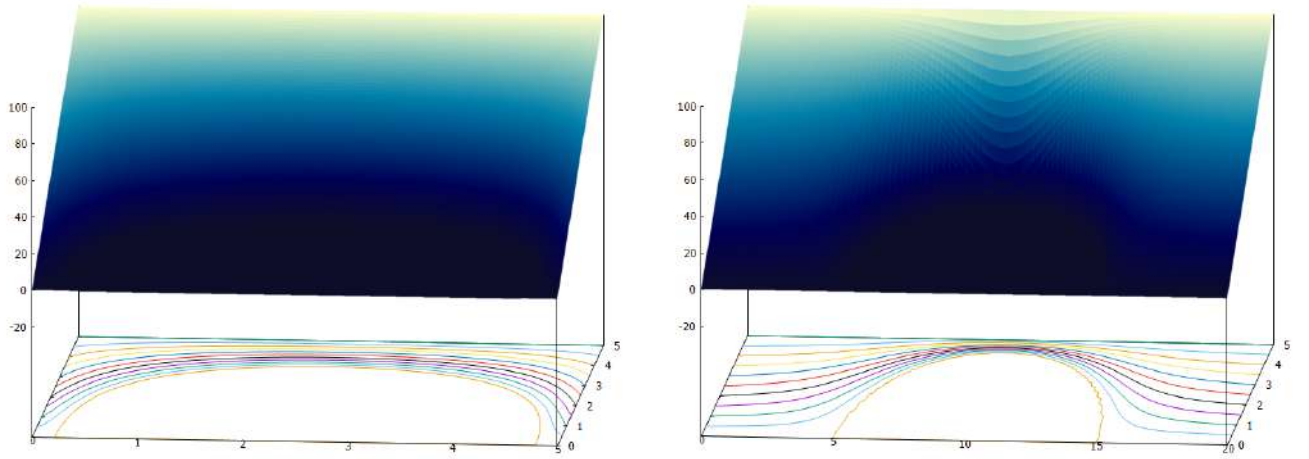
a) $r_1 = 5, r_q = 2.5$ b) $r_1 = 20, r_q = 10$

Fig. 3: $z_1 = 0, z_2 = 5, z_q = 2.5, U_0 = 100, \tau = -20$.

Fig. 3 demonstrates the change in the shape of the emitter when varying the values of $r = r_1$, the outer boundary in the variable r, and r_q.
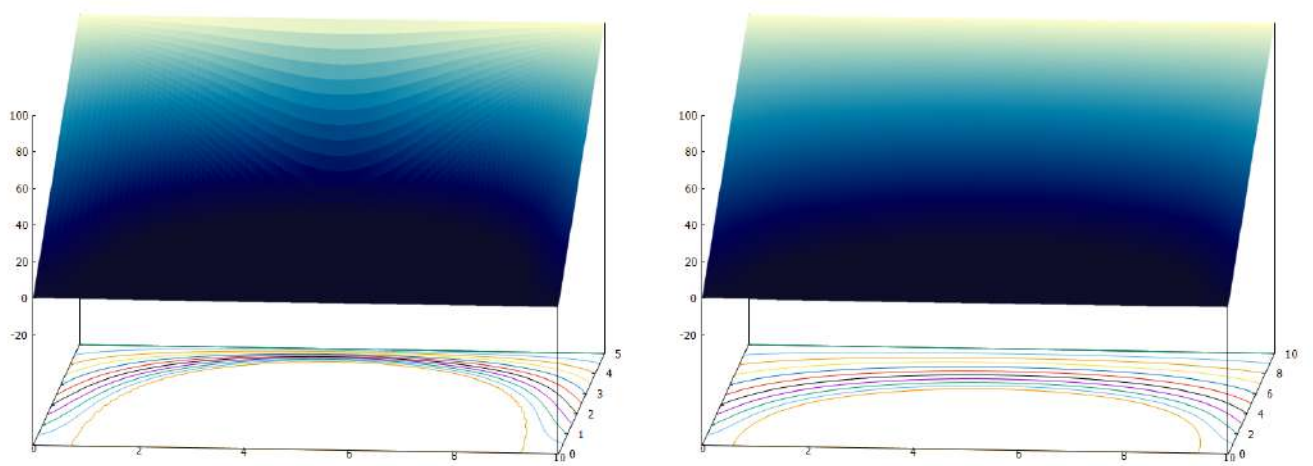
a) $z_2 = 5, z_q = 2.5$ b) $z_2 = 10, z_q = 5$

Fig. 4: $z_1 = 0, r_1 = 10, r_q = 5, U_0 = 100, \tau = -20$.

Fig. 4 represents the change in the shape of the emitter when varying the values of z_2, the outer boundary in the variable z, and z_q.

I.2   Modeling of an axially symmetric field emission system with dielectrics

In this paragraph, an axially symmetric diode system based on a field emitter with a sharp edge is modeled, with the entire inner region filled with two different dielectrics.

Physical formulation of the problem for calculating the potential in a field emission system with dielectrics
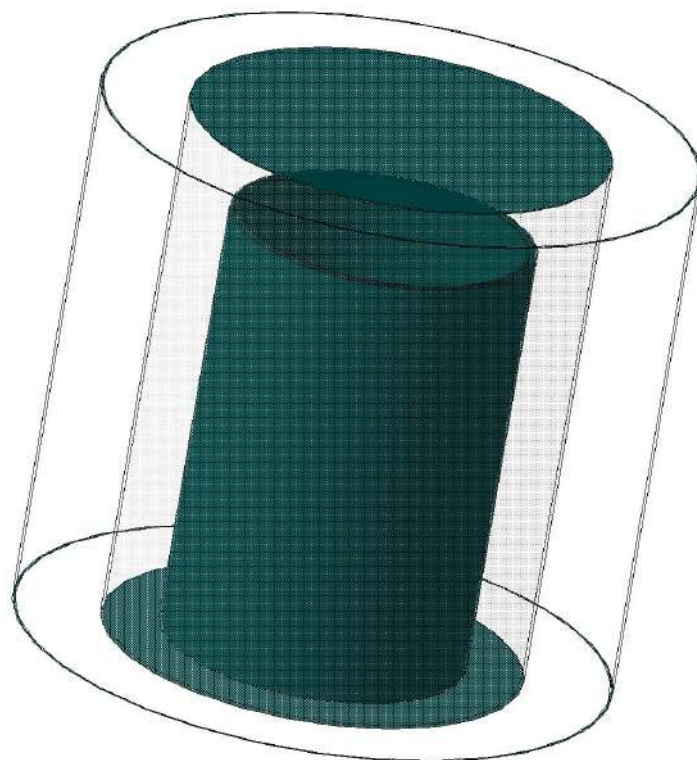

Fig. 5: Schematic image of the system.

The field emitter with a sharp edge is located on a flat substrate. The anode is a plane parallel to the substrate [99].

On Fig. 6, a schematic representation of the diode system on the (r, z) plane is shown.
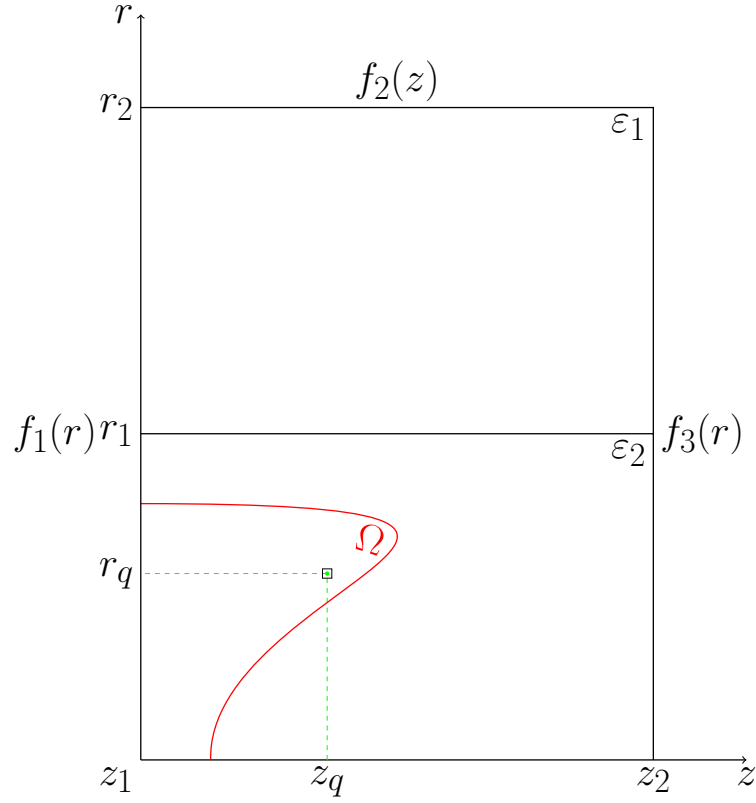
Fig. 6: A schematic representation of an electron-optical system with a sharp edge emitter on a plane.

Problem parameters:

$z = z_1$: surface of the cathode substrate,

$z = z_2$: surface of the anode,

$r = r_1$: plane separating the dielectrics,

$r = r_2$: outer boundary of the system in the variable r,

$U(r, z_1) = f_1(r)$: boundary condition on the substrate,

$U(r, z_2) = f_3(z)$: boundary condition on the anode,

$U(r_2, z) = f_2(z)$: boundary condition on the lateral surface of the system.

The mathematical model of a field emission system with dielectrics

To determine the potential distribution $U(r, z)$ in the system, the Laplace equation I.1 is solved with the following boundary conditions:

$$f_1(r) = 0, \quad 0 \le r \le r_2;$$

$$f_2(z) = U_0 \frac{z - z_1}{z_2 - z_1}, \quad z_1 \le z \le z_2;$$

$$f_3(r) = U_0, \quad 0 \le r \le r_2.$$

The influence of the sharp edge on the potential distribution is replaced by the influence of a circular charged wire with coordinates (r_q, z_q) and linear charge density τ. This leads to the solution of the Poisson equation I.2 with the boundary conditions:

$$
\begin{aligned}
U|_{z=z_1} &= 0, \\
U|_{z=z_2} &= U_0, \\
U|_{r=r_2} &= U_0 \frac{z - z_1}{z_2 - z_1},
\end{aligned}
\tag{I.1}
$$

where the right-hand side of the Poisson equation is determined by the formula I.4.

The solution to the problem of finding the potential distribution in the system with the influence of two dielectrics and one charged wire

Define:

$$
U(r, z) = \begin{cases}
U_{11}(r, z), & r < r_1 \ \& \ z < z_q; \\
U_{12}(r, z), & r < r_1 \ \& \ z > z_q; \\
U_2(r, z), & r > r_1.
\end{cases}
$$

Then the solution to the Poisson equation with boundary conditions I.1 in accordance with formulas I.10, I.11 will have the following form:

for $z < z_q$

$$
\begin{aligned}
U_{11}(r, z) = U_0 \Big(\frac{z - z_1}{z_2 - z_1} \Big) + \sum_{m=1}^{\infty} g_m \frac{I_0(\mu_m r)}{I_0(\mu_m r_1)} \sin \mu_m (z - z_1) + \\
+ \frac{2 \tau r_q}{\varepsilon_0 r_1} \sum_{s=1}^{\infty} \frac{J_0\big(\frac{\gamma_s r_q}{r_1} \big) \operatorname{sh}\big(\frac{\gamma_s}{r_1}(z_2 - z_q) \big) \operatorname{sh}\big(\frac{\gamma_s}{r_1}(z - z_1) \big)}{\gamma_s J_1^2(\gamma_s) \operatorname{sh}\big(\frac{\gamma_s}{r_1}(z_2 - z_1) \big)} J_0\big(\frac{\gamma_s r}{r_1} \big),
\end{aligned}
\tag{I.2}
$$

for $z > z_q$:

$$U_{12}(r,z) = U_0(\frac{z - z_1}{z_2 - z_1}) + \sum_{m=1}^{\infty} g_m \frac{I_0(\mu_m r)}{I_0(\mu_m r_1)} \sin \mu_m(z - z_1) +$$

$$+\frac{2\tau r_q}{\varepsilon_0 r_1} \sum_{s=1}^{\infty} \frac{J_0(\frac{\gamma_s r_q}{r_1}) \operatorname{sh}(\frac{\gamma_s}{r_1}(z_q - z_1)) \operatorname{sh}(\frac{\gamma_s}{r_1}(z_2 - z))}{\gamma_s J_1^2(\gamma_s)(\operatorname{sh}(z_2 - z_1)\frac{\gamma_s}{r_1})} J_0(\frac{\gamma_s r}{r_1}), \qquad (\text{I.3})$$

$$U_2(r,z) = \sum_{m=1}^{\infty} g_m \frac{\widetilde{W_0}(\mu_m, r, r_2)}{\widetilde{W_0}(\mu_m, r_1, r_2)} \sin \mu_m(z - z_1) + U_0(\frac{z - z_1}{z_2 - z_1}), \qquad (\text{I.4})$$

where

$\mu_m = \dfrac{\pi m}{z_2 - z_1}$, γ_s - the zeros of the Bessel function. $J_0(\gamma_s) = 0$, a function $\widetilde{W_0}$ The function is a linear combination of modified Bessel functions of the first and second kinds [66]:

$$\widetilde{W_0}(\mu_m, r, r_2) = I_0(\mu_m r)K_0(\mu_m r_2) - K_0(\mu_m r)I_0(\mu_m r_2).$$

Calculating of the coefficients determined by the boundary continuity conditions at the interface of the two dielectrics.

Using the continuity condition of the potential and the electric displacement vector at the interface of two dielectrics, the coefficients of the potential expansion can be determined. $r = r_1$:

for $z_1 \le z \le z_q$:

$$\frac{\partial U_{11}}{\partial r}\Big|_{r=r_1} = \frac{\varepsilon_1}{\varepsilon_2} \frac{\partial U_2}{\partial r}\Big|_{r=r_1},$$

for $z_q \le z \le z_2$:

$$\frac{\partial U_{12}}{\partial r}\Big|_{r=r_1} = \frac{\varepsilon_1}{\varepsilon_2} \frac{\partial U_2}{\partial r}\Big|_{r=r_1}.$$

Let's calculate the coefficient g_m.

$$(U_{11}(r,z))'_{r=r_1} = \sum_{m=1}^{\infty} g_m \mu_m \frac{I_1(\mu_m r_1)}{I_0(\mu_m r_1)} \sin \mu_m(z - z_1) -$$

$$-\frac{1}{\varepsilon_0} \sum_{s=1}^{\infty} \frac{2\tau r_q J_0(\frac{\gamma_s}{r_1}r_q)}{r_1 J_1^2(\gamma_s)} \frac{J_1(\gamma_s)}{r_1} \frac{\operatorname{sh}(\frac{\gamma_s}{r_1}(z_2 - z_q))}{\operatorname{sh}(\frac{\gamma_s}{r_1}(z_2 - z_1))} \operatorname{sh}(\frac{\gamma_s}{r_1}(z - z_1)),$$

$$(U_{12}(r,z))'_{r=r_1} = \sum_{m=1}^{\infty} g_m \mu_m \frac{I_1(\mu_m r_1)}{I_0(\mu_m r_1)} \sin \mu_m(z - z_1) -$$

$$-\frac{1}{\varepsilon_0} \sum_{s=1}^{\infty} \frac{2\tau r_q J_0(\frac{\gamma_s}{r_1} r_q)}{r_1 J_1^2(\gamma_s)} \frac{J_1(\gamma_s)}{r_1} \frac{\mathrm{sh}(\frac{\gamma_s}{r_1})(z_q - z_1)}{\mathrm{sh}(\frac{\gamma_s}{r_1})(z_2 - z_1)} \mathrm{sh}(\frac{\gamma_s}{r_1})(z_2 - z),$$

$$\frac{\varepsilon_1}{\varepsilon_2}(U_2(r,z))'_{r=r_1} = \frac{\varepsilon_1}{\varepsilon_2} \sum_{m=1}^{\infty} g_m \mu_m \frac{\widetilde{W_1}(\mu_m, r_1, r_2)}{\widetilde{W_0}(\mu_m, r_1, r_2)} \sin(\mu_m(z - z_1)),$$

where $\widetilde{W_1}(\mu_m, r_1, r_2) = I_1(\mu_m r_1)K_0(\mu_m r_2) + I_0(\mu_m r_2)K_1(\mu_m r_1)$

Thus:

$$\frac{z_2 - z_1}{2} g_m \mu_m \left(\frac{I_1(\mu_m r_1)}{I_0(\mu_m r_1)} - \frac{\varepsilon_1}{\varepsilon_2} \frac{\widetilde{W_1}(\mu_m, r_1, r_2)}{\widetilde{W_0}(\mu_m, r_1, r_2)}\right) =$$

$$= \frac{1}{\varepsilon_0} \sum_{s=1}^{\infty} \frac{2\tau r_q J_0(\frac{\gamma_s}{r_1} r_q) J_1(\gamma_s)}{r_1^2 J_1^2(\gamma_s)} \frac{\frac{\gamma_s}{r_1}}{(\frac{\gamma_s}{r_1})^2 + \mu_m^2} \sin(\mu_m(z_q - z_1)).$$

As a result, we obtain:

$$g_m = \frac{A_m}{B_m}, \tag{I.5}$$

where:

$$A_m = \frac{1}{\varepsilon_0} \frac{2\tau r_q}{r_1^3} \sum_{s=1}^{\infty} \frac{J_0(\frac{\gamma_s}{r_1} r_q) J_1(\gamma_s)}{J_1^2(\gamma_s)} \frac{\frac{\gamma_s}{r_1}}{(\frac{\gamma_s}{r_1})^2 + \mu_m^2} \sin(\mu_m(z_q - z_1))$$

$$B_m = \frac{\pi m}{2}\left(\frac{I_1(\mu_m r_1)}{I_0(\mu_m r_1)} - \frac{\varepsilon_1}{\varepsilon_2} \frac{\widetilde{W_1}(\mu_m, r_1, r_2)}{\widetilde{W_0}(\mu_m, r_1, r_2)}\right)$$

The formulas I.1-I.5 enable us to compute the distribution of the electrostatic potential throughout the entire space of the investigated diode system.

The results of the numerical calculation of the potential in the field emission system with dielectrics

Based on the obtained formulas for the potential distribution, graphs were constructed. Fig. 7 illustrate the differences in the behavior of the zero equipotential contour,

outlining the shape of the cathode edge, depending on the dielectric values at the interface of the regions. It can be observed that when the ratio $\dfrac{\varepsilon_1}{\varepsilon_2}$ decreases by a factor of 10, the zero equipotential becomes relatively flat, and the shape of the cathode is not clearly pronounced.

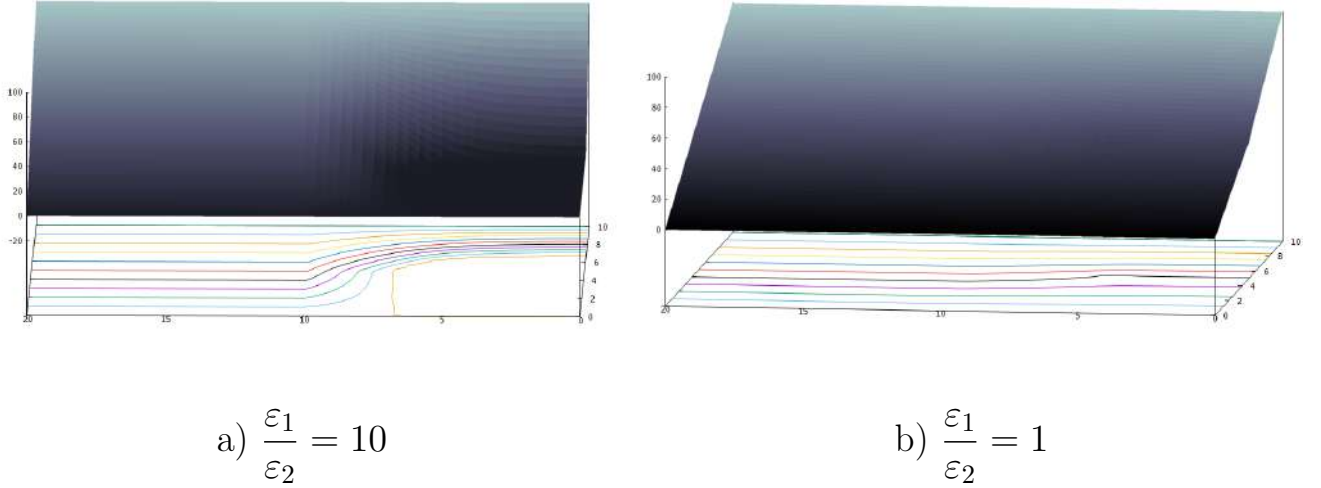All parameter values are given in dimensionless units.

$$\text{a)} \quad \frac{\varepsilon_1}{\varepsilon_2} = 10 \qquad\qquad\qquad \text{b)} \quad \frac{\varepsilon_1}{\varepsilon_2} = 1$$

Fig. 7: $r_1 = 10,\ r_q = 5,\ r_2 = 20,\ z_1 = 10,\ z_q = 5, \tau = -100, U_0 = 100.$

If the value of the dielectric permittivity ratio is kept constant but not equal to unity, and the charge density τ is increased as shown in Fig. 8, the shape of the cathode changes less significantly compared to the problem discussed in the first paragraph, Fig. 3-4.
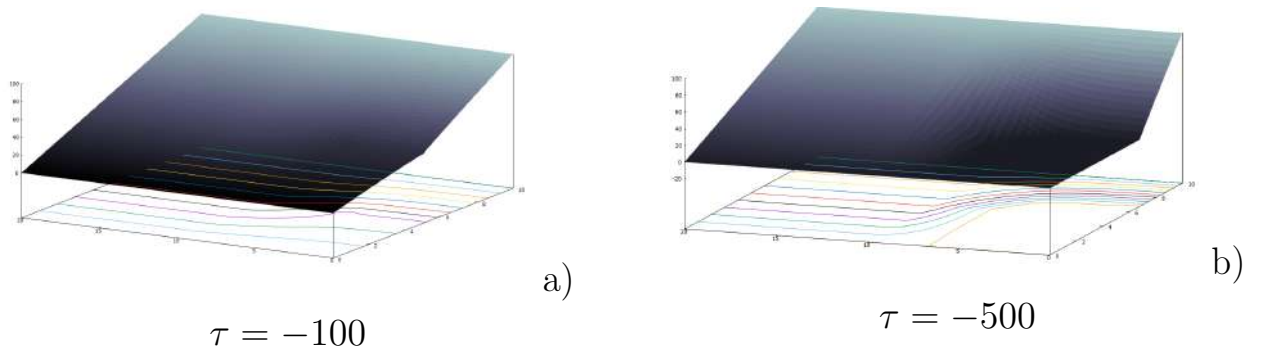

a)

$$\tau = -100$$

b)

$$\tau = -500$$

Fig. 8: $r_1 = 10, r_q = 5, r_2 = 20, z_1 = 10, z_q = 5, \dfrac{\varepsilon_1}{\varepsilon_2} = 5, U_0 = 100.$

I.3   Modeling of an axially symmetric triode field emission system with a modulator

Physical formulation of the problem for calculating the potential in a field emission system with a modulator

This section considers the modeling of an electron gun with a hollow cathode in the form of a triode system with a modulator, taking into account the influence of dielectrics on the potential distribution.
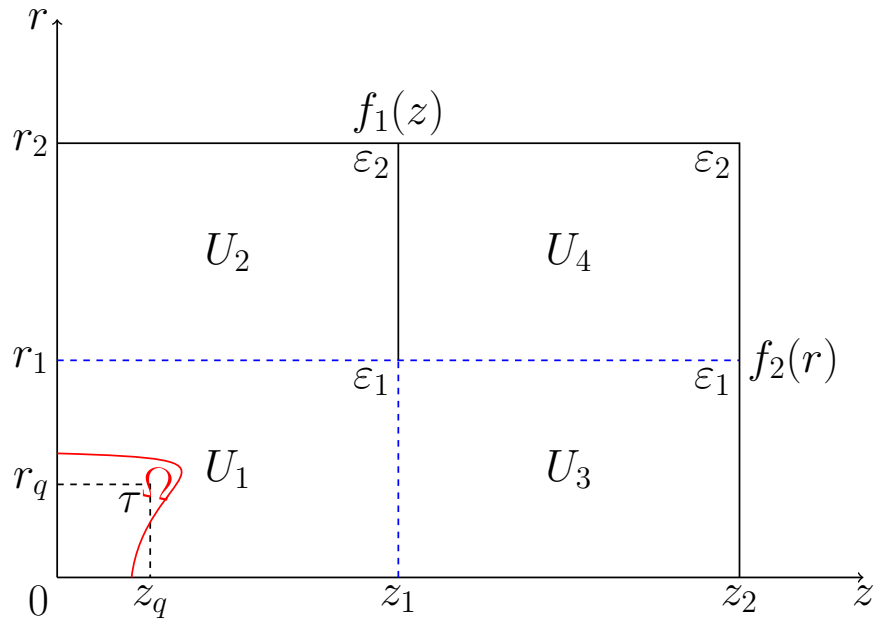

Fig. 9: Schematic representation of the electron-optical system on a plane.

The considered system is axially symmetric, which allows us to reduce the problem from three-dimensional to two-dimensional. To find the distribution of the electrostatic potential, we replace the influence of the cathode with the effect of a circular charged wire with a linear charge density τ. The schematic representation of the system on a plane is shown in the figure. The coordinates of the charged wire are (r_q, z_q). The modulator has the form of a diaphragm. The internal region of the system is filled with two dielectrics with dielectric permittivities ε_1 при $r < r_1$ and ε_2 for $r > r_1$.

System parameters:

$r = 0$ - surface of the cathode substrate, $0 \leq z \leq z_2$;

$z = z_2$ - surface of the anode, $0 \leq r \leq r_2$;

$z = z_1$ - surface of the modulator, for $r_1 \leq r \leq r_2$;

$r = r_2$ - outer boundary of the region, $0 \leq z \leq z_2$;

$r = r_1$ - boundary between the two dielectrics, $0 \leq z \leq z_2$.

Mathematical model

The distribution of the electrostatic potential $U(r, z)$ in the cylindrical coordinate system satisfies the Laplace's equation:

$$\triangle V = \frac{1}{r}\left(\frac{\partial}{\partial r}r\frac{\partial V}{\partial r}\right) + \frac{\partial^2 V}{\partial z^2} = 0,$$
$$V(r, z)|_\Omega = 0,$$
$$\Omega - \text{surface of the cathode.}$$

(I.1)

with boundary conditions:

$$V(r_2, z) = f_1(z),$$
$$0 \leq z \leq z_2;$$
$$V(r, z_1) = f_3(r), \quad r_1 \leq r \leq r_2;$$
$$V(r, z_2) = f_2(r), \quad 0 \leq r \leq r_2.$$

(I.2)

Due to the replacement of the cathode's influence with the effect of the charged wire, the original boundary problem I.1, I.2 is reduced to solving the Poisson's equation:

$$\triangle V(r, z) = -\frac{\rho(r, z)}{\varepsilon_0},$$

(I.3)

boundary conditions:

$$V(r_2, z) = f_1(z),$$
$$V(r, z_1) = f_3(r),$$
$$V(r, z_2) = f_2(r),$$

(I.4)

where $\rho(r, z)$:

$$\rho(r, z) = \begin{cases} \rho, & |r - r_q| < \delta \ \& \ |z - z_q| < \varepsilon_1; \\ 0, & |r - r_q| > \delta \ V \ |z - z_q| > \varepsilon_2, \end{cases}$$

(I.5)

$$\tau = \lim_{\delta_1 \to 0, \delta_2 \to 0} 4\delta_1\delta_2\rho.$$

(I.6)

To find the solution to the Poisson's equation I.3, I.4 for the entire system, we divide the internal region of the system into four subdomains:

$$U(r, z) = \begin{cases} U_1(r, z), \ 0 \leq r \leq r_1 \ \& \ 0 < z \leq z_1; \\ U_2(r, z), \ r_1 \leq r \leq r_2 \ \& \ 0 \leq z \leq z_1; \\ U_3(r, z), \ 0 \leq r \leq r_1 \ \& \ z_1 \leq z \leq z_2; \\ U_4(r, z), \ r_1 \leq r \leq r_2 \ \& \ z_1 \leq z \leq z_2. \end{cases} \quad \text{(I.7)}$$

The distribution of the potential is obtained as series expansions in terms of eigenfunctions for each of the mentioned regions. The coefficients of the series are determined from the following conditions:

$$U_1|_{r=r_1} = U_2|_{r=r_1}; \qquad \frac{\partial U_1}{\partial r}\Big|_{r=r_1} = \frac{\varepsilon_2}{\varepsilon_1} \frac{\partial U_2}{\partial r}\Big|_{r=r_1};$$

$$U_1|_{z=z_1} = U_3|_{z=z_1}; \qquad \frac{\partial U_1}{\partial z}\Big|_{z=z_1} = \frac{\partial U_3}{\partial z}\Big|_{z=z_1}; \qquad \text{(I.8)}$$

$$U_3|_{r=r_1} = U_4|_{r=r_1}; \qquad \frac{\partial U_3}{\partial r}\Big|_{r=r_1} = \frac{\varepsilon_2}{\varepsilon_1} \frac{\partial U_4}{\partial r}\Big|_{r=r_1}.$$

The solution of the Poisson's equation

The distribution of the potential $F(r, z)$, given by a charged wire according to the formulas in Section I.1, will have the following form:

$$F(r, z) = \sum_{m=1}^{\infty} \frac{1}{\varepsilon_0} \frac{2\tau r_q J_0(\mu_m r_q)}{\gamma_m r_1 J_1^2(\gamma_m)} J_0(\mu_m r) \frac{\text{sh}(\mu_m(z_1 - z_q)) \, \text{sh}(\mu_m z)}{\text{sh}(\mu_m z_1)},$$

for $0 \leqslant z \leqslant z_q$,

$$F(r, z) = \sum_{m=1}^{\infty} \frac{1}{\varepsilon_0} \frac{2\tau r_q J_0(\mu_m r_q)}{\gamma_m r_1 J_1^2(\gamma_m)} J_0(\mu_m r) \frac{\text{sh}(\mu_m(z_q - z_1)) \, \text{sh}(\mu_m(z_1 - z))}{\text{sh}(\mu_m z_1)},$$

for $z_q \leqslant z \leqslant z_1$, where $\mu_m = \dfrac{\gamma_m}{r_1}$, γ_m - the zeros of Bessel's function $J_0(\gamma_m) = 0$.

Depending on the region I.7, the value of the electrostatic potential can be expressed as follows:

for $(0 \leq z \leq z_1)$ и $(0 \leq r \leq r_1)$:

$$U_1(r,z) = \sum_{m=1}^{\infty} b_m \frac{\operatorname{sh}\dfrac{\gamma_m}{r_1}z}{\operatorname{sh}\dfrac{\gamma_m}{r_1}z_1} J_0(\frac{\gamma_m r}{r_1}) + \sum_{n=1}^{\infty} a_n \frac{I_0\left(\dfrac{\pi n r}{z_1}\right)}{I_0\left(\dfrac{\pi n r_1}{z_1}\right)} \sin\frac{\pi n z}{z_1} + F(r,z), \quad (I.9)$$

for $(0 \le z \le z_1)$ и $(r_1 \le r \le r_2)$:

$$U_2(r,z) = \sum_{q=1}^{\infty} d_q W_0(\lambda_q, r, r_2)\frac{\operatorname{sh}\lambda_q z}{\operatorname{sh}\lambda_q z_1} +$$

$$+ \sum_{n=1}^{\infty}\left(a_n \frac{\widetilde{W}_0(\alpha_n, r, r_2)}{\widetilde{W}_0(\alpha_n, r_1, r_2)} + g_n \frac{\widetilde{W}_0(\alpha_n, r_1, r)}{\widetilde{W}_0(\alpha_n, r_1, r_2)} \right) \sin(\alpha_n(z - z_1)),$$

$$(I.10)$$

where W_0 и $\widetilde{W}_0$ are linear combinations of Bessel functions:

$$W_0(\lambda_q, r, r_2) = J_0(\lambda_q r)Y_0(\lambda_q r_2) - J_0(\lambda_q r_2)Y_0(\lambda_q r),$$

$$\widetilde{W}_0(\beta_q, r, r_2) = I_0(\beta_q r)K_0(\beta_q r_2) - I_0(\beta_q r_2)K_0(\beta_q r).$$

The distribution of the potential $(z_1 \le z \le z_2)$ и $(0 \le r \le r_1)$ takes the form of:

$$U_3(r,z) = \sum_{m=1}^{\infty}\left(b_m \frac{\operatorname{sh}\mu_m(z_2 - z)}{\operatorname{sh}\mu_m(z_2 - z_1)} + t_m \frac{\operatorname{sh}\mu_m(z - z_1)}{\operatorname{sh}\mu_m(z_2 - z_1)} \right) J_0(\frac{\gamma_m r}{r_1}) +$$

$$+ \sum_{k=0}^{\infty} c_k \frac{I_0(\beta_k r)}{I_0(\beta_k r_1)} \sin(\beta_k(z - z_1)),$$

$$(I.11)$$

for $(z_1 \le z \le z_2)$ и $(r_1 \le r \le r_2)$:

$$U_4(r,z) = \sum_{q=1}^{\infty}\left(d_q \frac{\operatorname{sh}\lambda_q(z_2 - z)}{\operatorname{sh}\lambda_q(z_2 - z_1)} + s_q \frac{\operatorname{sh}\lambda_q(z - z_1)}{\operatorname{sh}\lambda_q(z_2 - z_1)} \right) W_0(\lambda_q, r, r_2) +$$

$$+ \sum_{k=0}^{\infty}\left(c_k \frac{\widetilde{W}_0(\beta_k, r, r_2)}{\widetilde{W}_0(\beta_k, r_1, r_2)} + h_k \frac{\widetilde{W}_0(\beta_k, r_1, r)}{\widetilde{W}_0(\beta_k, r_1, r_2)} \right) \sin(\beta_k(z - z_1)).$$

$$(I.12)$$

where γ_m - solution of the equation $J_0(\gamma_m) = 0$, $\mu_m = \dfrac{\gamma_m}{r_1}$, $\alpha_n = \dfrac{\pi n}{z_1}$, $\beta_k = \dfrac{\pi k}{z_2 - z_1}$ - eigenvalues.

λ_q - zeros of the linear combination of the Bessel functions of the first and second kind:

$$W_0(\lambda_q, r_1, r_2) = 0,$$

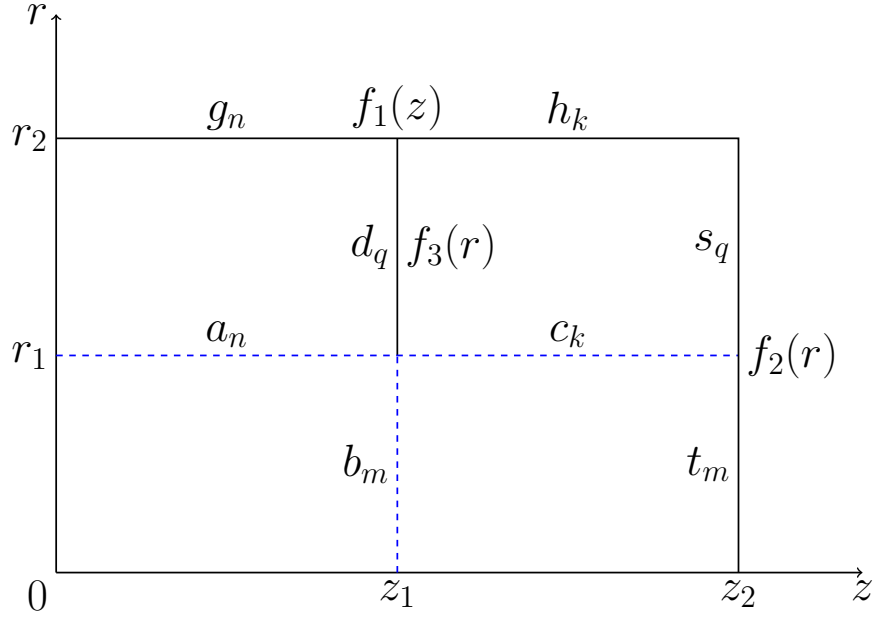## Finding coefficients in the series I.9-I.12

Fig. 10: Notation of coefficients in the expansions of boundary functions.

To determine the potential distribution in the entire region of the modeled system, it is necessary to find the coefficients in the expansions of the potential in terms of eigenfunctions (see Fig. 10).

These coefficients represent the expansion coefficients of the functions on the boundaries of the subdomains of the system.

Based on the continuity conditions of the displacement vector at the interfaces between the regions I.8, we can establish equations that allow us to compute these coefficients. It is necessary to compute the partial derivatives of the potential distribution with respect to the variables z and r for each of the regions according to I.8.

$$\varepsilon_1 \frac{\partial U_1}{\partial r}\Big|_{r=r_1} = \varepsilon_2 \frac{\partial U_2}{\partial r}\Big|_{r=r_1}$$

$$\sum_{n=1}^{\infty} a_n \alpha_n \frac{I_1(\alpha_n r_1)}{I_0(\alpha_n r_1)} \sin(\alpha_n z) - \sum_{m=1}^{\infty} b_m \mu_m \frac{\operatorname{sh}(\mu_m z)}{\operatorname{sh}(\mu_m z_1)} J_1(\gamma_m) + \frac{\partial F}{\partial r}\Big|_{r=r_1} =$$

$$= \frac{\varepsilon_2}{\varepsilon_1} \sum_{q=1}^{\infty} \lambda_q d_q W_1(\lambda_q, r_1, r_2) \frac{\operatorname{sh} \lambda_q z}{\operatorname{sh} \lambda_q z_1} +$$

$$+ \sum_{n=1}^{\infty} \left(a_n \frac{\widetilde{W}_1(\lambda_q, r_1, r_2)}{\widetilde{W}_0(\lambda_q, r_1, r_2)} - g_n \frac{\widetilde{W}_1(\lambda_q, r_1, r_1)}{\widetilde{W}_0(\lambda_q, r_1, r_2)} \right) \sin(\alpha_n z),$$

where

$$\frac{\partial F}{\partial r}\Big|_{r=r_1} = -\frac{1}{\varepsilon_0} \sum_{m=1}^{\infty} \frac{2\tau r_q}{\gamma_m r_1 J_1(\gamma_m)} \mu_m J_1(\mu_m r_q) \frac{\mathrm{sh}(\mu_m(z_1 - z_q))\,\mathrm{sh}(\mu_m z)}{\mathrm{sh}(\mu_m z_1)},$$

for $0 \leqslant z \leqslant z_q$,

$$\frac{\partial F}{\partial r}\Big|_{r=r_1} = -\frac{1}{\varepsilon_0} \sum_{m=1}^{\infty} \frac{2\tau r_q}{\gamma_m r_1 J_1(\gamma_m)} \mu_m J_0(\mu_m r_q) \frac{\mathrm{sh}(\mu_m z_q)\,\mathrm{sh}(\mu_m(z_1 - z))}{\mathrm{sh}(\mu_m z_1)}.$$

for $z_q \leqslant z \leqslant z_1$.

Let's multiply the previous equation by $\sin(\alpha_n z)$ and integrate with respect to the variable z:

$$a_n \alpha_n \frac{z_1}{2}\left(\frac{I_1(\alpha_n r_1)}{I_0(\alpha_n r_1)} - \frac{\varepsilon_2}{\varepsilon_1}\frac{\widetilde{W_1}(\alpha_n, r_1, r_2)}{\widetilde{W_0}(\alpha_n, r_1, r_2)}\right) - \sum_{m=1}^{\infty} b_m \mu_m J_1(\gamma_m) \int_0^{z_1} \frac{\mathrm{sh}(\mu_m z)}{\mathrm{sh}(\mu_m z_1)} \sin(\alpha_n z) =$$

$$= -\frac{\varepsilon_2}{\varepsilon_1} g_n \frac{\widetilde{W_1}(\alpha_n, r_1, r_1)}{\widetilde{W_0}(\alpha_n, r_1, r_2)} \alpha_n \frac{z_1}{2} + \frac{\varepsilon_2}{\varepsilon_1} \sum_{q=1}^{\infty} d_q \lambda_q W_1(\lambda_q, r_1, r_2) \int_0^{z_1} \frac{\mathrm{sh}(\lambda_q z)}{\mathrm{sh}(\lambda_q z_1)} \sin(\alpha_n z) dz +$$

$$+ \frac{1}{\varepsilon_0} \sum_{m=1}^{\infty} \frac{2\tau r_q J_0(\mu_m r_q)}{\gamma_m r_1 J_1^2(\gamma_m)} \mu_m J_1(\gamma_m)\left[\int_0^{z_q} \mathrm{sh}(\mu_m z)\sin(\alpha_n z)dz\frac{\mathrm{sh}(\mu_m(z_1 - z_q))}{\mathrm{sh}(\mu_m z_1)} + \right.$$

$$\left. + \int_{z_q}^{z_1} \mathrm{sh}(\mu_m(z_1 - z))\sin(\alpha_n(z))dz\frac{\mathrm{sh}(\mu_m z_q)}{\mathrm{sh}(\mu_m z_1)}\right].$$

After calculation we have:

$$a_n \alpha_n \frac{z_1}{2}\left(\frac{I_1(\alpha_n r_1)}{I_0(\alpha_n r_1)} - \frac{\varepsilon_2}{\varepsilon_1}\frac{\widetilde{W_1}(\alpha_n, r_1, r_2)}{\widetilde{W_0}(\alpha_n, r_1, r_2)}\right) + \sum_{m=1}^{\infty} b_m \mu_m J_1(\gamma_m)\frac{\alpha_n}{\mu_m^2 + \alpha_n^2}(-1)^n =$$

$$= -\frac{\varepsilon_2}{\varepsilon_1} g_n \alpha_n \frac{z_1}{2}\frac{\widetilde{W_1}(\alpha_n, r_1, r_1)}{\widetilde{W_0}(\alpha_n, r_1, r_2)} - \frac{\varepsilon_2}{\varepsilon_1} \sum_{q=1}^{\infty} d_q \lambda_q W_1(\lambda_q, r_1, r_2)\frac{\alpha_n}{\lambda_q^2 + \alpha_n^2}(-1)^n +$$

$$+ \frac{1}{\varepsilon_0} \sum_{m=1}^{\infty} \frac{2\tau r_q J_0(\mu_m r_q)}{\gamma_m r_1 J_1^2(\gamma_m)} \mu_m J_1(\gamma_m)\frac{\mu_m}{\mu_m^2 + \alpha_n^2}\sin(\alpha_n z_q).$$

$$\tag{I.13}$$

At the boundary between the regions with potentials U_1 and U_3, the following equation holds true:

$$\frac{\partial U_1}{\partial z}\Big|_{z=z_1} = \frac{\partial U_3}{\partial z}\Big|_{z=z_1},$$

for $0 \leq r \leq r_1$, therefore:

$$\sum_{n=1}^{\infty} a_n \alpha_n (-1)^n \frac{I_0(\alpha_n r)}{I_0(\alpha_n r_1)} + \sum_{m=1}^{\infty} b_m \mu_m \operatorname{cth}(\mu_m z_1) J_0(\mu_m r) -$$

$$- \frac{1}{\varepsilon_0} \frac{2\tau r_q}{r_1} \sum_{m=1}^{\infty} \frac{J_0(\mu_m r_q)}{\gamma_m J_1^2(\gamma_m)} \mu_m \frac{\operatorname{sh}(\mu_m z_q)}{\operatorname{sh}(\mu_m z_1)} J_0(\mu_m r) =$$

$$= \sum_{m=1}^{\infty} \Big[- b_m \mu_m \operatorname{cth}(\mu_m(z_2 - z_1)) + t_m \mu_m \frac{1}{\operatorname{sh}(\mu_m(z_2 - z_1))} \Big] J_0(\mu_m r) +$$

$$+ \sum_{k=1}^{\infty} c_k \beta_k \frac{I_0(\beta_k r)}{I_0(\beta_k r_1)},$$

by multiplying the last equation by $r J_0(\mu_m r)$ and integrating with respect to r, we obtain:

$$\sum_{n=1}^{\infty} a_n \alpha_n (-1)^n \frac{r_1 \mu_m}{\mu_m^2 + \alpha_n^2} J_1(\gamma_m) +$$

$$+ b_m \mu_m [\operatorname{cth}(\mu_m z_1) + \operatorname{cth}(\mu_m(z_2 - z_1))] \frac{r_1^2}{2} J_1^2(\gamma_m) -$$

$$- \sum_{k=1}^{\infty} c_k \beta_k \frac{r_1 \mu_m}{\mu_m^2 + \beta_k^2} J_1(\gamma_m) = \frac{1}{\varepsilon_0} \frac{2\tau r_q}{r_1} \frac{J_0(\mu_m r_q)}{\gamma_m J_1^2(\gamma_m)} \mu_m \frac{\operatorname{sh}(\mu_m z_q)}{\operatorname{sh}(\mu_m z_1)} \frac{r_1^2}{2} J_1^2(\gamma_m) + \qquad (I.14)$$

$$+ t_m \mu_m \frac{1}{\operatorname{sh}(\mu_m(z_2 - z_1))} \frac{r_1^2}{2} J_1^2(\gamma_m).$$

Next, we equate the derivatives at $r = r_1$ on the boundary between the regions with the potential distributions given by the functions $U_3(r, z)$ and $U_4(r, z)$:

$$\frac{\partial U_3}{\partial r}\Big|_{r=r_1} = \frac{\varepsilon_1}{\varepsilon_2} \frac{\partial U_4}{\partial r}\Big|_{r=r_1},$$

$$- \sum_{m=1}^{\infty} \Big[b_m \mu_m \frac{\operatorname{sh}(\mu_m(z_2 - z))}{\operatorname{sh}(\mu_m(z_2 - z_1))} + t_m \mu_m \frac{\operatorname{sh}(\mu_m(z - z_1))}{\operatorname{sh}(\mu_m(z_2 - z_1))} \Big] J_1(\gamma_m) +$$

$$+ \sum_{k=1}^{\infty} c_k \beta_k \frac{I_1(\beta_k r_1)}{I_0(\beta_k r_1)} \sin(\beta_k(z - z_1)) =$$

$$= \frac{\varepsilon_2}{\varepsilon_1} \Bigg[\Big(\sum_{k=1}^{\infty} c_k \beta_k \frac{\widetilde{W_1}(\beta_k, r_1, r_2)}{\widetilde{W_0}(\beta_k, r_1, r_2)} - h_k \beta_k \frac{1}{\beta_k r_1} \frac{1}{\widetilde{W_0}(\beta_k, r_1, r_2)} \Big) \sin(\beta_k(z - z_1)) +$$

$$+ \sum_{q=1}^{\infty} \Big(d_q \frac{\operatorname{sh}(\lambda_q(z_2 - z))}{\operatorname{sh}(\lambda_q(z_2 - z_1))} + s_q \frac{\operatorname{sh}(\lambda_q(z - z_1))}{\operatorname{sh}(\lambda_q(z_2 - z_1))} \Big) \lambda_q W_1(\lambda_q, r_1, r_2) \Bigg],$$

where:

$$\widetilde{W_0}(\beta_k, r_1, r)'\Big|_{r=r_1} = \beta_k [-I_0(\beta_k r_1) K_1(\beta_k r_1) - I_1(\beta_k r_1) K_0(\beta_k r_1)] = -\frac{1}{r_1}.$$

We multiply the last equation by $\sin(\beta_k(z - z_1))$ and integrate it with respect to z:

$$-\sum_{m=1}^{\infty} b_m \frac{\mu_m J_1(\gamma_m)}{\text{sh}(\mu_m(z_2 - z_1))} \int_{z_1}^{z_2} \text{sh}(\mu_m(z_2 - z)) \sin(\beta_k(z - z_1)) dz +$$

$$+ c_k \beta_k \frac{z_2 - z_1}{2} \left(\frac{I_1(\beta_k r_1)}{I_0(\beta_k r_1)} - \frac{\varepsilon_2}{\varepsilon_1} \frac{\widetilde{W_1}(\beta_k, r_1, r_2)}{\widetilde{W_0}(\beta_k, r_1, r_2)} \right) =$$

$$= \sum_{m=1}^{\infty} t_m \frac{\mu_m J_1(\gamma_m)}{\text{sh}(\mu_m(z_2 - z_1))} \int_{z_1}^{z_2} \text{sh}(\mu_m(z - z_1)) \sin(\beta_k(z - z_1)) dz -$$

$$- h_k \frac{1}{r_1} \frac{1}{\widetilde{W_0}(\beta_k, r_1, r_2)} \frac{z_2 - z_1}{2} +$$

$$+ \sum_{q=1}^{\infty} d_q \lambda_q \frac{W_1(\lambda_q, r_1, r_2)}{\text{sh}(\lambda_q(z_2 - z_1))} \int_{z_1}^{z_2} \text{sh}(\lambda_q(z_2 - z)) \sin(\beta_k(z - z_1)) dz +$$

$$+ \sum_{q=1}^{\infty} s_q \lambda_q \frac{W_1(\lambda_q, r_1, r_2)}{\text{sh}(\lambda_q(z_2 - z_1))} \int_{z_1}^{z_2} \text{sh}(\lambda_q(z - z_1)) \sin(\beta_k(z - z_1)) dz,$$

now we have:

$$-\sum_{m=1}^{\infty} b_m \mu_m J_1(\gamma_m) \frac{\beta_k}{\mu_m^2 + \beta_k^2} + c_k \beta_k \frac{z_2 - z_1}{2} \left(\frac{I_1(\beta_k r_1)}{I_0(\beta_k r_1)} - \frac{\varepsilon_2}{\varepsilon_1} \frac{\widetilde{W_1}(\beta_k, r_1, r_2)}{\widetilde{W_0}(\beta_k, r_1, r_2)} \right) =$$

$$= -\sum_{m=1}^{\infty} t_m \mu_m J_1(\gamma_m) \frac{\beta_k (-1)^k}{\mu_m^2 + \beta_k^2} - h_k \frac{1}{r_1} \frac{1}{\widetilde{W_0}(\beta_k, r_1, r_2)} \frac{z_2 - z_1}{2} \frac{\varepsilon_2}{\varepsilon_1} +$$

$$+ \frac{\varepsilon_2}{\varepsilon_1} \sum_{q=1}^{\infty} d_q \lambda_q W_1(\lambda_q, r_1, r_2) \frac{\beta_k}{\lambda_q^2 + \beta_k^2} - \frac{\varepsilon_2}{\varepsilon_1} \sum_{q=1}^{\infty} s_q \lambda_q W_1(\lambda_q, r_1, r_2) \frac{\beta_k}{\lambda_q^2 + \beta_k^2} (-1)^k.$$
$$(I.15)$$

For convenience, let's represent equations I.13 - I.15 in the following form:

$$\varepsilon_1 \frac{\partial U_1}{\partial r} \Big|_{r=r_1} = \varepsilon_2 \frac{\partial U_2}{\partial r} \Big|_{r=r_1} :$$

$$a_n \left(\frac{I_1(\alpha_n r_1)}{I_0(\alpha_n r_1)} - \frac{\varepsilon_2}{\varepsilon_1} \frac{\widetilde{W_1}(\alpha_n, r_1, r_2)}{\widetilde{W_0}(\alpha_n, r_1, r_2)} \right) + \left[\sum_{m=1}^{\infty} b_m J_1(\gamma_m) \frac{\mu_m}{\mu_m^2 + \alpha_n^2} \right] \frac{2(-1)^n}{z_1} =$$

$$= -\frac{\varepsilon_2}{\varepsilon_1} g_n \frac{\widetilde{W_1}(\alpha_n, r_1, r_2)}{\widetilde{W_0}(\alpha_n, r_1, r_2)} - \frac{\varepsilon_2}{\varepsilon_1} \left[\sum_{q=1}^{\infty} d_q \lambda_q W_1(\lambda_q, r_1, r_2) \frac{\alpha_n}{\lambda_q^2 + \alpha_n^2} \right] \frac{2(-1)^n}{z_1 - z} + \quad (I.16)$$

$$+ \frac{1}{\varepsilon_0} \sum_{m=1}^{\infty} \frac{4 \tau r_q J_0(\mu_m r_q)}{\pi n (r_1)^2 J_1(\gamma_m)} \frac{\mu_m}{\mu_m^2 + \alpha_n^2} \sin(\alpha_n z_q),$$

where

$$\widetilde{W_1}(\alpha_n, r_1, r_2) = \frac{1}{\alpha_n r_1}; \quad W_1(\lambda_q, r_1, r_2) = -\frac{2}{\pi \lambda_q r_1} \frac{J_0(\lambda_q r_2)}{J_0(\lambda_q r_1)}.$$

$$\varepsilon_1 \frac{\partial U_1}{\partial z} \Big|_{z=z_1} = \varepsilon_2 \frac{\partial U_3}{\partial z} \Big|_{z=z_1} :$$

$$\frac{2}{r_1 J_1(\gamma_m)} \sum_{n=1}^{\infty} a_n (-1)^n \frac{\alpha_n}{\alpha_n^2 + \mu_m^2} + b_m[\text{cth}(\mu_m z_1) + \text{cth}(\mu_m(z_2 - z_1))]-$$

$$-\frac{2}{r_1 J_1(\gamma_m)} \sum_{k=1}^{\infty} c_k \frac{\beta_k}{\beta_k^2 + \mu_m^2} = \frac{1}{\varepsilon_0} \frac{2\tau r_q}{r_1} \frac{J_0(\mu_m r_q)}{\gamma_m J_1^2(\gamma_m)} \frac{\text{sh}(\mu_m z_q)}{\text{sh}(\mu_m z_1)} + t_m \frac{1}{\text{sh}(\mu_m(z_2 - z_1))}.$$

$$\text{(I.17)}$$

$$\varepsilon_1 \frac{\partial U_3}{\partial r}\Big|_{r=r_1} = \varepsilon_2 \frac{\partial U_4}{\partial r}\Big|_{r=r_1} :$$

$$-\frac{2}{z_2 - z_1} \sum_{m=1}^{\infty} b_m \frac{\mu_m}{\beta_k^2 + \mu_m^2} J_1(\gamma_m) + c_k \left(\frac{I_1(\beta_k r_1)}{I_0(\beta_k r_1)} - \frac{\varepsilon_2}{\varepsilon_1} \frac{\widetilde{W}_1(\beta_k, r_1, r_2)}{\widetilde{W}_0(\beta_k, r_1, r_2)} \right) =$$

$$= \frac{\varepsilon_2}{\varepsilon_1} \frac{2}{z_2 - z_1} \sum_{q=1}^{\infty} [d_q - s_q(-1)^k] \frac{\lambda_q}{\lambda_q^2 + \beta_k^2} W_1(\lambda_q, r_1, r_2) - \quad \text{(I.18)}$$

$$-\frac{2}{z_2 - z_1} \sum_{m=1}^{\infty} t_m \frac{\mu_m}{\beta_k^2 + \mu_m^2} (-1)^k J_1(\gamma_m) - \frac{\varepsilon_2}{\varepsilon_1} h_k \frac{1}{\beta_k r_1} \frac{1}{\widetilde{W}_0(\beta_k, r_1, r_2)},$$

where

$$W_1(\lambda_q, r_1, r_2) = -\frac{2}{\pi \lambda_q r_1} \frac{J_0(\lambda_q r_2)}{J_0(\lambda_q r_1)}.$$

In equations I.16 - I.18, let's calculate the values of the known coefficients for which the values of the electrostatic potential are specified on the boundaries of the system. Let's calculate the coefficient d_q:

$$U_2(r, z_1) = f_3(r) = \sum_{q=1}^{\infty} d_q W_0(\lambda_q, r, r_2).$$

Let's multiply the expression by $r W_0(\lambda_q, r, r_2)$ and integrate it with respect to r:

$$d_q \frac{2}{\pi^2 \lambda_q^2} \frac{J_0^2(\lambda_q r_1) - J_0^2(\lambda_q r_2)}{J_0^2(\lambda_q r_1)} = \int_{r_1}^{r_2} f_3(r) r W_0(\lambda_q, r, r_2) dr,$$

let's assume that $f_3(r) = const = f_3$, then:

$$d_q = \pi f_3 \frac{J_0(\lambda_q r_1)}{J_0(\lambda_q r_1) + J_0(\lambda_q r_2)}.$$

then let's find the coefficient g_n:

$$U_2(r_2, z) = \sum_{n=1}^{\infty} g_n \sin(\alpha_n z) = f_1(z),$$

Multiply both sides by $\sin(\alpha z)$ and integrate with respect to z:

$$g_n = \frac{2}{z_1} \int\limits_0^{z_1} f_1(z) \sin(\alpha_n z) dz.$$

Let's $f_1(z) = const = f_1$:

$$g_n = f_1 \frac{2}{z_1} \frac{(-1)^n}{\alpha_n} ((-1)^n - 1) = f_1 \frac{2}{\pi n} (1 - (-1)^n).$$

the following equality holds true for t_m:

$$U_3(r, z_2) = f_2(r) = \sum_{m=1}^{\infty} t_m J_0(\mu_m r),$$

Multiply by $r J_0(\mu_m r)$ and integrate with respect to r:

$$t_m = \frac{2}{r_1^2 J_1^2(\gamma_m)} \int\limits_0^{r_1} f_2(r) r J_0(\mu_m r) dr.$$

Let's $f_2(r) = const = f_2$, then:

$$t_m = \frac{2f_2}{r_1^2 J_1^2(\gamma_m)} \frac{r_1^2}{\gamma_m} J_1(\gamma_m) = f_2 \frac{2}{\gamma_m J_1(\gamma_m)}.$$

Let's find s_q:

$$U_4(r, z_2) = f_2(r) = \sum_{m=1}^{\infty} s_q W_0(\lambda_q, r, r_2),$$

Multiply by $r W_0(\lambda_q, r, r_2)$ and integrate with respect to r:

$$s_q = \frac{\pi^2 \lambda_q^2}{2} \frac{J_0^2(\lambda_q r_1)}{J_0^2(\lambda_q r_1) - J_0^2(\lambda_q r_2)} \int\limits_{r_1}^{r_2} f_2(r) r W_0(\lambda_q, r, r_2) dr.$$

Let's $f_2(r) = const = f_2$, then:

$$s_q = f_2 \pi \frac{J_0(\lambda_q r_1)}{J_0(\lambda_q r_1) + J_0(\lambda_q r_2)}.$$

Let's find h_k:

$$U_4(r_2, z) = f_1(z) = \sum_{k=1}^{\infty} h_k \sin(\beta_k(z - z_1)),$$

multiply by the eigenfunctions and integrate with respect to z:

$$h_k = \frac{2}{z_2 - z_1} \int_{z_1}^{z_2} f_1(z) \sin(\beta_k(z - z_1))dz.$$

If $f_1(z) = const = f_1$, then:

$$h_k = f_1 \frac{2}{\pi k}(1 - (-1)^k).$$

We can construct the matrix of the system I.16 - I.18 that will allow us to compute the unknown coefficients. It will be composed of the coefficients corresponding to the unknown coefficients:

$$M = \begin{pmatrix} A_1 & B_1 & C_1 \\ A_2 & B_2 & C_2 \\ A_3 & B_3 & C_{3,} \end{pmatrix}$$

on the right-hand side of the system I.16 - I.18, there is a vector determined by coefficients whose values are known to us:

$$D = \begin{pmatrix} D_1 \\ D_2 \\ D_3 \end{pmatrix} \tag{I.19}$$

To compute the matrix M, we need to evaluate each of the blocks $A_i, B_i, C_i (i = 1, 2, 3)$:

$$A_1 = \begin{pmatrix} a_{11}^1 & \ldots & 0 & 0 & 0 \\ \vdots & \ddots & \ldots & 0 & 0 \\ 0 & \ldots & a_{ij}^1 & \ldots & 0 \\ 0 & 0 & \ldots & \ddots & \vdots \\ 0 & 0 & 0 & \ldots & a_{nn}^1 \end{pmatrix} \quad B_1 = \begin{pmatrix} b_{11}^1 & \ldots & b_{1j}^1 & \ldots & b_{1m}^1 \\ \vdots & \ddots & \ldots & \ldots & \vdots \\ b_{i1}^1 & \ldots & b_{ij}^1 & \ldots & b_{im}^1 \\ \vdots & \ldots & \ldots & \ddots & \vdots \\ b_{n1}^1 & \ldots & b_{nj}^1 & \ldots & b_{nm}^1 \end{pmatrix} \quad C_1 = \begin{pmatrix} \varnothing \end{pmatrix},$$

where:

$$a_{ij}^1 = \begin{cases} \left(\dfrac{I_1(\alpha_j r_1)}{I_0(\alpha_j r_1)} - \dfrac{\varepsilon_1}{\varepsilon_2} \dfrac{\widetilde{W}_1(\alpha_j, r_1, r_2)}{\widetilde{W}_0(\alpha_j, r_1, r_2)} \right), & i = j = 1 \div n; \\ 0, & i \neq j, \ i, j = 1 \div n; \end{cases}$$

$$b_{ij}^1 = \frac{2(-1)^i}{z_1} \frac{\mu_j}{\mu_j^2 + \alpha_i^2} J_1(\gamma_j), \ i = 1 \div n, j = 1 \div m;$$

$$c_{ij}^1 = 0, \ i, j = 1 \div n.$$

(I.20)

Similarly, let's express the following blocks of the matrix M:

$$A_2 = \begin{pmatrix} a_{11}^2 & \cdots & a_{1j}^2 & \cdots & a_{1n}^2 \\ \vdots & \ddots & \cdots & \cdots & \vdots \\ a_{i1}^2 & \cdots & a_{ij}^2 & \cdots & a_{in}^2 \\ \vdots & \cdots & \cdots & \ddots & \vdots \\ a_{m1}^2 & \cdots & a_{mj}^2 & \cdots & a_{mn}^2 \end{pmatrix} \qquad B_2 = \begin{pmatrix} b_{11}^2 & \cdots & 0 & 0 & 0 \\ \vdots & \ddots & \cdots & 0 & 0 \\ 0 & \cdots & b_{ij}^2 & \cdots & 0 \\ 0 & 0 & \cdots & \ddots & \vdots \\ 0 & 0 & 0 & \cdots & b_{mm}^2 \end{pmatrix}$$

$$C_2 = \begin{pmatrix} c_{11}^2 & \cdots & c_{1j}^2 & \cdots & c_{1k}^2 \\ \vdots & \ddots & \cdots & \cdots & \vdots \\ c_{i1}^2 & \cdots & c_{ij}^2 & \cdots & c_{ik}^2 \\ \vdots & \cdots & \cdots & \ddots & \vdots \\ c_{m1}^2 & \cdots & c_{mj}^2 & \cdots & c_{mk}^2 \end{pmatrix},$$

where:

$$a_{ij}^2 = \frac{2}{r_1 J_1(\gamma_i)} (-1)^j \frac{\alpha_j}{\alpha_j^2 + \mu_i^2}, \ i = 1 \div m, j = 1 \div n;$$

$$b_{ij}^2 = \begin{cases} \operatorname{cth}(\mu_i z_1) + \operatorname{cth}(\mu_i(z_2 - z_1)), & i = j = 1 \div m; \\ 0, & j \neq i, \ i, j = 1 \div m; \end{cases}$$

(I.21)

$$c_{ij}^2 = -\frac{2}{r_1 J_1(\gamma_i)} \frac{\beta_j}{\beta_j^2 + \mu_i^2}, \ i = 1 \div m, j = 1 \div n.$$

Third line takes a form:

$$A_3 = \begin{pmatrix} \varnothing \end{pmatrix} \quad B_3 = \begin{pmatrix} b_{11}^3 & \cdots & b_{1j}^3 & \cdots & b_{1m}^3 \\ \vdots & \ddots & \cdots & \cdots & \vdots \\ b_{i1}^3 & \cdots & b_{ij}^3 & \cdots & b_{im}^3 \\ \vdots & \cdots & \cdots & \ddots & \vdots \\ b_{k1}^3 & \cdots & b_{kj}^3 & \cdots & b_{km}^3 \end{pmatrix} \quad C_3 = \begin{pmatrix} c_{11}^3 & \cdots & 0 & 0 & 0 \\ \vdots & \ddots & \cdots & 0 & 0 \\ 0 & \cdots & c_{ij}^3 & \cdots & 0 \\ 0 & 0 & \cdots & \ddots & \vdots \\ 0 & 0 & 0 & \cdots & c_{kk}^3, \end{pmatrix}$$

where:

$$\begin{aligned} &a_{ij}^3 = 0, \ i = 1 \div k, j = 1 \div m; \\ &b_{ij}^3 = -\frac{2}{z_2 - z_1} \frac{\mu_j}{\mu_j^2 + \beta_i^2} J_1(\gamma_m), \ i = 1 \div k, j = 1 \div m; \\ &c_{ij}^3 = \begin{cases} \dfrac{I_1(\beta_i r_1)}{I_0(\beta_i r_1)} - \dfrac{\varepsilon_1 \widetilde{W_1}(\beta_i, r_1, r_2)}{\varepsilon_2 \widetilde{W_0}(\beta_i, r_1, r_2)}, & i = 1 = j \div k; \\ 0, & i \neq j, \ i, j = 1 \div k. \end{cases} \end{aligned} \tag{I.22}$$

Let's represent the right-hand side of the system I.16 - I.18 according to how the rows of matrix M were presented.

Then the first components D_1 of vector D will have the following form:

$$\begin{aligned} d_n^1 = &-\frac{\varepsilon_2}{\varepsilon_1} g_n \frac{\widetilde{W_1}(\alpha_n, r_1, r_2)}{\widetilde{W_0}(\alpha_n, r_1, r_2)} - \frac{\varepsilon_2}{\varepsilon_1} \frac{2(-1)^n}{z_1} \sum_{q=1}^{\infty} d_q \frac{\lambda_q}{\lambda_q^2 + \alpha_n^2} W_1(\lambda_q, r_1, r_2), + \\ &+ \frac{1}{\varepsilon_0} \tau \frac{4r_q}{r_1^2 \pi n} \sum_{m=1}^{\infty} \frac{J_0(\mu_m r_q)}{J_1(\gamma_m)} \frac{\mu_m}{\mu_m^2 + \alpha_n^2} \sin(\alpha_n z_q), \end{aligned} \tag{I.23}$$

The second components D_2 of vector D will have the following form:

$$d_m^2 = \frac{1}{\varepsilon_0} \tau \frac{2r_q}{r_1} \frac{J_0(\mu_m r_q)}{\gamma_m J_1^2(\gamma_m)} \frac{\text{sh}(\mu_m z_q)}{\text{sh}(\mu_m z_1)} + t_m \frac{1}{\text{sh}(\mu_m(z_2 - z_1))}, \tag{I.24}$$

For the third component D_3 of vector D, the following expression holds true:

$$\begin{aligned} d_k^3 = &\frac{\varepsilon_2}{\varepsilon_1} \frac{2}{z_2 - z_1} \sum_{q=1}^{\infty} (d_q - s_q(-1)^k) \frac{\lambda_q}{\lambda_q^2 + \beta_k^2} W_1(\lambda_q, r_1, r_2) - \\ &- \frac{2}{z_2 - z_1} \sum_{m=1}^{\infty} t_m \frac{\mu_m}{\mu_m^2 + \beta_k^2} (-1)^k J_1(\gamma_m) - \frac{\varepsilon_2}{\varepsilon_1} h_k \frac{1}{\beta_k r_1} \frac{1}{\widetilde{W_0}(\beta_k, r_1, r_2)}. \end{aligned} \tag{I.25}$$

Formulas I.9 - I.12, I.16 - I.25 define the potential distribution throughout the entire region of the studied triode system.

The main results of this chapter have been published in the papers [11, 32, 33, 35, 99].

II   Modeling planar-symmetric two-dimensional diode systems with blade-shaped field cathodes in the Cartesian coordinate system.

The following sources were used in writing Chapter II: [5, 12, 13, 14, 15].

This chapter presents methods for modeling planar-symmetric diode emission systems with blade-shaped field emitters located on a flat substrate [7, 44]. The anode is a plane parallel to the substrate. The method of separation of variables in Cartesian coordinates is used to calculate the distribution of electrostatic potential throughout the system. Additionally, diode systems with two different dielectric materials filling their inner region are investigated [98].

II.1   Modeling a diode field emission system with a charged wire.

Formulation of the physical problem of calculating the potential of a system with a charged wire

Let's consider the problem of modeling a diode system using a charged wire in Cartesian coordinates (x, y, z). Neglecting edge effects, we assume that the shape of the blade-shaped cathode does not vary along the z variable. Thus, the potential distribution $V(x, y)$ depends on two coordinates (x, y). The cathode is located on a flat substrate, and the anode is a plane parallel to the cathode substrate.

System parameters:

$y = 0$ - cathode substrate;

$y = y_1$ - anode surface;

$x = 0, x = x_1$ - outer boundaries of the system along the x variable.

Boundary conditions:

$$
\begin{aligned}
&V(x, 0) = 0, \;\; 0 \leq x \leq x_1, \\
&V(x, y_1) = U_0, \; 0 \leq x \leq x_1, \\
&V(0, y) = \frac{U_0 y}{y_0}, \;\; 0 \leq y \leq y_0, \\
&V(x_1, y)\frac{U_0 y}{y_0}, \;\; 0 \leq y \leq y_0.
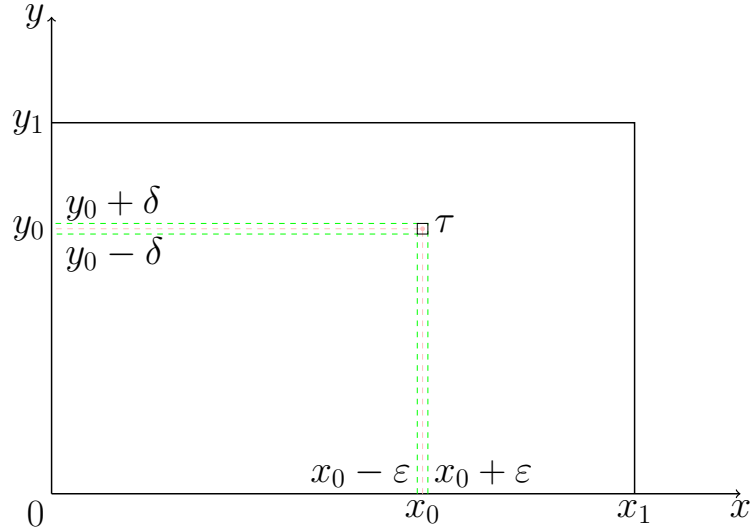\end{aligned} \tag{II.1}
$$

Fig. 11: A schematic representation of a system with a charged wire on a plane

Let's represent the potential distribution throughout the entire system as follows:

$$V(x,y) = U_0 \frac{y}{y_1} + U(x,y), \ 0 \le x \le x_1, 0 \le y \le y_1. \tag{II.2}$$

The influence of the field-emitting cathode on the field distribution is replaced by the influence of a charged wire with a charge density of τ, positioned in the xOy plane at coordinates $x = x_0$, $y = y_0$. Fig. 11 illustrates the schematic representation of the system with a charged wire in the two-dimensional domain (x,y). It is assumed that the surface of the actual cathode coincides with the zero equipotential. The potential of the emitter substrate is zero, and the potential of the anode is U_0. The lateral boundaries of the system along the x variable are defined by a linear function.

The mathematical model of a system with a charged wire in a bounded domain

Assuming a uniform distribution of charge density ρ, the charge is evenly spread within a small volume of a rectangle. [12, 17]:

$$x_0 - \varepsilon < x < x_0 + \varepsilon; \quad y_0 - \delta < y < y_0 + \delta,$$

then $\tau = \lim_{\varepsilon \to 0, \ \delta \to 0} 4\varepsilon\delta\rho$, the problem reduces to solving the Poisson's equation:

$$\triangle U(x,y) = \frac{\partial^2 U}{\partial x^2} + \frac{\partial^2 U}{\partial y^2} = -\frac{\rho(x,y)}{\varepsilon_0}, \tag{II.3}$$

where

$$\rho(x, y) = \begin{cases} \rho, & |x - x_0| < \varepsilon \text{ и } |y - y_0| < \delta, \\ 0, & |x - x_0| > \varepsilon \text{ или } |y - y_0| > \delta, \end{cases} \tag{II.4}$$

with the following boundary conditions:

$$U(0, y) = 0, \ U(x, 0) = 0, \ U(x_1, y) = 0, \ U(x, y_1) = 0. \tag{II.5}$$

Calculating the potential distribution of a system with a charged wire

The eigenfunctions are found with respect to the variable y. The differential equation for the eigenfunctions takes the following form:

$$Y'' + \lambda Y = 0,$$

the integral:

$$Y_n(y) = C_1 \sin(\sqrt{\lambda_n}y) + C_2 \cos(\sqrt{\lambda_n}y),$$

The eigenfunctions have to satisfy following conditions:

$$Y_n(0) = Y_n(y_1) = 0.$$

From the first equation, we can conclude that $C_2 = 0$. Using the second equation, we find:

$$\lambda_n = \frac{n^2\pi^2}{y_1^2},$$

then system of functions defines the eigenfunctions we need to find:

$$Y_n(y) = \sin\frac{n\pi}{y_1}y$$

The solution is sought in the form of a series:

$$U(x, y) = \sum_{n=1}^{\infty} \nu_n(x) \sin\frac{\pi n}{y_1}y. \tag{II.6}$$

Multiplying both sides of the equation by $\sin\left(\frac{\pi n}{y_1}y\right)$ and integrating with respect to y from 0 to y_1, we obtain:

$$\nu_n(x) = \frac{2}{y_1} \int_0^{y_1} U(x, y)) \sin\frac{\pi n}{y_1}y\,dy.$$

Multiplying equation II.6 by $\sin\left(\frac{\pi n}{y_1}y\right)$ and integrating with respect to y from 0 to y_1 in order to find $\nu_n(x)$:

$$\int\limits_0^{y_1} \frac{\partial^2 U}{\partial x^2}\sin\frac{\pi n}{y_1}y\,dy + \int\limits_0^{y_1} \frac{\partial^2 U}{\partial y^2}\sin\frac{\pi n}{y_1}y\,dy = -\frac{1}{\varepsilon_0}\int\limits_0^{y_1}\rho(x,y)\sin\frac{\pi n}{y_1}y\,dy.$$

Considering conditions II.4, we have:

$$\nu_n''(x) - \left(\frac{n\pi}{y_1}\right)^2\nu_n(x) = -\frac{2}{y_1\varepsilon_0}\phi(x)\int\limits_{y_0-\delta}^{y_0+\delta}\sin\frac{n\pi}{y_1}y\,dy,$$

where:

$$\phi(x) = \begin{cases} \rho, & |x-x_0| < \varepsilon, \\ 0, & |x-x_0| > \varepsilon, \end{cases} \tag{II.7}$$

from which we can derive the final form of the equation:

$$\nu_n''(x) - \left(\frac{n\pi}{y_1}\right)^2\nu_n(x) = -\frac{4\delta}{\varepsilon_0 y_1}\phi(x)\sin\frac{n\pi y_0}{y_1}.$$

The solution can be represented in the following form:

$$\nu_n(x) = C_1(x)\,\mathrm{ch}\,\frac{n\pi}{y_1}x + C_2(x)\,\mathrm{sh}\,\frac{n\pi}{y_1}x.$$

Taking into account the homogeneous boundary conditions, we find that $C_1 = 0$. Then, for C_2, the following expression holds [17]:

$$C_2 = \lim_{\varepsilon\to 0,\ \delta\to 0}\frac{8\rho\varepsilon\delta\sin\frac{n\pi}{y_1}y_0\sin\frac{n\pi}{y_1}(x_1-x_0)}{n\pi\varepsilon_0\sin\frac{n\pi}{y_1}x_1} = \frac{2\tau\sin\frac{n\pi}{y_1}y_0\sin\frac{n\pi}{y_1}(x_1-x_0)}{n\pi\varepsilon_0\sin\frac{n\pi}{y_1}x_1}.$$

Thus, we obtain the solution to the boundary problem II.1-II.4:
for $x \le x_0$

$$U(x,y) = \frac{2\tau}{\pi\varepsilon_0}\sum_{n=1}^{\infty}\frac{\mathrm{sh}(\frac{\pi n}{y_1}(x_1-x_0))}{n\,\mathrm{sh}(\frac{\pi n}{y_1}x_1)}\mathrm{sh}(\frac{\pi n}{y_1}x)\sin(\frac{\pi n}{y_1}y_0)\sin(\frac{\pi n}{y_1}y), \tag{II.8}$$

for $x \ge x_0$

$$U(x,y) = \frac{2\tau}{\pi\varepsilon_0} \sum_{n=1}^{\infty} \frac{\mathrm{sh}(\frac{\pi n}{y_1}x_0)}{n\,\mathrm{sh}(\frac{\pi n}{y_1}x_1)}\,\mathrm{sh}(\frac{\pi n}{y_1}(x_1 - x))\sin(\frac{\pi n}{y_1}y_0)\sin(\frac{\pi n}{y_1}y). \qquad (\mathrm{II.9})$$

Therefore, equations II.1, II.8, II.9 provide the potential distribution $V(x,y)$ throughout the entire space of the studied system.

The results of the numerical calculation of the potential distribution in the system with a charged wire are as follows:

Based on the obtained solution, a C++ program has been written. The program generates plots illustrating the potential distribution throughout the entire system. All parameter values are given in dimensionless units.
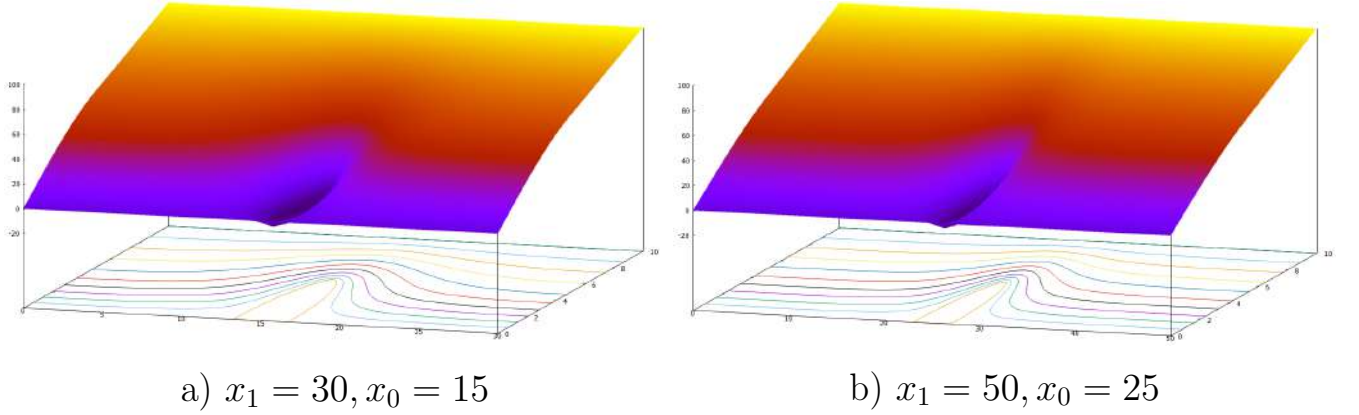

a) $x_1 = 30, x_0 = 15$ b) $x_1 = 50, x_0 = 25$

Fig. 12: $y_1 = 10, y_0 = 5, \tau = -10, U_0 = 100$.

It is worth noting that in Fig. 12 (a) and (b), the shape of the cathode remains almost same, as well as the length of the cathode base. This fact reflects the adequacy of the constructed model. The simulation results show the necessary shape and dimensions of the cathode, while variations in the system size contribute to changes in the potential distribution within the diode system region but have a minimal impact on the cathode shape.
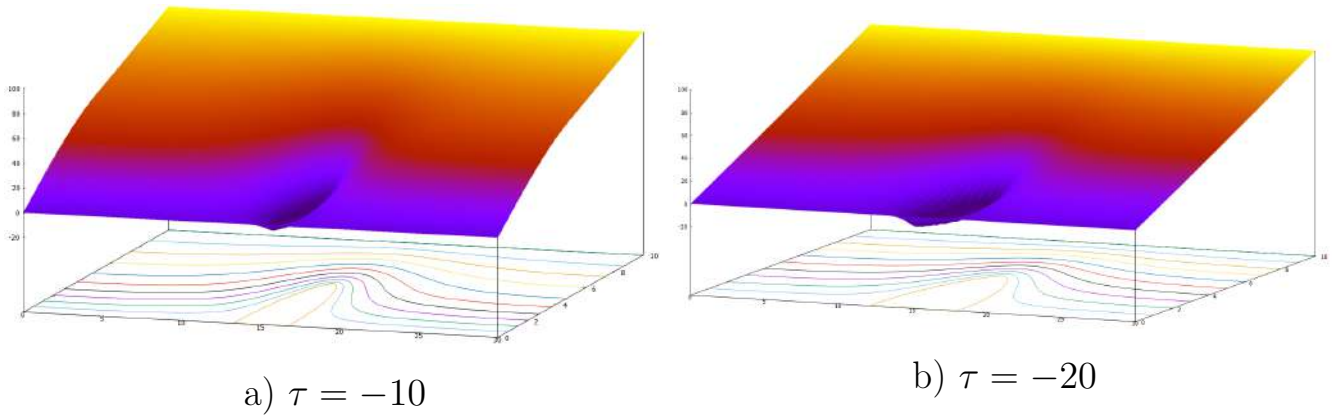
a) $\tau = -10$

b) $\tau = -20$

Fig. 13: $y_1 = 10, y_0 = 5, x_1 = 50, x_0 = 25, U_0 = 100$.

Considering Fig. 13, panels (a) and (b) exhibit different values of the charge density τ. The plots demonstrate that a doubling of the value of τ leads to a change in the shape of the cathode, specifically an increase in the length of its base.

II.2   Modeling of a system with an arbitrary number of charged wires.

The physical setup of the problem of calculating the potential distribution in a system with charged wires.

The problem under investigation is the modeling of a diode system with an arbitrary number of charged wires in Cartesian coordinates (x, y, z).
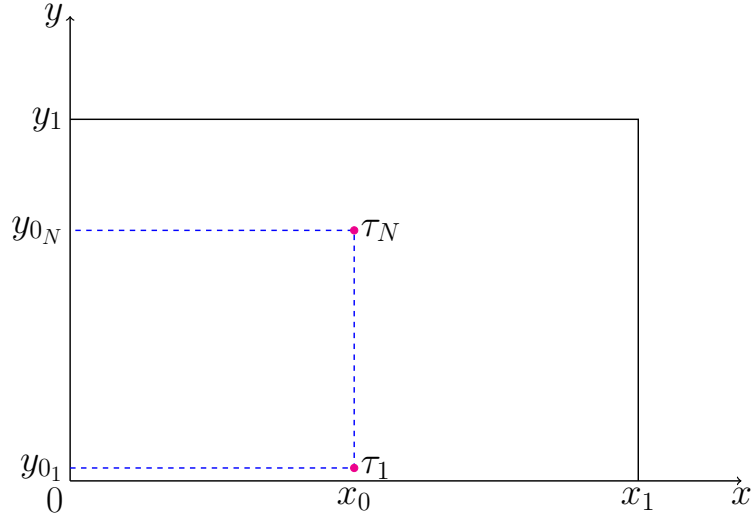

Fig. 14: A schematic representation of a two-dimensional system with N charged wires.

   Neglecting edge effects, we assume that the shape of the blade cathode does not vary with respect to the variable z. Thus, the potential distribution $V(x, y)$ depends on two coordinates (x, y), where $0 \leq x \leq x_1$ and $0 \leq y \leq y_1$. The cathode substrate is represented by the plane $y = 0$, the anode surface is defined by $y = y_1$, and the external boundaries of the system along the x variable are given by $x = 0$ and $x = x_1$.

   To account for the influence of the field cathode on the field distribution, we replace it with the influence of N charged wires with charge densities τ_i $(i = 1...N)$ located in the xOy plane at coordinates $x = x_0$ and $y = y_{0_i}$. Fig. 14 illustrates a schematic representation of the system with N charged wires in the two-dimensional (x, y) domain. We assume that the actual cathode surface coincides with the zero equipotential. The potential of the emitter substrate is zero, and the potential of the anode is U_0. The lateral boundaries of the system with respect to the x variable,

specifically at $x = 0$ and $x = x_1$, are described by the linear function:

$$V(0, y) = V(x_1, y) = U_0 \frac{y}{y_1}.$$

As in the previous paragraph, we assume that:

$$V(x, y) = U_0 \frac{y}{y_1} + U(x, y). \tag{II.1}$$

Mathematical model of a system with an arbitrary number of charged wires.

Let's assume that charges with densities ρ_i are uniformly distributed inside rectangles of small volume

$$x_0 - \varepsilon < x < x_0 + \varepsilon; \ \ y_{0_i} - \delta < y < y_{0_i} + \delta, i = 1...N.$$

then $\tau_i = \lim_{\varepsilon \to 0, \ \delta \to 0} 4\varepsilon\delta\rho_i$, and the problem reduces to solving the Poisson equation:

$$\triangle U(x, y) = \frac{\partial^2 U}{\partial x^2} + \frac{\partial^2 U}{\partial y^2} = -\frac{\rho(x, y)}{\varepsilon_0}, \tag{II.2}$$

where

$$\rho(x, y) = \begin{cases} \rho_i, & |x - x_0| < \varepsilon \text{ and } |y - y_{0_i}| < \delta, \\ 0, & |x - x_0| > \varepsilon \text{ or } |y - y_{0_i}| > \delta. \end{cases} \tag{II.3}$$

with homogeneous boundary conditions:

$$U(0, y) = 0, \ U(x, 0) = 0, \ U(x_1, y) = 0, \ U(x, y_1) = 0. \tag{II.4}$$

Computing the potential distribution of a system with an arbitrary number of charged wires

According to the formulas presented in the previous paragraph, we will seek the solution of the boundary problem II.2-II.4 in the form of a series:

$$U(x, y) = \sum_{n=1}^{\infty} \nu_n(x) \sin \frac{\pi n}{y_1} y.$$

The function $\nu(x)$ is a solution of a the differential equation:

$$\nu_n''(x) - \left(\frac{n\pi}{y_1}\right)^2 \nu_n(x) = -\frac{4\delta}{\varepsilon_0 y_1} \sum_{i=1}^{N} \phi_i(x) \sin \frac{n\pi y_{0_i}}{y_1},$$

where

$$\phi(x) = \begin{cases} \rho_i, & |x - x_0| < \varepsilon; \\ 0, & |x - x_0| > \varepsilon, \ i = 1 \div N. \end{cases}$$

The solution of the equation:

$$\nu_n(x) = C_1(x)\operatorname{ch}\frac{n\pi}{y_1}x + C_2(x)\operatorname{sh}\frac{n\pi}{y_1}x.$$

Taking into account the boundary condition II.4, we find that $C_1 = 0$. Therefore, for C_2, the following expression holds:

$$C_2 = \frac{2\sum_{i=1}^{N} \tau_i \sin \frac{n\pi}{y_1} y_{0_i} \sin \frac{n\pi}{y_1}(x_1 - x_0)}{n\pi\varepsilon_0 \sin \frac{n\pi}{y_1}x_1}.$$

Thus, the solution of the II.2-II.4:

for $x \le x_0$

$$U(x, y) = \sum_{n=1}^{\infty} \frac{2}{n\pi\varepsilon_0} \frac{\operatorname{sh}(\frac{\pi n}{y_1}(x_2 - x_0))}{\operatorname{sh}(\frac{\pi n}{y_1}x_2)} \operatorname{sh}(\frac{\pi n}{y_1}x) \sum_{i=1}^{N} \tau_i \sin(\frac{\pi n}{y_1}y_{0_i}) \sin(\frac{\pi n}{y_1}y), \quad \text{(II.5)}$$

for $x > x_0$

$$U(x, y) = \sum_{n=1}^{\infty} \frac{2}{n\pi\varepsilon_0} \frac{\operatorname{sh}(\frac{\pi n}{y_1}x_0)}{\operatorname{sh}(\frac{\pi n}{y_1}x_2)} \operatorname{sh}(\frac{\pi n}{y_1}(x_2 - x_0)) \sum_{i=1}^{N} \tau_i \sin(\frac{\pi n}{y_1}y_{0_i}) \sin(\frac{\pi n}{y_1}y). \quad \text{(II.6)}$$

Thus, formulas II.1, II.5, and II.6 provide the distribution of the potential $V(x, y)$ throughout the entire region of the studied system.

The results of the numerical calculation of the potential for the system with an arbitrary number of charged wires are as follows:

Based on the constructed solution, a program has been written, and based on its results, graphs of the potential distribution throughout the system have been generated.

All parameter values are given in dimensionless units.
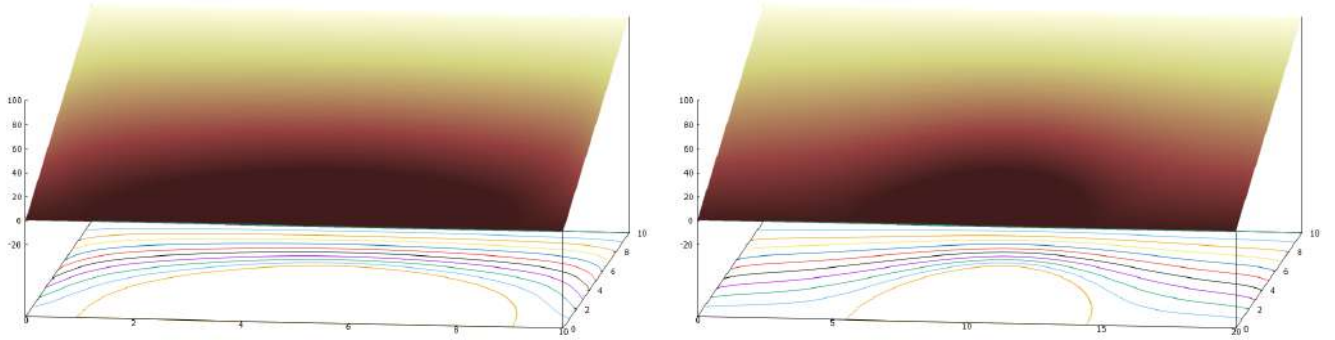
a) $x_1 = 10, x_0 = 5$ b) $x_1 = 20, x_0 = 10$

Fig. 15: $y_1 = 10, y_{0i} = 5(i = 1 \div N), \tau_i = -10, U_0 = 100, N = 10$.

It is worth noting that in figures 15 (a) and (b), when varying the boundaries of the system along the x variable, the shape of the cathode remains almost unchanged, as well as the length of its base. This fact reflects the adequacy of the constructed model. The simulation results yield the desired shape and size of the cathode, while changes in the system's dimensions primarily affect the potential distribution in the diode system but have a minor impact on the cathode's shape.
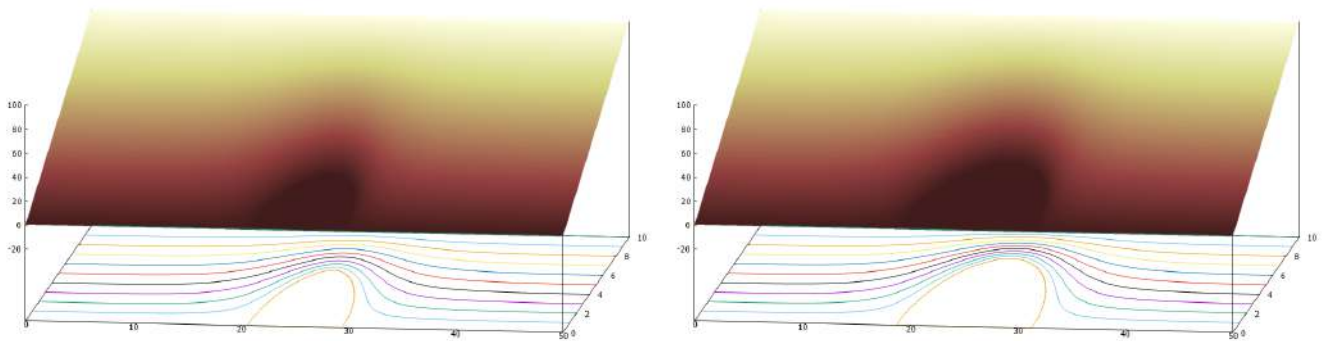
a) $\tau_i = -10, i = 1 \div N$ b) $\tau_i = -20, i = 1 \div N$

Fig. 16: $y_1 = 10, y_{0i} = 5(i = 1 \div N), x_1 = 50, x_0 = 25, N = 10$.

Let's consider figures 16. Fig. (a) and (b) differ in the value of charge density τ. The graphs show that when the value of τ is doubled, the length of the cathode's base increases.

II.3 Modeling a diode system with an arbitrary number of charged wires, considering the influence of the dielectric layer on the substrate.

The physical problem formulation involves calculating the potential of a system consisting of charged wires and a dielectric layer on a substrate.

The two-dimensional problem of calculating an emission system is solved in the Cartesian coordinate system (x, y). The anode is a plane parallel to the substrate. The internal region of the system is filled with two different dielectrics [73]. The influence of the field apex is replaced by the influence of a system of N charged wires with linear charge densities τ_i, where the wire coordinates are (x_0, y_{0i}) for $i = 1...N$. The boundary between the dielectrics with permittivities ε_1 and ε_2 is represented by the plane $y = y_1$. The field cathode is located on the flat substrate at $y = 0$. The outer boundaries of the considered system are defined by $x = 0$, $x = x_1$, and $y = y_2$ with first-type boundary conditions specified. The potential of the substrate at $y = 0$ is zero. The cathode surface coincides with the surface of zero equipotential.
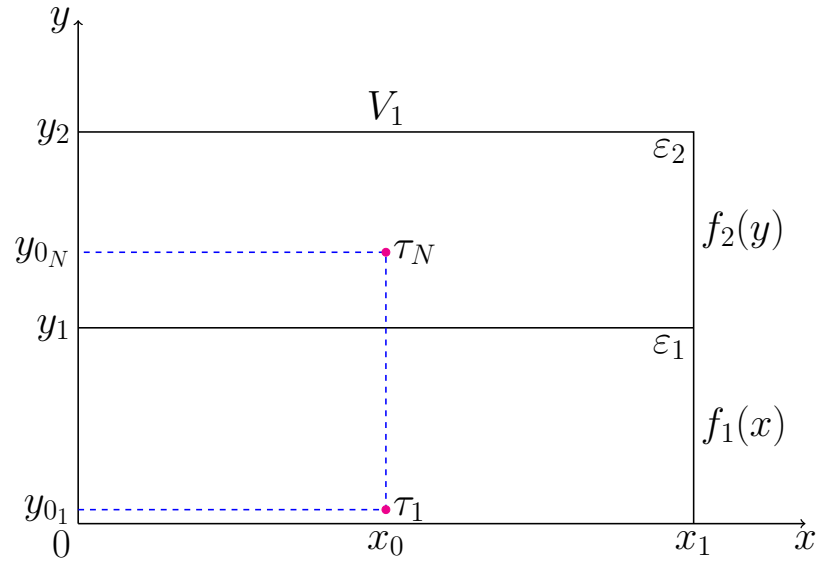

Fig. 17: Schematic image of the system on a plane

Mathematical model

The distribution of the electrostatic potential $U(x, y)$ in the Cartesian coordinate system satisfies the Laplace's equation:

$$\frac{\partial U^2}{\partial x^2} + \frac{\partial U^2}{\partial y^2} = 0.$$

$$U(x, y)|_\Omega = 0, \tag{II.1}$$

where Ω - a cathode surface.

$$U(0, y) = U(x_1, y) = f(y),$$

$$U(x, y_2) = V_1, \tag{II.2}$$

$$U(x, 0) = 0,$$

$$f(y) = \begin{cases} f_1(y) = V_1 \dfrac{y\varepsilon_2}{y_2\varepsilon_1 + y_1(\varepsilon_2 - \varepsilon_1)}, & 0 \leqslant y \leqslant y_1, \\ f_2(y) = V_1 \dfrac{y\varepsilon_1 + y_1(\varepsilon_2 - \varepsilon_1)}{y_2\varepsilon_1 + y_1(\varepsilon_2 - \varepsilon_1)}, & y_1 \leqslant y \leqslant y_2. \end{cases} \tag{II.3}$$

Due to the fact that the influence of the cathode is replaced by the influence of the charged wires, the original boundary problem II.1-II.3 is reduced to solving the Poisson's equation with the corresponding boundary condition:

$$\triangle U(x, y) = \frac{\partial^2 U}{\partial x^2} + \frac{\partial^2 U}{\partial y^2} = -\frac{\rho(x, y)}{\varepsilon_0}, \tag{II.4}$$

где

$$\rho(x, y) = \begin{cases} \rho_i, & |x - x_0| < \varepsilon \text{ и } |y - y_{0_i}| < \delta_i, \\ 0, & |x - x_0| > \varepsilon \text{ или } |y - y_{0_i}| > \delta_i. \\ & i = 1 \div N, \tau_i = \lim_{\varepsilon \to 0, \; \delta \to 0} 4\varepsilon\delta\rho_i. \end{cases} \tag{II.5}$$

The computation of the potential distribution in a system with charged wires and dielectrics

To solve the problem II.4–II.5, the entire internal region of the system is divided into two subdomains along the boundary between the dielectrics $y = y_1$.

$$U(x, y) = \begin{cases} U_1(x, y), & 0 \leqslant y_{0i} \leqslant y_1, \; 1 \leq i \leq j, \\ U_2(x, y), & y_1 \leqslant y_{0i} \leqslant y_2, \; j + 1 \leq i \leq N. \end{cases} \tag{II.6}$$

The potential distribution II.6 can be expressed according to the formulas in §II.2 as follows [20]:

$$U_1(x, y) = f_1(y) + \sum_{m=1}^{\infty} A_m \frac{\operatorname{sh} \alpha_m y}{\operatorname{sh} \alpha_m y_1} \sin \alpha_m x + \sum_{i=1}^{j} \frac{2\tau_i}{\pi \varepsilon_0} \times$$

$$\times \begin{cases} \displaystyle\sum_{n=1}^{\infty} \frac{\operatorname{sh} \beta_n(x_1 - x_0) \operatorname{sh} \beta_n x}{n \operatorname{sh} \beta_n x_1} \sin \beta_n y_{0_i} \sin \beta_n y, \\ \\ \qquad 0 \leqslant x \leqslant x_0; \\ \\ \displaystyle\sum_{n=1}^{\infty} \frac{\operatorname{sh} \beta_n(x_1 - x) \operatorname{sh} \beta_n x_0}{n \operatorname{sh} \beta_n x_1} \sin \beta_n y_{0_i} \sin \beta_n y, \\ \\ \qquad x_0 \leqslant x \leqslant x_1; \end{cases} \tag{II.7}$$

$$U_2(x, y) = f_2(y) + \sum_{m=1}^{\infty} A_m \frac{\operatorname{sh} \alpha_m(y_2 - y)}{\operatorname{sh} \alpha_m(y_2 - y_1)} \sin \alpha_m x + \sum_{i=j+1}^{N} \frac{2\tau_i}{\pi \varepsilon_0} \times$$

$$\times \begin{cases} \displaystyle\sum_{k=1}^{\infty} \frac{\operatorname{sh} \gamma_k(x_1 - x_0) \operatorname{sh} \gamma_k x}{k \operatorname{sh} \gamma_k x_1} \sin \gamma_k(y_{0_i} - y_1) \sin \gamma_k(y - y_1), \\ \\ \qquad 0 \leqslant x \leqslant x_0; \\ \\ \displaystyle\sum_{k=1}^{\infty} \frac{\operatorname{sh} \gamma_k(x_1 - x) \operatorname{sh} \gamma_k x_0}{k \operatorname{sh} \gamma_k x_1} \sin \gamma_k(y_{0_i} - y_1) \sin \gamma_k(y - y_1), \\ \\ \qquad x_0 \leqslant x \leqslant x_1; \end{cases} \tag{II.8}$$

where

$$\alpha_m = \frac{\pi m}{x_1}, \quad \beta_n = \frac{\pi n}{y_1}, \quad \gamma_k = \frac{\pi k}{y_2 - y_1}.$$

Thus, the expansions II.7-II.8 ensure the continuity of the potential $U(x, y)$ at the boundary between the dielectrics $y = y_1$ and satisfy the boundary conditions II.2–II.3.

The condition for continuity of the normal component of the electric displacement vector at the boundary between the dielectrics is given by:

$$\left. \frac{\partial U_1}{\partial y} \right|_{y=y_1} = \left. \frac{\partial U_2}{\partial y} \right|_{y=y_1}$$

leads to the computation of the unknown coefficients A_m in the series II.7 and II.8 in an explicit form:

$$A_m = \frac{4}{\varepsilon_0 \pi m(\varepsilon_1 \operatorname{cth}(\alpha_m y_1) + \varepsilon_2 \operatorname{cth}(\alpha_m(y_2 - y_1)))} \times$$

$$\times \left(\frac{\varepsilon_1}{y_1} \left(\sum_{i=1}^{j} \sum_{n=1}^{\infty} \tau_i (-1)^n \sin(\beta_n y_{0_i}) \frac{\beta_n}{\beta_n^2 + \alpha_m^2} \sin(\alpha_m x_0) \right) + \right.$$

$$\left. + \frac{\varepsilon_2}{(y_2 - y_1)} \left(\sum_{i=j+1}^{N} \sum_{k=1}^{\infty} \tau_i \sin(\gamma_k(y_{0_i} - y_1)) \frac{\gamma_k}{\gamma_k^2 + \alpha_m^2} \sin(\alpha_m x_0) \right) \right).$$

(II.9)

Therefore, formulas II.6-II.9 provide the distribution of the potential $U(x, y)$ throughout the entire region of the investigated system.

The results of the numerical calculation of the potential in the system with charged wires and dielectrics

It should be noted that the obtained images from the simulation correspond to the expected results. As the ratio of the dielectric permittivities $\frac{\varepsilon_1}{\varepsilon_2}$ increases, the shape of the cathode changes, as shown in Fig. 18.

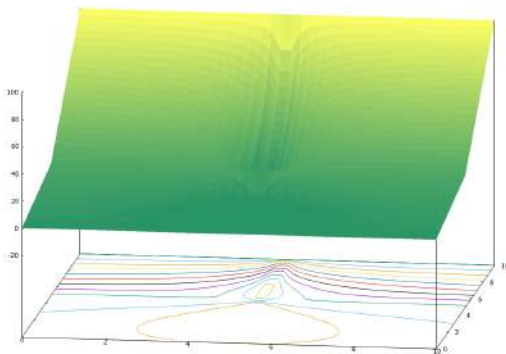All parameter values are given in dimensionless units.
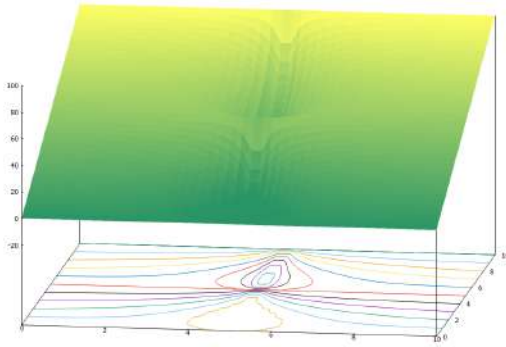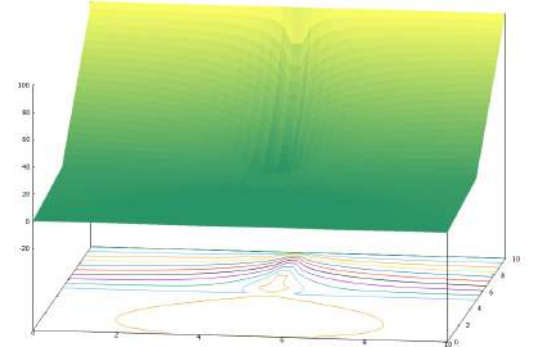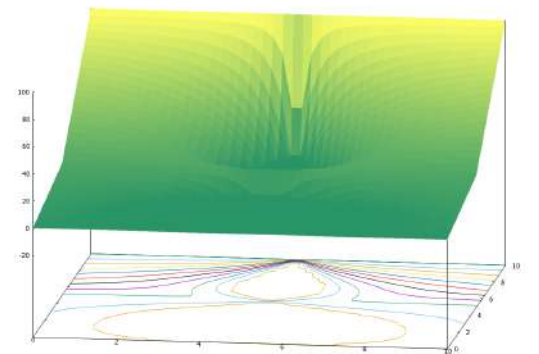

a) $\dfrac{\varepsilon_1}{\varepsilon_2} = 1$ b) $\dfrac{\varepsilon_1}{\varepsilon_2} = 10$

Fig. 18: $y_1 = 5,\ y_2 = 10,\ y_{0_i} = [0, 5],\ N = 50,\ x_1 = 10,\ x_0 = 5,\ \tau = -100,\ V_1 = 100$

When increasing the value of τ, it can be observed that in Fig. 19, the apex becomes larger relative to the dimensions of the system.

a) $\tau = -100$ b) $\tau = -300$

Fig. 19: $y_1 = 5,\ y_2 = 10,\ y_{0_i} = [0, 5],\ N = 50, x_1 = 10, x_0 = 5, \dfrac{\varepsilon_1}{\varepsilon_2} = 5,\ V_1 = 100$

II.4 Modeling a diode emission system with dielectric layers on the lateral surfaces

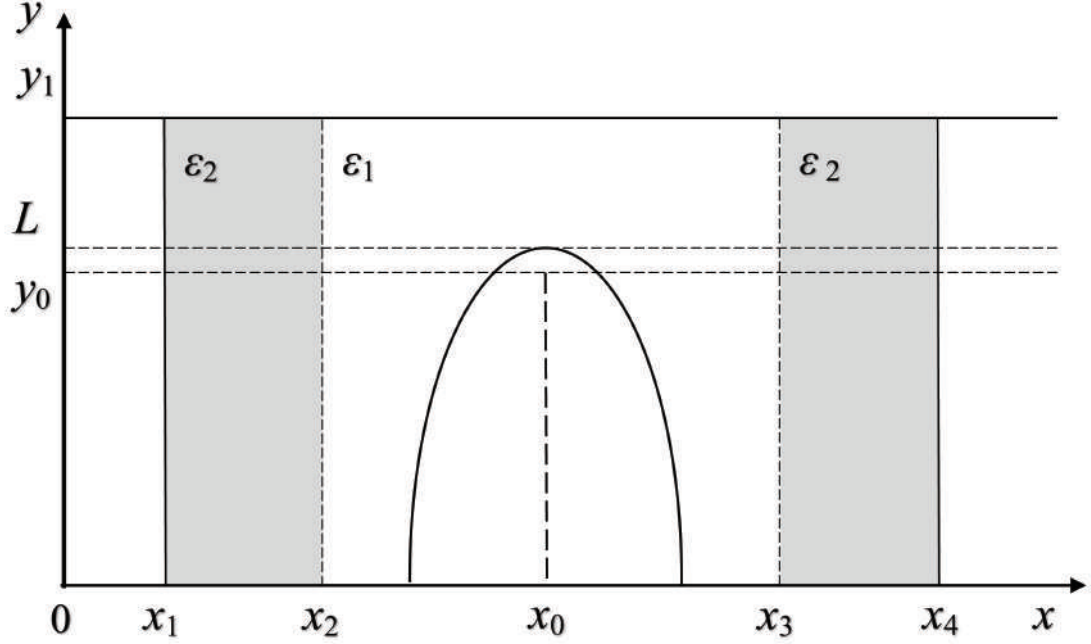### Physical problem formulation for potential calculation

Fig. 20: Schematic picture of the diode system.

We replace the influence of the field cathode on the potential distribution with the influence of a charged plane with charge density τ [14, 16]. Fig. 20 presents a schematic representation of the diode emission system.

Problem parameters:

Domain of the diode system— $(x_1 \leq x \leq x_4, 0 \leq y \leq y_1)$;

Boundary between dielectrics with permittivities ε_2 and ε_1— $x = x_2, 0 \leq y \leq y_1$;

Boundary between dielectrics with permittivities ε_1 and ε_2— $x = x_3, 0 \leq y \leq y_1$;

Charged plane surface— $x = x_0 = (x_2 + x_3)/2, 0 \leq y \leq y_0$;

Substrate surface— $y = 0$; Anode surface— $y = y_1$;

Substrate potential— $U(x,0) = 0, x_1 \leq x \leq x_4$; Anode potential— $U(x, y_1) = U_0, x_1 \leq x \leq x_4$;

Potential distribution on the lateral boundaries of the domain—

$$U(x_1, y) = U(x_4, y) = U_0 \frac{y}{y_1}, \ 0 \le y \le y_1.$$

Mathematical model of the diode system with a charged plane and dielectric layers

The distribution of the electrostatic potential $U(x, y)$ satisfies the Poisson's equation:

$$\triangle U(x, y) = \frac{\partial^2 U}{\partial x^2} + \frac{\partial^2 U}{\partial y^2} = -\frac{\rho(x, y)}{\varepsilon_0}, \tag{II.1}$$

and boundary conditions:

$$U(x_1, y) = U(x_4, y) = U_0 \frac{y}{y_1},$$
$$U(x, y_1) = U_0, \quad U(x, 0) = 0, \tag{II.2}$$

$$\rho(x, y) = \begin{cases} \rho, & |x - x_0| < \varepsilon \text{ and } 0 \le y \le y_0; \\ 0, & |x - x_0| > \varepsilon \text{ or } y_0 < y \le y_1, \end{cases} \tag{II.3}$$

$$\tau = \lim_{\varepsilon \to 0} 2\varepsilon \, y_0 \, \rho. \tag{II.4}$$

Computation of the potential distribution

We represent the function $U(x, y)$ as the sum of the solution $U_1(x, y)$ and a linear term $U_0 \frac{y}{y_0}$. To solve the boundary problem II.1-II.4, we divide the entire domain of the modeled system ($x_1 \le x \le x_4$, $0 \le y \le y_1$) into three parts.

$$U(x, y) = U_0 y/y_1 + U_1(x, y),$$

$$U_1(x, y) = \begin{cases} U_1^I(x, y), & x_1 \le x \le x_2; \\ U_1^{II}(x, y), & x_2 \le x \le x_3; \\ U_1^{III}(x, y), & x_3 \le x \le x_4. \end{cases}$$

Then, the functions $U_1^I(x, y)$, $U_1^{II}(x, y)$, $U_1^{III}(x, y)$ can be represented as expansions using eigenfunctions:

$$U_1^I(x, y) = \sum_{n=1}^{\infty} a_n \frac{\text{sh}(\lambda_n(x - x_1))}{\text{sh}(\lambda_n(x_2 - x_1))} \sin \lambda_n y, \quad x_1 \le x \le x_2; \tag{II.5}$$

$$U_1^{II}(x, y) = \sum_{n=1}^{\infty} \left(a_n \frac{\mathrm{sh}(\lambda_n(x_3 - x))}{\mathrm{sh}(\lambda_n(x_3 - x_2))} + \right.$$
$$\left. + b_n \frac{\mathrm{sh}(\lambda_n(x - x_2))}{\mathrm{sh}(\lambda_n(x_3 - x_2))} \right) \sin \lambda_n y + U_\tau(x, y), \quad x_2 \le x \le x_2; \tag{II.6}$$

$$U_1^{III}(x, y) = \sum_{n=1}^{\infty} b_n \frac{\mathrm{sh}(\lambda_n(x_4 - x))}{\mathrm{sh}(\lambda_n(x_4 - x_3))} \sin \lambda_n y, \quad x_3 \le x \le x_4, \tag{II.7}$$

where $\lambda_n = \dfrac{\pi n}{y_1}$.

The function $U_\tau(x, y)$ [13]:

$$U_\tau(x, y) = \begin{cases} \dfrac{\tau}{y_0} \sum\limits_{m=1}^{\infty} \dfrac{2 \sin \alpha_m(x_0 - x_2)}{\alpha_m \, \pi m \varepsilon_0} \left[1 - \dfrac{\mathrm{sh}(\alpha_m(y_1 - y))}{\mathrm{sh}(\alpha_m y_1)} - \right. \\ \qquad \left. - \dfrac{\mathrm{sh}(\alpha_m y) \, \mathrm{ch}(\alpha_m(y_1 - y_0))}{\mathrm{sh}(\alpha_m y_1)} \right] \times \\ \qquad \times \sin \alpha_m(x - x_2), \quad 0 \le y \le y_0; \\[2ex] \dfrac{\tau}{y_0} \sum\limits_{m=1}^{\infty} \dfrac{2 \sin \alpha_m(x_0 - x_2)}{\alpha_m \, \pi m \varepsilon_0} \dfrac{\mathrm{sh}(\alpha_m(y_1 - y))}{\mathrm{sh}(\alpha_m y_1)} \times \\ \qquad \times (\mathrm{ch}(\alpha_m y_0) - 1) \sin \alpha_m(x - x_2), \quad y_0 \le y \le y_1, \end{cases} \tag{II.8}$$

where $\alpha_m = \dfrac{\pi m}{x_3 - x_2}$, τ - constant charge density on a plane $x = x_0$, $0 < y < y_0$.

The potential distribution $U(x, y)$ is a continuous function on the boundaries of the domain separation $x = x_2$ and $x = x_3$ for $0 \le y \le y_0$ according to formulas II.5-II.8.

Determination of the expansion coefficients from the interface boundary conditions

The coefficients a_n, b_n in the expansions II.5–II.7 can be found from the continuity conditions of the electric displacement vector at $x = x_2$ and $x = x_3$.

$$\varepsilon_2 \frac{\partial U_1^I(x,y)}{\partial x}\bigg|_{x=x_2} = \varepsilon_1 \frac{\partial U_1^{II}(x,y)}{\partial x}\bigg|_{x=x_2},$$

$$\varepsilon_1 \frac{\partial U_1^{II}(x,y)}{\partial x}\bigg|_{x=x_3} = \varepsilon_2 \frac{\partial U_1^{III}(x,y)}{\partial x}\bigg|_{x=x_3}.$$

The interface boundary conditions and the orthogonality of the eigenfunction system in the expansions II.5–II.8 lead to explicit expressions for the coefficients a_n and b_n:

$$a_n = A_n \frac{\delta_n + \gamma_n}{\beta_n \delta_n - \gamma_n^2}, \qquad b_n = A_n \frac{\beta_n + \gamma_n}{\beta_n \delta_n - \gamma_n^2}, \qquad (\text{II.9})$$

where

$$A_n = \tau \frac{4(1 - \cos \lambda_n y_0)}{\varepsilon_0\, y_0\, y_1\, \lambda_n^2} \sum_{m=1,3,5,\dots}^{\infty} \frac{\sin \alpha_m (x_0 - x_2)}{\pi m} \frac{\alpha_m^2}{\alpha_m^2 + \lambda_n^2},$$

$$\beta_n = \frac{\varepsilon_2}{\varepsilon_1} \operatorname{cth}(\lambda_n(x_2 - x_1)) + \operatorname{cth}(\lambda_n(x_3 - x_2)),$$

$$\gamma_n = \frac{1}{\operatorname{sh}(\lambda_n(x_3 - x_2))},$$

$$\delta_n = \frac{\varepsilon_2}{\varepsilon_1} \operatorname{cth}(\lambda_n(x_4 - x_3)) + \operatorname{cth}(\lambda_n(x_3 - x_2)).$$

The linear charge density τ is computed based on the condition:

$$U(x_0, L) = 0,$$

in order for the zero equipotential to pass through the vertex of the cathode ($x = x_0$, $y = L$), the formulas II.5–II.9 define the potential distribution in the entire space of the system under consideration.

Numerical calculation results of the potential in the diode system with dielectric layers

Fig. 21 and 22 show the plots of the potential distribution and equipotential lines for different values of the ratio of dielectric permittivities $\frac{\varepsilon_2}{\varepsilon_1}$, considering the given geometric parameters of the system and calculated values of τ, with the condition that the zero equipotential passes through the vertex of the cathode (x_0, L) [21].
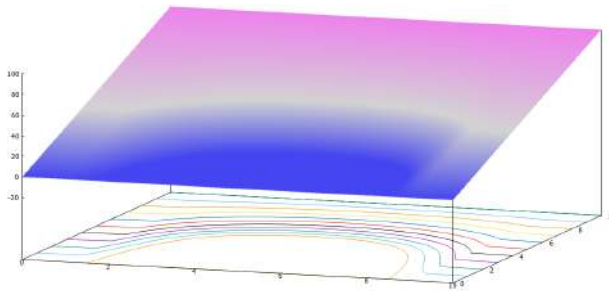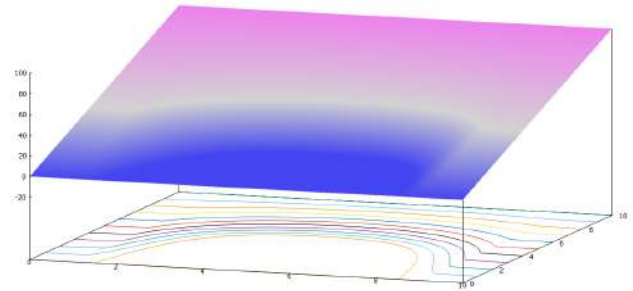
All parameter values are given in dimensionless units.
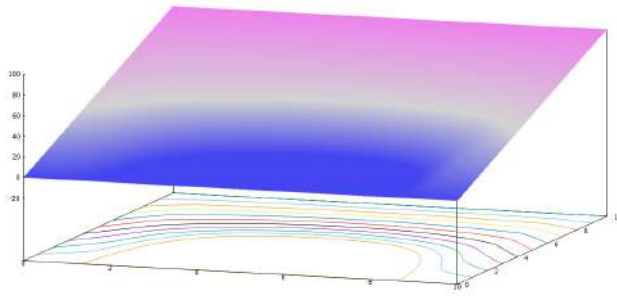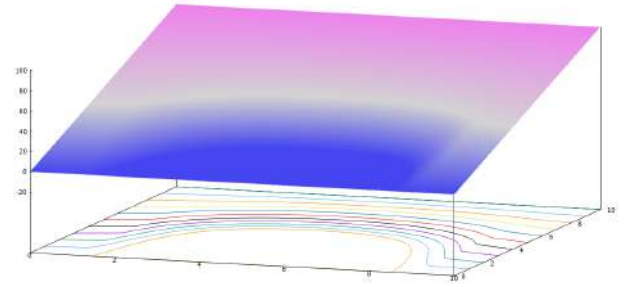
$$\tau = -417.7326, \ \frac{\varepsilon_2}{\varepsilon_1} = 1 \qquad\qquad \tau = -476.5427, \ \frac{\varepsilon_2}{\varepsilon_1} = 5$$

$$\tau = -492.7033, \ \frac{\varepsilon_2}{\varepsilon_1} = 20 \qquad\qquad \tau = -494.6468, \ \frac{\varepsilon_2}{\varepsilon_1} = 50$$

Fig. 21: $y_0 = 5, \ x_1 = 0, \ x_2 = 1, \ x_3 = 9, \ x_4 = 10, \ y_1 = 10, \ U_1 = 100,$ $L = 5,00005, U_0 = 100$.

It should be noted that as the ratio of $\frac{\varepsilon_2}{\varepsilon_1}$ increases, the value of the charge density τ also increases. The influence of the dielectric layers on the obtained distribution of the electrostatic potential is shown in Fig. 21.

Fig. 22 demonstrates the effect of changing the boundaries of the dielectric layers in the system. The boundaries of the dielectric layers are defined by the parameters x_2 and x_3. Thus, it is possible to change the shape of the cathode to the desired form not only by adjusting the ratio of dielectric permittivities but also by changing the arrangement of the dielectric layers within the considered system.

$\tau = -164.8959, \ \frac{\varepsilon_2}{\varepsilon_1} = 1;$

$\tau = -689.0760, \ \frac{\varepsilon_2}{\varepsilon_1} = 5$
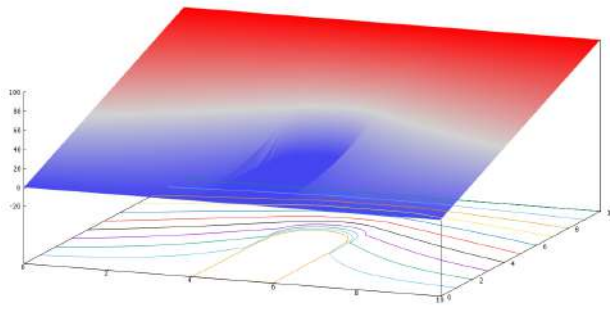
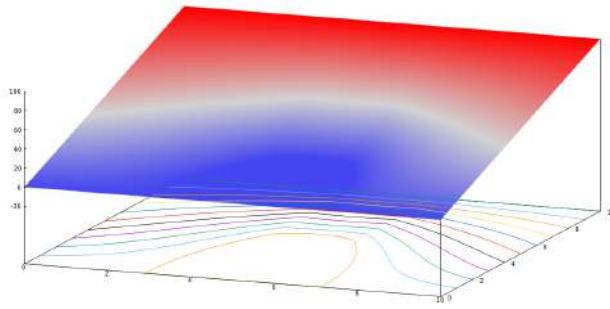$\tau = -2654.7514, \ \frac{\varepsilon_2}{\varepsilon_1} = 20$

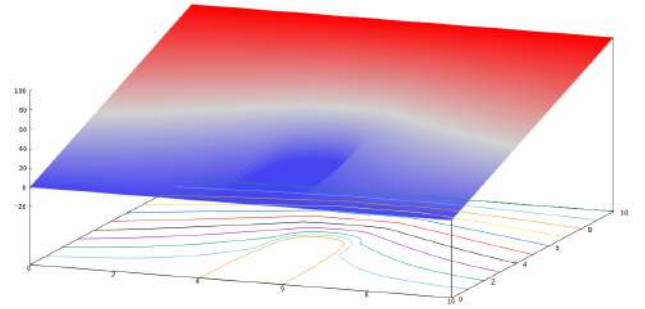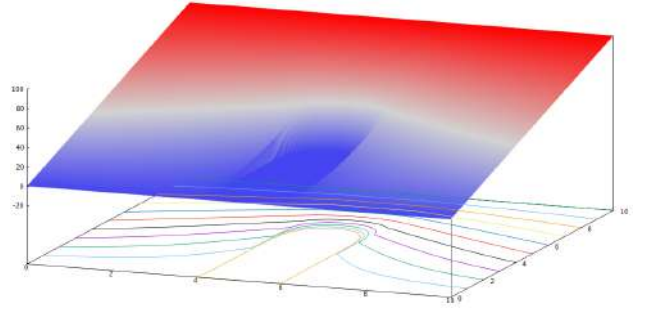$\tau = -3965.2016, \ \frac{\varepsilon_2}{\varepsilon_1} = 30$

Fig. 22: Parameters: $y_0 = 5, \ x_1 = 0, \ x_4 = 10, \ x_2 = 4, \ x_3 = 6, \ y_1 = 10,$ $U_1 = 100, \ L = 5,00005, U_0 = 100.$

II.5 Calculation of the electric field intensity

The electric field intensity is a crucial characteristic of a field emission system as it allows for the calculation of current density, total current, and so on [21].

In this section, the field intensity is calculated not in the entire system region, as the focus is on the values of intensity at the cathode apex and in its small vicinity δ:

$$L = y_0 + \delta.$$

The values of field intensity for an axisymmetric system with a single field emitter are presented in Fig. 23:
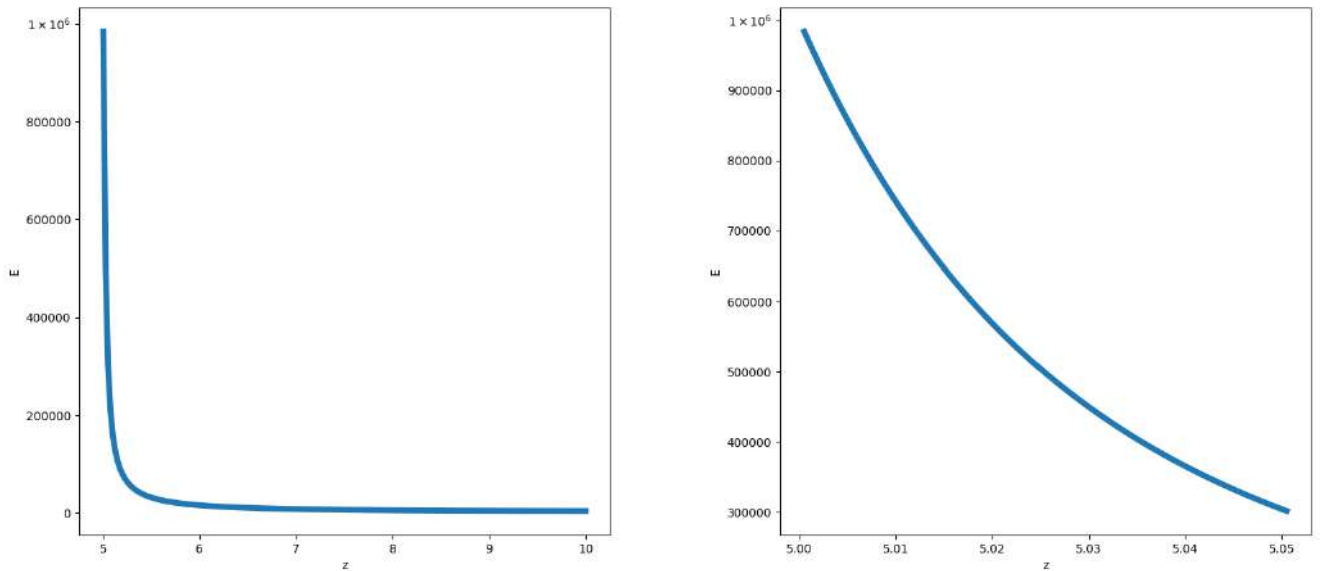
Fig. 23: Parameters: $r_1 = 10,\ z_1 = 10,\ r_q = 5,\ z_q = 5,\ U_0 = U_1 = 100,$
$\tau = -100,\ L = 0.0005$

The values of the field intensity for the case of a periodic system of emitters modeled by a charged plane in Cartesian coordinates are presented in Fig. **??**. It should be noted that the maximum value of the field intensity for a flat system modeled by a charged plane is lower by a factor of 10^3 compared to the values for an axisymmetric system in cylindrical coordinates.

Fig. 24: Parameters: $x_1 = 10$, $y_1 = 10$, $x_0 = 5$, $y_0 = 5$, $V_0 = V_1 = 100$, $\tau = -100$, $L = 0.0005$

In Fig. 24, a periodic system of emitters containing dielectric layers is presented. From these graphs, it can be observed that the maximum field intensity near the emitter tip is relatively small, reaching only 12×10^3. However, this value is higher than that for the non-periodic system. It is important to note that these field intensity values are expected to decrease when creating a real device due to the mutual shielding effect of the emitters on each other [72].

The system with charged wires, depicted in the figure, exhibits much higher values of electric field intensity near the cathode apex (up to 4×10^4)than periodic system due to the lack of the mutual shielding effect (fig.25).
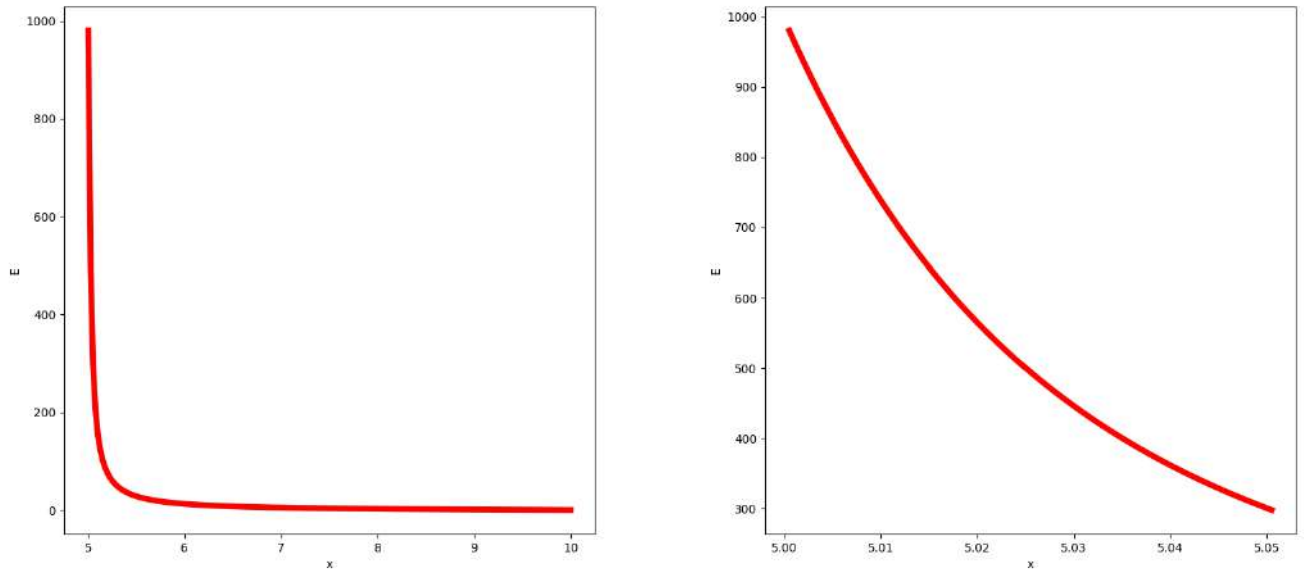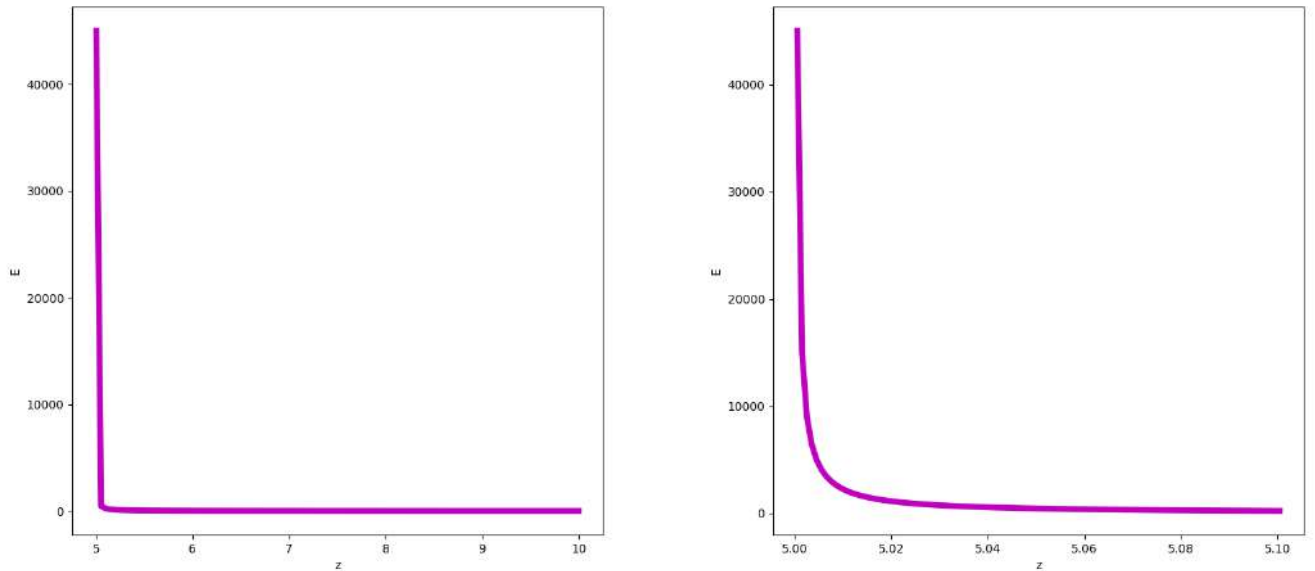

Fig. 25: Parameters: $x_1 = 10$, $y_1 = 10$, $x_0 = 5$, $y_0 = 5$, $V_0 = V_1 = 100$, $\tau = -100$, $L = 0.0005$

The main results of this chapter have been published in the papers [5, 12, 13, 14].

III Modeling of planar symmetric periodic blade-shaped field emitter systems

The following sources were used in writing Chapter III: [6], [97].

Periodic blade-shaped field emitter systems are widely used in electron vacuum devices for various purposes [26, 45, 64, 71, 77, 83, 87, 88, 106, 108, 112]. It should be noted that there are significantly fewer works dedicated to the modeling of such emission systems compared to experimental studies on this topic [2, 42, 53].

In this chapter, a method for modeling planar symmetric periodic blade-shaped field emitter systems on a flat substrate using charged planes in Cartesian coordinates is developed. The anode is a plane parallel to the substrate. The distribution of the electrostatic potential is analytically determined for periodic emitter systems with and without dielectric layers in the system region. It is represented as series expansions in eigenfunctions, and the coefficients of the series are explicitly calculated.

III.1 Modeling of a periodic system of field emitters using charged planes

Physical formulation of the potential calculation problem for a periodic system of charged planes

In this section, a periodic system of blade-shaped field emitters on a flat substrate is modeled. The anode is a plane parallel to the substrate in the Cartesian coordinate system (x, y). Due to the periodicity of the system, it is sufficient to consider one elementary cell with boundaries $0 \leq x \leq x_1$ (see Fig. 26). The influence of each field emitter on the potential distribution U(x, y) in the elementary cell is replaced by the influence of a charged plane with charge density τ and coordinates $x = x_1/2$, $0 \leq y \leq y_0$ [62, 72, 92].
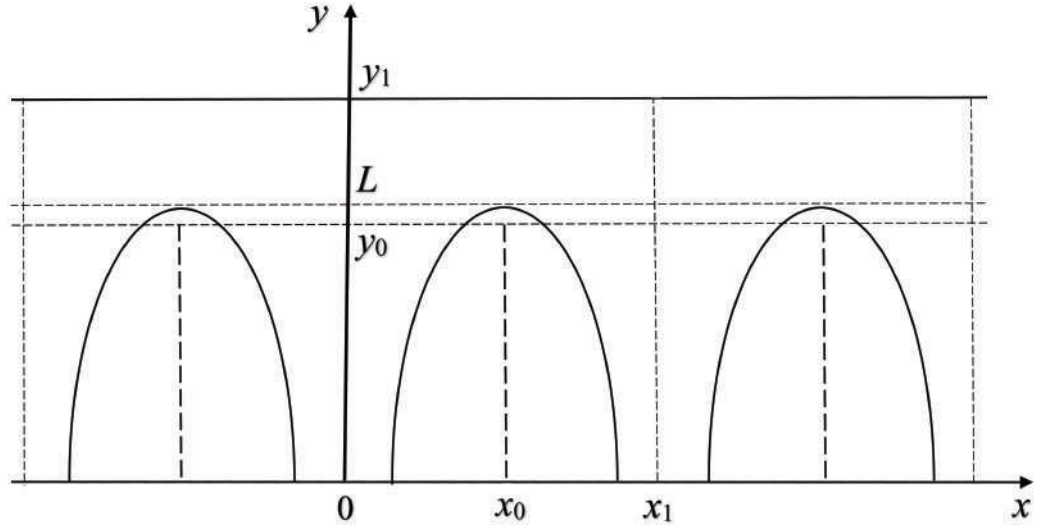
Fig. 26: Schematic image of the system on a plane.

Parameters:

$y = 0$ - Cathode substrate plane, $y = y_1$ - Anode plane, $x = 0, x = x_1$ - Boundaries of one cell of the system in the x-direction, L - Height of the field emitter, $U(x, 0) = 0$ - Potential of the substrate, $U(x, y_1) = U_0$ - Potential of the anode.

Mathematical model of the periodic system of charged planes

To compute the potential distribution $U(x, y)$ in the entire domain of one cell ($0 \leq x \leq x_1$, $0 \leq y \leq y_1$), it is necessary to solve the boundary value problem for the Poisson equation:

$$
\begin{cases}
\dfrac{\partial^2 U(x, y)}{\partial x^2} + \dfrac{\partial^2 U(x, y)}{\partial y^2} = -\dfrac{1}{\varepsilon_0}\rho(x, y), \\[2mm]
U(x, 0) = 0, \quad 0 \leq x \leq x_1, \\[2mm]
U(x, y_1) = U_0, \quad 0 \leq x \leq x_1, \\[2mm]
\dfrac{\partial U(x, y)}{\partial x}\bigg|_{x = 0} = 0, \quad 0 \leq y \leq y_1, \\[2mm]
\dfrac{\partial U(x, y)}{\partial x}\bigg|_{x = x_1} = 0, \quad 0 \leq y \leq y_1.
\end{cases}
\tag{III.1}
$$

We assume that a charged wire with a linear charge density $\tau(y)$ creates a spatial

distribution of charge $\rho(x, y)$ within a small volume rectangle ($|x - x_0| < \delta$, $0 \leq y \leq y_0$) [29, 62]:

$$\rho(x, y) = \begin{cases} \rho(y), & |x - x_0| < \delta \text{ and } 0 \leq y \leq y_0, \\ 0, & |x - x_0| > \delta \text{ or } y_0 \leq y \leq y_1, \end{cases} \tag{III.2}$$

so

$$\tau(y) = \lim_{\delta \to 0} 2\delta \, y_0 \, \rho(y). \tag{III.3}$$

Compution the potential distribution in a periodic system of charged planes

Let us express the solution to the boundary problem III.1-III.2 in the form of an expansion:

$$U(x, y) = U_0 \, y/y_1 + U_1(x, y). \tag{III.4}$$

To determine the function $U_1(x, y)$ from the equation III.4, we need to solve the Poisson's equation with homogeneous boundary conditions of the first kind with respect to the variable y and homogeneous boundary conditions of the second kind with respect to the variable x:

$$\begin{cases} \dfrac{\partial^2 U_1(x, y)}{\partial x^2} + \dfrac{\partial^2 U_1(x, y)}{\partial y^2} = -\dfrac{1}{\varepsilon_0}\rho(x, y), \\[2mm] U_1(x, 0) = 0, \quad 0 \leq x \leq x_1, \\[2mm] U_1(x, y_1) = 0, \quad 0 \leq x \leq x_1, \\[2mm] \dfrac{\partial U_1(x, y)}{\partial x}\bigg|_{x = 0} = 0, \quad 0 \leq y \leq y_1, \\[2mm] \dfrac{\partial U_1(x, y)}{\partial x}\bigg|_{x = x_1} = 0, \quad 0 \leq y \leq y_1. \end{cases} \tag{III.5}$$

By solving equation III.5, we can obtain $U_1(x, y)$ in the form of a series:

$$U_1(x, y) = \sum_{n=0}^{\infty} v_n(y) \cos(\alpha_n x), \quad \alpha_n = \frac{\pi n}{x_1}, \tag{III.6}$$

where the function $\nu_n(y)$ satisfies the diffirential equation:

$$\nu_n''(y) - \alpha_n^2 \nu_n(y) = \frac{\gamma_n}{x_1}\phi_n(y), \quad \gamma_n = \begin{cases} 1, n = 0 \\ 2, n > 0 \end{cases}$$

$$\nu_n(y) = -\frac{1}{\varepsilon_0}\int\limits_0^{x_1} \rho(x,y)\cos\alpha_n x\, dx.$$

If $n = 0$

$$v_0(y) = -\frac{y_1 - y}{x_1\, y_1}\int\limits_0^y \eta\phi_0(\eta)\, d\eta + \frac{y}{x_1\, y_1}\int\limits_y^{y_0} (\eta - y_1)\phi_0(\eta)\, d\eta, \quad 0 \le y \le y_0,$$

$$v_0(y) = -\frac{y_1 - y}{x_1\, y_1}\int\limits_0^{y_0} \eta\phi_0(\eta)\, d\eta, \qquad\qquad\qquad y_0 < y \le y_1,$$

(III.7)

If $n > 0$

$$v_n(y) = -\frac{2}{\pi n}\frac{1}{\operatorname{sh}\alpha_n y_1}\left[\int\limits_0^y \phi_n(\eta)\operatorname{sh}\alpha_n\eta\operatorname{sh}\alpha_n(y_1 - y)\, d\eta - \right.$$

$$\left. -\int\limits_y^{y_0} \phi_n(\eta)\operatorname{sh}\alpha_n(\eta - y_1)\operatorname{sh}\alpha_n y\, d\eta\right], \qquad 0 \le y \le y_0,$$

(III.8)

$$v_n(y) = -\frac{2}{\pi n}\frac{1}{\operatorname{sh}\alpha_n y_1}[\int\limits_0^{y_0} \phi_n(\eta)\operatorname{sh}\alpha_n\eta\operatorname{sh}\alpha_n(y_1 - y)\, d\eta, \qquad y_0 < y \le y_1.$$

Thus, equations III.5, III.6, III.7, and III.8 determine the distribution of the potential $U(x,y)$ at any point in the studied system.

In this section, based on the obtained analytical formulas for the potential distribution III.4-III.8, we present graphs and equipotential line patterns for the elementary cell of the periodic multi-emitter system.

All parameter values are given in dimensionless units.
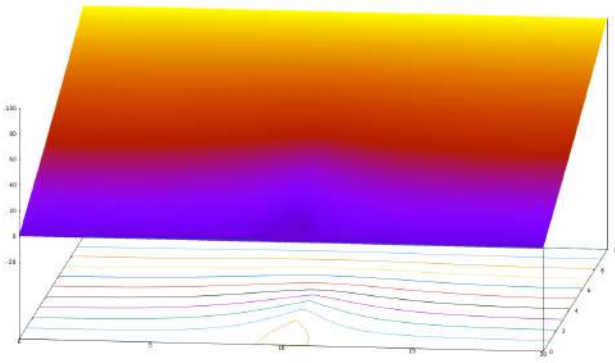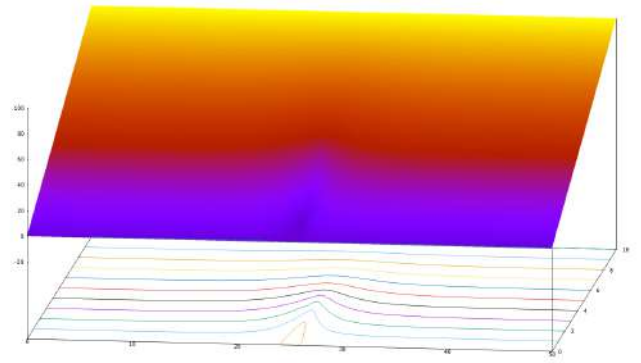
a) $x_1 = 20,\ x_0 = 10.$ b) $x_1 = 50,\ x_0 = 25.$

Fig. 27: $y_1 = 10,\ y_0 = 5\,\tau = -20, U_0 = 100.$
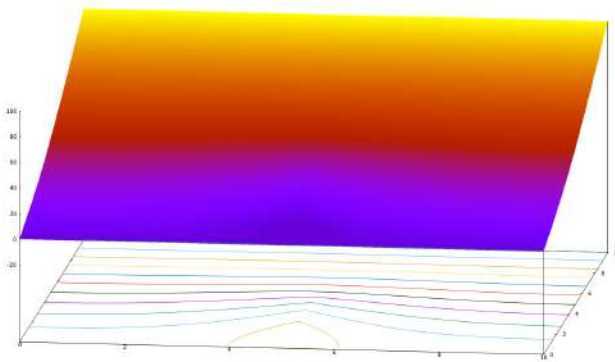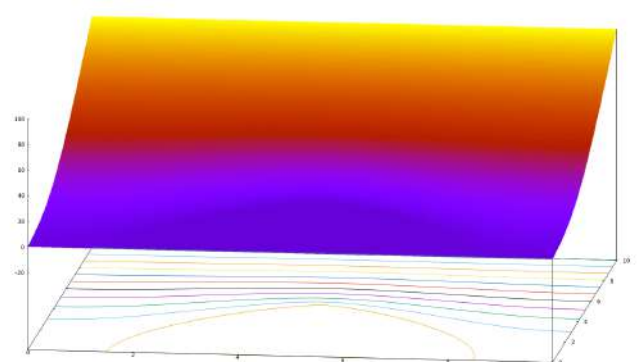
a) $\tau = -20.$ b) $\tau = -50.$

Fig. 28: $y_1 = 10,\ y_0 = 5,\ x_1 = 10,\ x_0 = 5, U_0 = 100$

The figures 27-28 depict the field plots for various values of geometric parameters (Fig.27) and specified charge density values τ (Fig.28), where $\tau(y) = \tau(\frac{y}{y_0}), \tau = const.$
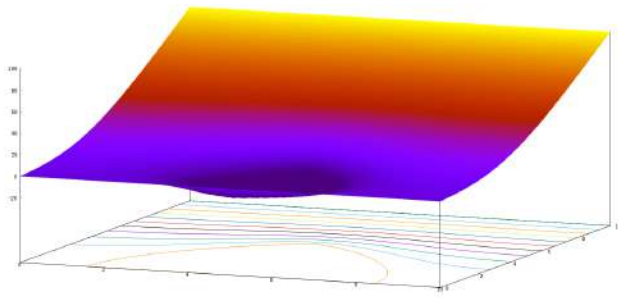
$x_1 = 10, \ \tau = -49.285;$
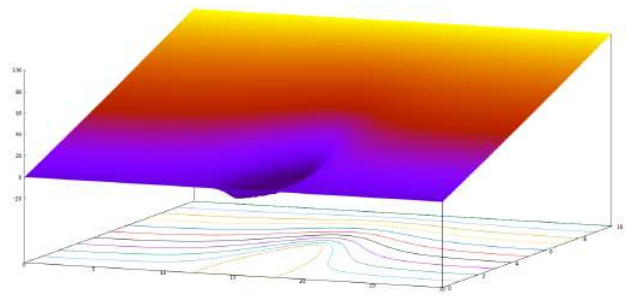
$x_1 = 30, \ \tau = -54.756;$
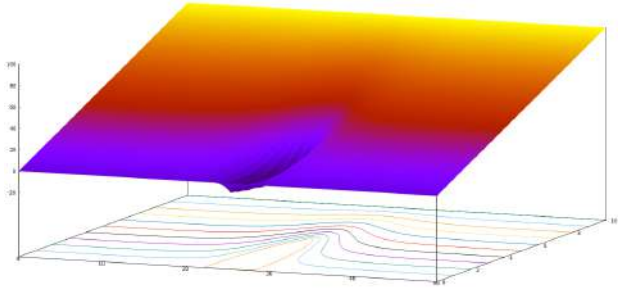
$x_1 = 50, \ \tau = -55.374;$
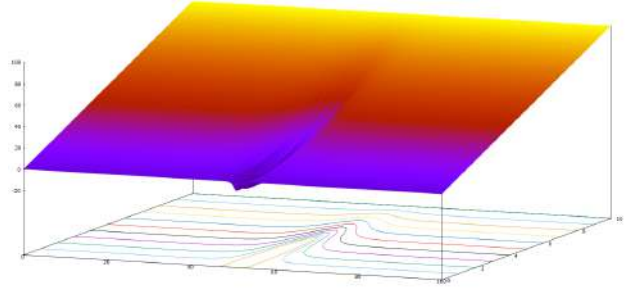
$x_1 = 100, \ \tau = -56.955.$

Fig. 29: Параметры системы: $y_1 = 10, \ U_0 = 100, \ l = 0.00005, U_0 = 100.$

The figures 29 present the field plots for various values of geometric parameters and computed values of τ. The values of τ were determined by satisfying the condition that the zero equipotential, coinciding with the cathode surface, passes at a specified distance l from the cathode vertex $U(x_0, y_0 + l) = 0$, where the vertex of each emitter is $L = y_0 + l$.

III.2   Periodic system of field emitters with dielectric layers on a substrate

Physical problem formulation
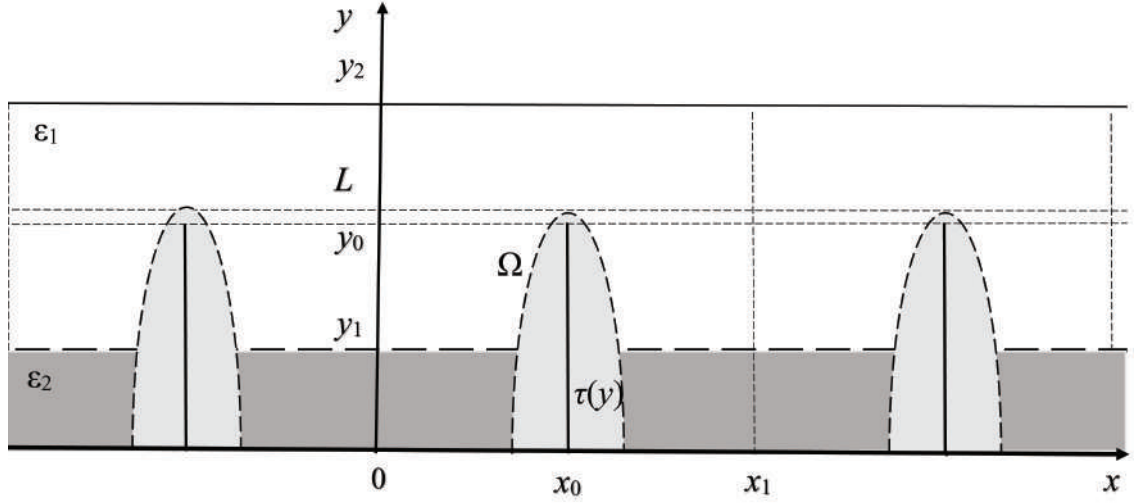
Fig. 30: Schematic image of the system.

In this section, we consider the problem of calculating the potential distribution in the Cartesian coordinates (x, y) for a periodic system of field emitters with a dielectric layer on the substrate (see Fig. 30). The parameters of the system are as follows:

$x = 0, x = x_1$ — boundaries of an individual cell,

$y = 0$ — substrate of the cathode;

$y = y_2$ — surface of the anode;

Ω — emitter surface;

L — emitter length;

$y = y_1$ — plane separating the dielectrics;

ε_2 — dielectric permittivity for $0 \leq y \leq y_1$;

ε_1 — dielectric permittivity for $y_1 \leq y \leq y_2$;

$x = x_0$ — coordinate of the charged plane along the x axis;

y_0 — length of the charged plane along the y axis;

$\tau(y), 0 \leq y \leq y_0$ — linear charge density;

$U(x, 0) = 0$ — boundary conditions on the substrate;

$U(x, y_2) = U_0$ — boundary conditions on the anode.

The influence of the field emitter in the cell is replaced by the influence of a charged plane with a charge density $\tau(y)$.

Mathematical Model

The potential distribution satisfies the Poisson equation:

$$\frac{\partial^2 U(x,y)}{\partial x^2} + \frac{\partial^2 U(x,y)}{\partial y^2} = -\frac{1}{\varepsilon_0}\rho(x,y), \tag{III.1}$$

with boundary conditions:

$$\begin{cases} U(x,0) = 0, & 0 \leq x \leq x_1, \\ U(x,y_2) = U_0, & 0 \leq x \leq x_1, \\ \left.\dfrac{\partial U(x,y)}{\partial x}\right|_{x=0} = 0, & 0 \leq y \leq y_2, \\ \left.\dfrac{\partial U(x,y)}{\partial x}\right|_{x=x_1} = 0, & 0 \leq y \leq y_2. \end{cases} \tag{III.2}$$

Assuming that a charged filament with charge density $\tau(y)$ creates a spatial charge distribution $\rho(x,y)$ in a small rectangular region ($|x - x_0| < \delta$, $0 \leq y \leq y_0$):

$$\rho(x,y) = \begin{cases} \rho(y), & |x - x_0| < \delta \text{ and } 0 \leq y \leq y_0, \\ 0, & |x - x_0| > \delta \text{ or } y_0 \leq y \leq y_1, \end{cases} \tag{III.3}$$

then:

$$\tau(y) = \lim_{\delta \to 0} 2\delta\, y_0\, \rho(y). \tag{III.4}$$

Solution of the problem III.2–III.4 can be written as:

$$U(x,y) = \begin{cases} U_0 \dfrac{y\,\varepsilon_1}{y_2\varepsilon_2 + y_1(\varepsilon_1 - \varepsilon_2)} + U_1(x,y), & 0 \leq y \leq y_1, \\ U_0 \dfrac{y\,\varepsilon_2 + y_1(\varepsilon_1 - \varepsilon_2)}{y_2\varepsilon_2 + y_1(\varepsilon_1 - \varepsilon_2)} + U_2(x,y), & y_1 \leq y \leq y_2. \end{cases} \tag{III.5}$$

The functions $U_i(x,y)$ $(i = 1, 2)$ determine the potential distribution created by the charged filament for $0 \leq y \leq y_1$ and $y_1 \leq y \leq y_2$, respectively, according to the

boundary conditions:

$$U_1(x,0) = 0, \quad \left.\frac{\partial U_1(x,y)}{\partial x}\right|_{x=0} = \left.\frac{\partial U_1(x,y)}{\partial x}\right|_{x=x_1} = 0,$$

$$U_2(x,y_2) = 0, \quad \left.\frac{\partial U_2(x,y)}{\partial x}\right|_{x=0} = \left.\frac{\partial U_2(x,y)}{\partial x}\right|_{x=x_1} = 0.$$

The function $U_1(x,y)$ can be represented as:

$$U_1(x,y) = \sum_{n=0}^{\infty} v_{1,n}(y)\cos(\alpha_n x), \tag{III.6}$$

where

$$\alpha_n = \frac{\pi\, n}{x_1}. \tag{III.7}$$

By substituting equations III.3 to III.7 into the Poisson equation III.1, we obtain the function $v_{1,n}(y)$ that satisfies the ordinary differential equation:

$$v''_{1,n}(y) - \alpha_n^2 v_{1,n}(y) = \varphi_{1,n}(y), \qquad 0 \le y \le y_1,$$

$$\varphi_{1,0}(y) = -\frac{1}{\varepsilon_0 x_1}\lim_{\delta\to 0}\int_{x_0-\delta}^{x_0+\delta}\rho(x,y)\,dx = -\frac{1}{\varepsilon_0 x_1 y_0}\tau(y),$$

$$\varphi_{1,n}(y) = -\frac{2}{\varepsilon_0 x_1}\lim_{\delta\to 0}\int_{x_0-\delta}^{x_0+\delta}\rho(x,y)\cos(\alpha_n x)\,dx = -\frac{2\,\cos(\alpha_n x_0)}{\varepsilon_0 x_1 y_0}\tau(y),\; n \ne 0.$$

$$\tag{III.8}$$

The solution of the equations III.8 for $v_{1,n}(0) = 0$:

$$v_{1,0}(y) = -\frac{1}{\varepsilon_0 x_1 y_0}\int_0^y \tau(\eta)(y-\eta)\,d\eta + C_{1,0}y,$$

$$v_{1,n}(y) = -\frac{2\,\cos(\alpha_n x_0)}{\varepsilon_0 x_1 y_0 \,\alpha_n}\int_0^y \tau(\eta)\,\mathrm{sh}(\alpha_n(y-\eta))\,d\eta + C_{1,n}\,\mathrm{sh}(\alpha_n y),\; n \ne 0,$$

$$\tag{III.9}$$

where $C_{1,n}$ — integration constants, $n \ge 0$.

The distribution of potential $U_2(x,y)$ for $y_1 \le y \le y_2$ can be obtained in a similar manner as $U_1(x,y)$ and can be expressed as:

$$U_2(x,y) = \sum_{n=0}^{\infty} v_{2,n}(y)\cos(\alpha_n x), \tag{III.10}$$

and the functions $v_{2,n}(y)$ satisfy the ordinary differential equation:

$$v_{2,n}''(y) - \alpha_n^2 v_{2,n}(y) = \varphi_{2,n}(y), \qquad y_1 \leq y \leq y_2,$$

$$\varphi_{2,0}(y) = \begin{cases} -\dfrac{1}{\varepsilon_0 x_1} \lim_{\delta \to 0} \displaystyle\int\limits_{x_0-\delta}^{x_0+\delta} \rho(x,y)\,dx = -\dfrac{1}{\varepsilon_0 x_1 y_0}\tau(y), & y_1 \leq y \leq y_0, \\[4mm] 0, & y_0 \leq y \leq y_2, \end{cases}$$

$$\varphi_{2,n}(y) = \begin{cases} -\dfrac{2}{\varepsilon_0 x_1} \lim_{\delta \to 0} \displaystyle\int\limits_{x_0-\delta}^{x_0+\delta} \rho(x,y)\cos(\alpha_n x)\,dx = \\[4mm] \qquad\qquad = -\dfrac{2\,\cos(\alpha_n x_0)}{\varepsilon_0 x_1 y_0}\tau(y), & y_1 \leq y \leq y_0, \\[4mm] 0, & y_0 \leq y \leq y_2, \end{cases} \tag{III.11}$$

The solution of equation III.11 for $v_{2,n}(y_2) = 0$:

$$v_{2,0}(y) = \begin{cases} \dfrac{1}{\varepsilon_0 x_1 y_0} \displaystyle\int\limits_{y}^{y_0} \tau(\eta)(y-\eta)\,d\eta - C_{2,0}(y_2-y), & y_1 \leq y \leq y_0, \\[4mm] -C_{2,0}(y_2-y), & y_0 \leq y \leq y_2, \end{cases}$$

$$v_{2,n}(y) = \begin{cases} \dfrac{2\,\cos(\alpha_n x_0)}{\varepsilon_0 x_1 y_0 \alpha_n} \displaystyle\int\limits_{y}^{y_0} \tau(\eta)\,\mathrm{sh}(\alpha_n(y-\eta))\,d\eta + \\[4mm] \qquad + C_{2,n}\,\mathrm{sh}(\alpha_n(y_2-y)), & y_1 \leq y \leq y_0, \\[4mm] C_{2,n}\,\mathrm{sh}(\alpha_n(y_2-y)), & y_0 \leq y \leq y_2, \end{cases} \tag{III.12}$$

$C_{2,n}$ — integration constants, $n \geq 0$.

Calculation of unknown coeffitients

To calculate the unknown coefficients $C_{1,n}$, $C_{2,n}$ in III.9, III.12, it is necessary to use the continuity conditions III.5, III.6, III.10 and the continuity condition of the normal component of the electric displacement vector at $y = y_1$:

$$U_1(x,y_1) = U_2(x,y_1), \quad \varepsilon_2 \frac{\partial U_1(x,y)}{\partial y}\bigg|_{y=y_1} = \varepsilon_1 \frac{\partial U_2(x,y)}{\partial y}\bigg|_{y=y_1}. \tag{III.13}$$

Conditions III.13 set conditions for the functions $v_{i,n}(y)$ ($i = 1,2,\ n \geq 0$):

$$v_{1,n}(y_1) = v_{2,n}(y_1), \quad \varepsilon_2 \frac{\partial v_{1,n}(y)}{\partial y}\bigg|_{y=y_1} = \varepsilon_1 \frac{\partial v_{2,n}(y)}{\partial y}\bigg|_{y=y_1}. \tag{III.14}$$

Formulas III.9, III.12, III.14 allow us to calculate the coefficients $C_{1,n}$, $C_{2,n}$ explicitly:

$$C_{1,0} = \frac{1}{\varepsilon_0 x_1 \, y_0 (y_2 - (1 - \varepsilon_1/\varepsilon_2)y_1)} \times$$

$$\times \left[\int_0^{y_1} \tau(\eta) \, (y_2 - (1 - \varepsilon_1/\varepsilon_2)y_1 - \varepsilon_1/\varepsilon_2 \eta) \; d\eta + \int_{y_1}^{y_0} \tau(\eta)(\varepsilon_1/\varepsilon_2)(y_2 - \eta) \, d\eta \right],$$

$$C_{1,n} = -\frac{2\cos(\alpha_n x_0)}{\varepsilon_0 x_1 \, y_0 \, \alpha_n} \times$$

$$\times \left(\frac{\varepsilon_1}{\varepsilon_2} \operatorname{sh}(\alpha_n y_1) \operatorname{ch}(\alpha_n(y_2 - y_1)) + \operatorname{ch}(\alpha_n y_1) \operatorname{sh}(\alpha_n(y_2 - y_1)) \right)^{-1} \times$$

$$\times \int_0^{y_0} \tau(\eta) \left[\frac{\varepsilon_1}{\varepsilon_2} \operatorname{sh}(\alpha_n(\eta - y_1)) \operatorname{ch}(\alpha_n(y_2 - y_1)) - \right.$$

$$\left. - \operatorname{sh}(\alpha_n(y_2 - y_1)) \operatorname{ch}(\alpha_n(\eta - y_1)) \right] d\eta, \tag{III.15}$$

$$C_{2,0} = \frac{1}{\varepsilon_0 x_1 \, y_0 (y_2 - (1 - \varepsilon_1/\varepsilon_2)y_1)} \times$$

$$\times \left[-\int_0^{y_1} \tau(\eta)\eta \, d\eta + \int_{y_1}^{y_0} \tau(\eta)\big((1 - \varepsilon_1/\varepsilon_2)y_1 - \eta\big) \, d\eta \right],$$

$$C_{2,n} = \frac{2\cos(\alpha_n x_0)}{\varepsilon_0 x_1 \, y_0 \, \alpha_n} \times$$

$$\times \left(\frac{\varepsilon_1}{\varepsilon_2} \operatorname{sh}(\alpha_n y_1) \operatorname{ch}(\alpha_n(y_2 - y_1)) + \operatorname{ch}(\alpha_n y_1) \operatorname{sh}(\alpha_n(y_2 - y_1)) \right)^{-1} \times$$

$$\times \left[\int_0^{y_1} \tau(\eta) \operatorname{sh}(\alpha_n \eta) \, d\eta + \int_{y_1}^{y_0} \tau(\eta) \left[\frac{\varepsilon_1}{\varepsilon_2} \operatorname{sh}(\alpha_n y_1) \operatorname{ch}(\alpha_n(\eta - y_1)) + \right. \right.$$

$$\left. \left. + \operatorname{sh}(\alpha_n(\eta - y_1)) \operatorname{ch}(\alpha_n y_1) \right] d\eta \right]. \tag{III.16}$$

Thus, equations III.5–III.7, III.10, III.15, and III.16 represent the solution to the boundary problem III.2. The potential distribution $U(x, y)$ has been obtained analytically throughout the entire periodic system.

The main results of this chapter have been published in the papers [6], [97].

IV   Simulation of a blade-shaped cathode in polar coordinate system

The following references were used in writing Chapter IV: [43, 99].

Field emitters are widely used as cathode elements in electron vacuum devices for microscopy, lithography, microwave amplifiers, X-ray generators, and other applications. To increase the lifespan of field cathodes, coatings on the apex of the emitter with various materials, including dielectrics, are being investigated [22, 44, 45, 46].

IV.1   Simulation of a blade-shaped field emitter with a dielectric coating in polar coordinate system

Physical formulation of the problem: calculation of field emitter with dielectric coating on its apex

In this section, we present the simulation of a two-dimensional diode emission system based on a blade-shaped field emitter in a polar coordinate system. The apex of the emitter is a circular region covered with a dielectric material. The anode is a coaxial circle to the emitter's apex. On the cathode, boundary conditions of the first kind are specified, while on the anode, boundary conditions of the first and second kinds are specified. The calculation of the electrostatic potential is reduced to solving a system of linear algebraic equations with constant coefficients.

Parameters:

$r = R_1, \quad (\varphi \in [-\pi, \pi])$ — a surface of the emitter,

$r = R_3, \quad (\varphi \in [\varphi_0, \pi - \varphi_0])$ — a surface of the anode ,

$r = R_3, \quad (\varphi \in [-\varphi_0, \varphi_0])$ — anode's substrate,

$r = R_2, \quad (\varphi \in [-\pi, \pi])$ — the boundary between the two dielectrics with dielectric permittivities ε_1 и ε_2,

V_1 — the value of the potential at the emitter's vertex,

V_2 — the value of the potential at the anode,

$\dfrac{\partial U(r, \varphi)}{\partial r}\bigg|_{r=R_3} = Q$ — the value of the potential at the emitter substrate.
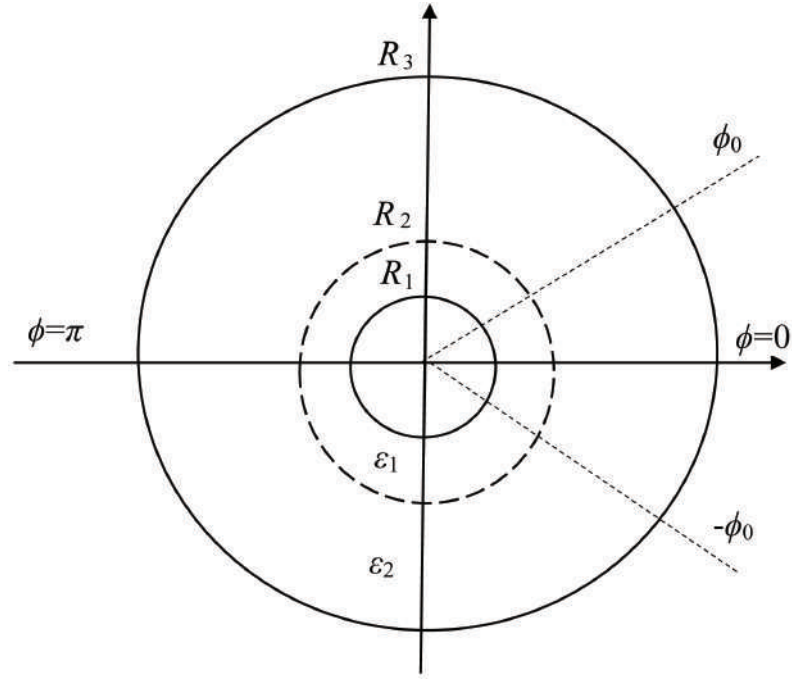
Fig. 31: Schematic image of the system in polar coordinate system.

Mathematical model

The distribution of the electrostatic potential $U(r, \varphi)$ can be found as the solution of the Laplace's equation:

$$\frac{1}{r}\frac{\partial}{\partial r}\left(r\frac{\partial U}{\partial r}\right) + \frac{1}{r^2}\frac{\partial^2 U}{\partial \varphi^2} = 0 \qquad \text{(IV.1)}$$

with boundary conditions:

$$\begin{cases} U(R_1, \varphi) = V_1, & \varphi \in [-\pi, \pi], \\ U(R_3, \varphi) = V_2, & \varphi \in [\varphi_0, 2\pi - \varphi_0], \\ \left.\dfrac{\partial U(r, \varphi)}{\partial r}\right|_{r=R_3} = Q, & \varphi \in [-\varphi_0, \varphi_0], \\ \varepsilon_1 \left.\dfrac{\partial U(r, \varphi)}{\partial r}\right|_{r=R_2-0} = \varepsilon_2 \left.\dfrac{\partial U(r, \varphi)}{\partial r}\right|_{r=R_2+0}, & \varphi \in [-\pi, \pi]. \end{cases} \qquad \text{(IV.2)}$$

Solution of the boundary problem IV.1, IV.2

To solve the boundary problem IV.1, IV.2, considering that the potential distribution $U(r, \varphi)$ for the entire region ($r \in [R_1, R_3]$, $\varphi \in [-\pi, \pi]$) is symmetric with respect to the planes $\varphi = 0$ and $\varphi = \pi$, the problem IV.1, IV.2 can be solved for ($r \in [R_1, R_3]$, $\varphi \in [0, \pi]$).

To find the solution of equation IV.1 with boundary conditions IV.2, the entire inner region of the diode system ($r \in [R_1, R_3]$, $\varphi \in [0, \pi]$) can be divided into the following subregions:

(1) $-$ ($r \in [R_1, R_2]$, $\varphi \in [0, \varphi_0]$);
(2) $-$ ($r \in [R_2, R_3]$, $\varphi \in [0, \varphi_0]$);
(3) $-$ ($r \in [R_1, R_2]$, $\varphi \in [\varphi_0, \pi]$);
(4) $-$ ($r \in [R_2, R_3]$, $\varphi \in [\varphi_0, \pi]$).

Let:

$$U(r, \varphi) = \begin{cases} U_1(r, \varphi), & r \in [R_1, R_2], \quad \varphi \in [0, \varphi_0], \\ U_2(r, \varphi), & r \in [R_2, R_3], \quad \varphi \in [0, \varphi_0], \\ U_3(r, \varphi), & r \in [R_1, R_2], \quad \varphi \in [\varphi_0, \pi], \\ U_4(r, \varphi), & r \in [R_2, R_3], \quad \varphi \in [\varphi_0, \pi]. \end{cases} \tag{IV.3}$$

Let's consider the functions with respect to the variable r - $V_1(r)$, $V_2(r)$, $V_3(r)$, $V_4(r)$ for each of the regions IV.3 respectively:

$$V_1(r) = Q R_3 \frac{\varepsilon_2}{\varepsilon_1} \ln (r/R_1) + V_1,$$

$$V_2(r) = Q R_3 \left(\ln (r/R_2) + \frac{\varepsilon_2}{\varepsilon_1} \ln (R_2/R_1) \right) + V_1,$$

$$V_3(r) = \frac{\varepsilon_2}{\varepsilon_1} \frac{(V_2 - V_1) \ln (r/R_1)}{\frac{\varepsilon_2}{\varepsilon_1} \ln (R_2/R_1) + \ln (R_3/R_2)} + V_1, \tag{IV.4}$$

$$V_4(r) = \frac{(V_2 - V_1) \ln (r/R_3)}{\frac{\varepsilon_2}{\varepsilon_1} \ln (R_2/R_1) + \ln (R_3/R_2)} + V_2.$$

The functions $V_1(r)$, $V_2(r)$, $V_3(r)$, $V_4(r)$ given by equation IV.4 satisfy the Laplace equation with the boundary conditions IV.2 for each corresponding region (i).

The potential distribution $U_i(r, \varphi)$ ($i, =, 1, 2, 3, 4$) in region (i) can be represented using the method of separation of variables, as described in reference [43]:

$$U_1(r, \varphi) = V_1(r) + \sum_{n=1}^{\infty} a_n e^{-\lambda_n(\varphi_0 - \varphi)} \frac{1 + e^{-2\lambda_n \varphi}}{1 + e^{-2\lambda_n \varphi_0}} \sin (\lambda_n \ln (r/R_1)) +$$
$$+ \sum_{m=0}^{\infty} c_m (r/R_2)^{\mu_m} \frac{1 - (r/R_1)^{-2\mu_m}}{1 - (R_1/R_2)^{2\mu_m}} \cos(\mu_m \varphi), \tag{IV.5}$$

$$U_2(r, \varphi) = V_2(r) + \sum_{k=0}^{\infty} b_k e^{-\nu_k(\varphi_0 - \varphi)} \frac{1 + e^{-2\nu_k \varphi}}{1 + e^{-2\nu_k \varphi_0}} \sin\left(\nu_k \ln\left(r/R_2\right)\right) +$$
$$+ \sum_{m=0}^{\infty} c_m \left(r/R_2\right)^{-\mu_m} \frac{1 + \left(r/R_3\right)^{2\mu_m}}{1 + \left(R_2/R_3\right)^{2\mu_m}} \cos(\mu_m \varphi), \tag{IV.6}$$

$$U_3(r, \varphi) = V_3(r) +$$
$$+ \sum_{n=1}^{\infty} \left(a_n + \frac{2(-1)^n}{\lambda_n} \frac{\varepsilon_2}{\varepsilon_1} \left(\frac{T_2 - T_1}{\frac{\varepsilon_2}{\varepsilon_1} \ln\left(R_2/R_1\right) + \ln\left(R_3/R_2\right)} - Q R_3 \right) \right) \times$$
$$\times e^{-\lambda_n(\varphi - \varphi_0)} \frac{1 + e^{-2\lambda_n(\pi - \varphi)}}{1 + e^{-2\lambda_n(\pi - \varphi_0)}} \sin\left(\lambda_n \ln\left(r/R_1\right)\right) + \tag{IV.7}$$
$$+ \sum_{p=0}^{\infty} d_p \left(r/R_2\right)^{\eta_p} \frac{1 - \left(r/R_1\right)^{-2\eta_p}}{1 - \left(R_1/R_2\right)^{2\eta_p}} \cos(\eta_p(\pi - \varphi)),$$

$$U_4(r, \varphi) = V_4(r) + \sum_{t=1}^{\infty} g_t \, e^{-\xi_t(\varphi - \varphi_0)} \frac{1 + e^{-2\xi_t(\pi - \varphi)}}{1 + e^{-2\xi_t(\pi - \varphi_0)}} \sin\left(\xi_t \ln\left(r/R_2\right)\right) +$$
$$+ \sum_{p=0}^{\infty} d_p \left(r/R_2\right)^{-\eta_p} \frac{1 - \left(r/R_3\right)^{2\eta_p}}{1 - \left(R_2/R_3\right)^{2\eta_p}} \cos(\eta_p(\pi - \varphi)), \tag{IV.8}$$

where

$$\lambda_n = \frac{\pi n}{\ln\left(R_2/R_1\right)}, \quad \mu_m = \frac{(2m+1)\pi}{2\varphi_0}, \quad \nu_k = \frac{(2k+1)\pi}{2\ln\left(R_3/R_2\right)},$$
$$\eta_p = \frac{(2p+1)\pi}{2(\pi - \varphi_0)}, \quad \xi_t = \frac{\pi t}{\ln\left(R_3/R_2\right)}, \tag{IV.9}$$

The computation of the unknown coefficients in the potential expansion IV.5 – IV.9

The functions $U_i(r, \varphi)$ $(i = 1, 2, 3, 4)$ given by equations IV.5 to IV.9, representing the potential distribution $U(r, \varphi)$ as series expansions in the eigenfunctions, satisfy the boundary conditions IV.2 on the surfaces of the cathode and anode. These formulas impose the following continuity conditions for the potential distribution on the interface boundaries:

$$U_1(R_2, \varphi) = U_2(R_2, \varphi), \quad \varphi \in [0, \varphi_0];$$
$$U_1(r, \varphi_0) = U_3(r, \varphi_0), \quad r \in [R_1, R_2];$$
$$U_3(R_2, \varphi) = U_4(R_2, \varphi), \quad \varphi \in [\varphi_0, \pi].$$

To compute the unknown coefficients a_n, b_k, c_m, d_p, g_t, additional continuity conditions for the potential distribution and the normal component of the displacement vector can be utilized on the remaining interface boundaries:

$$U_2(r, \varphi_0) = U_4(r, \varphi_0), \qquad\qquad r \in [R_2, R_3];$$

$$\varepsilon_1 \left.\frac{\partial U_1(r, \varphi)}{\partial r}\right|_{r=R_2} = \varepsilon_2 \left.\frac{\partial U_2(r, \varphi)}{\partial r}\right|_{r=R_2}, \quad \varphi \in [0, \varphi_0];$$

$$\left.\frac{\partial U_1(r, \varphi)}{\partial \varphi}\right|_{\varphi=\varphi_0} = \left.\frac{\partial U_3(r, \varphi)}{\partial \varphi}\right|_{\varphi=\varphi_0}, \qquad r \in [R_1, R_2]; \qquad\text{(IV.10)}$$

$$\varepsilon_1 \left.\frac{\partial U_3(r, \varphi)}{\partial r}\right|_{r=R_2} = \varepsilon_2 \left.\frac{\partial U_4(r, \varphi)}{\partial r}\right|_{r=R_2}, \quad \varphi \in [\varphi_0, \pi];$$

$$\left.\frac{\partial U_2(r, \varphi)}{\partial \varphi}\right|_{\varphi=\varphi_0} = \left.\frac{\partial U_4(r, \varphi)}{\partial r}\right|_{\varphi=\varphi_0}, \qquad r \in [R_2, R_3].$$

Using the continuity conditions IV.10 and the orthogonality of the eigenfunctions, we can formulate a linear algebraic system with the corresponding unknown coefficients a_n, b_k, c_m, d_p, g_t:

$$b_k \frac{1}{2} \ln (R_3/R_2) - (-1)^k \sum_{t=1}^{\infty} g_t \frac{(-1)^t \xi_t}{\nu_k^2 - \xi_t^2} =$$
$$= \frac{1}{\nu_k} \left(\frac{\varepsilon_2}{\varepsilon_1} \ln (R_2/R_1) + \frac{1}{\nu_k} (-1)^k \right) \times \qquad\text{(IV.11)}$$
$$\times \left(\frac{V_2 - V_1}{\dfrac{\varepsilon_2}{\varepsilon_1} \ln (R_2/R_1) + \ln (R_3/R_2)} - Q R_3 \right);$$

$$(-1)^m \sum_{n=1}^{\infty} a_n \frac{(-1)^n \lambda_n}{\lambda_n^2 + \mu_m^2} - (-1)^m \frac{\varepsilon_2}{\varepsilon_1} \sum_{k=0}^{\infty} b_k \frac{\nu_k}{\nu_k^2 + \mu_m^2} +$$
$$+ c_m \frac{\varphi_0}{2} \left(\coth (\mu_m (R_2/R_1)) + \frac{\varepsilon_2}{\varepsilon_1} \coth (\mu_m (R_3/R_2)) \right) = 0; \qquad\text{(IV.12)}$$

$$a_n \frac{1}{2} \ln\left(R_2/R_1\right) \left(\tanh(\lambda_n \varphi_0) + \tanh(\lambda_n(\pi - \varphi_0))\right) + (-1)^n \sum_{m=0}^{\infty} c_m \frac{(-1)^m \mu_m}{\lambda_n^2 + \mu_m^2} +$$

$$+(-1)^n \sum_{p=0}^{\infty} d_p \frac{(-1)^p \eta_p}{\lambda_n^2 + \eta_p^2} = -\tanh(\lambda_n(\pi - \varphi_0)) \times$$

$$\times \frac{2(-1)^n}{\lambda_n} \frac{\varepsilon_2}{\varepsilon_1} \left(\frac{V_2 - V_1}{\frac{\varepsilon_2}{\varepsilon_1} \ln\left(R_2/R_1\right) + \ln\left(R_3/R_2\right)} - Q R_3\right); \qquad \text{(IV.13)}$$

$$(-1)^p \sum_{n=1}^{\infty} a_n \frac{(-1)^n \lambda_n}{\lambda_n^2 + \eta_p^2} + d_p \frac{\pi - \varphi_0}{2} \left(\coth\left(\eta_p\left(R_2/R_1\right)\right) + \frac{\varepsilon_2}{\varepsilon_1} \coth\left(\eta_p\left(R_3/R_2\right)\right)\right) -$$

$$-(-1)^p \frac{\varepsilon_2}{\varepsilon_1} \sum_{t=1}^{\infty} g_t \frac{\xi_t}{\xi_t^2 + \eta_p^2} = -2\,(-1)^p \sum_{n=1}^{\infty} \frac{1}{\lambda_n^2 + \eta_p^2} \times$$

$$\times \frac{\varepsilon_2}{\varepsilon_1} \left(\frac{V_2 - V_1}{\frac{\varepsilon_2}{\varepsilon_1} \ln\left(R_2/R_1\right) + \ln\left(R_3/R_2\right)} - Q R_3\right); \qquad \text{(IV.14)}$$

$$-\sum_{m=0}^{\infty} c_m \frac{\mu_m}{\mu_m^2 + \nu_k^2} + b_k \frac{1}{2} \ln\left(R_3/R_2\right) \tanh(\nu_k \varphi_0) +$$

$$+\sum_{p=0}^{\infty} d_p \frac{(-1)^p \eta_p}{\nu_k} \left(\frac{\eta_p}{\eta_p^2 + \nu_k^2} \frac{(-1)^k}{\sinh\left(\eta_p\left(\ln\left(R_3/R_2\right)\right)\right)} - \frac{\nu_k}{\eta_p^2 + \nu_k^2}\right) + \qquad \text{(IV.15)}$$

$$+(-1)^k \sum_{t=1}^{\infty} g_t \frac{\xi_t}{\nu_k} \frac{(-1)^t \xi_t}{(\nu_k^2 - \xi_t^2)} \tanh(\xi_t\left(\pi - \varphi_0\right)) = 0.$$

So, the solution of the original boundary problem IV.1, IV.2 is reduced to solving the system of linear algebraic equations IV.11 – IV.15 for the coefficients involved in the potential expansion IV.5 – IV.9.

Results of numerical calculation of potential distribution in the diode system for a field emitter with a dielectric coating

Based on the derived formulas for the potential distribution IV.3 – IV.9, this section presents contour plots of equipotential lines throughout the entire diode system for various parameter values.

All parameter values are presented in dimensionless units.
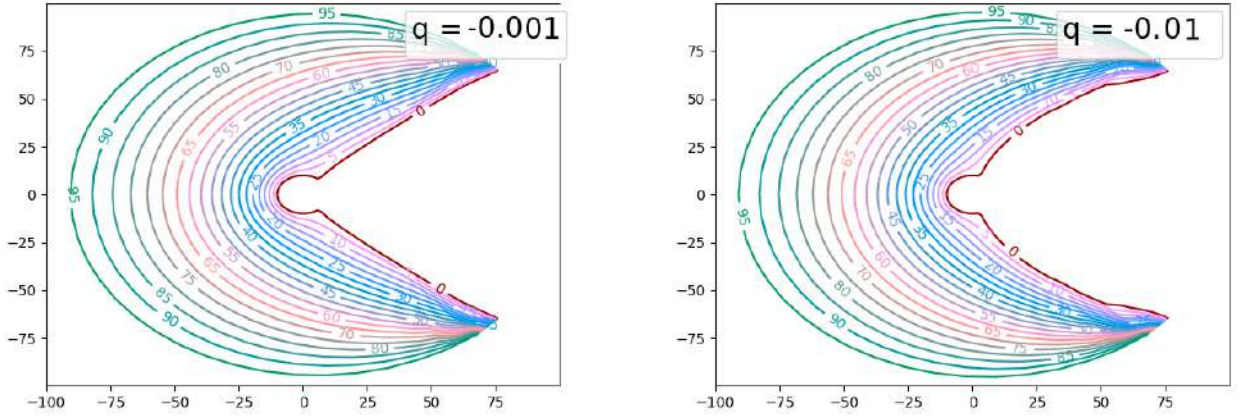
a) $Q = -0.001$ b) $Q = -0.01$

Fig. 32: $\varepsilon 1/\varepsilon 2 = 1$, $R_1 = 10$, $R_3 = 100$, $\varphi_0 = \pi/4$, $V_1 = 0$, $V_2 = 100$
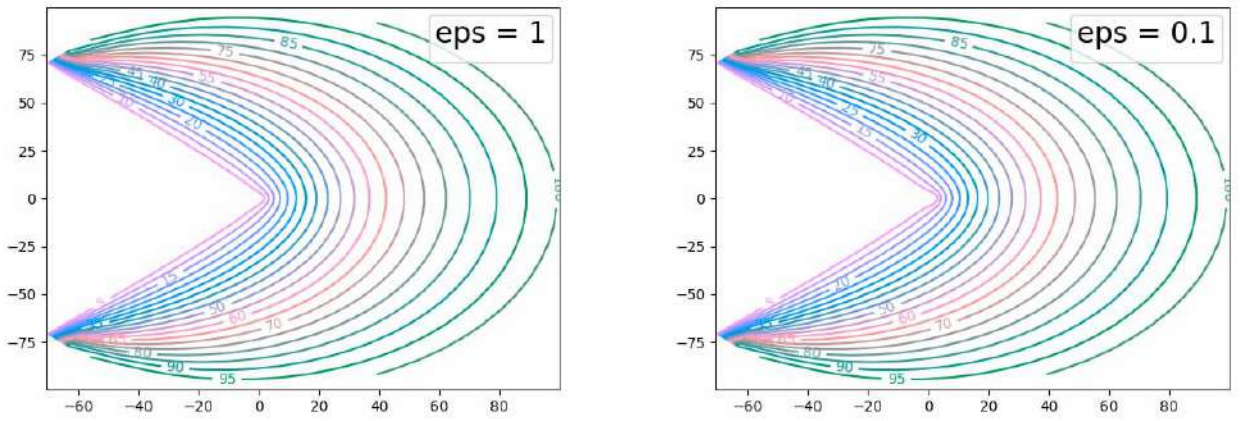
a) $\varepsilon_2/\varepsilon_1 = 1$ b) $\varepsilon_2/\varepsilon_1 = 0.1$

Fig. 33: $R_1 = 1$, $R_2 = 2$, $R_3 = 100$, $\varphi_0 = \pi/4$, $V_1 = 0$, $V_2 = 100$, $U(r, \varphi_0) = 0$

The figures 32 show the plots of potential distribution for various values of Q in the boundary conditions IV.2 when there is no dielectric layer on the cathode tip $(\varepsilon_2 = \varepsilon_1)$.

The figures 33 depict the plots of potential distribution for different values of the ratio of dielectric permittivities $\varepsilon_2/\varepsilon_1$ under homogeneous Dirichlet boundary conditions on the surface $\varphi_0 = \pi/4$ $(R_1 \leq r \leq R_3)$.
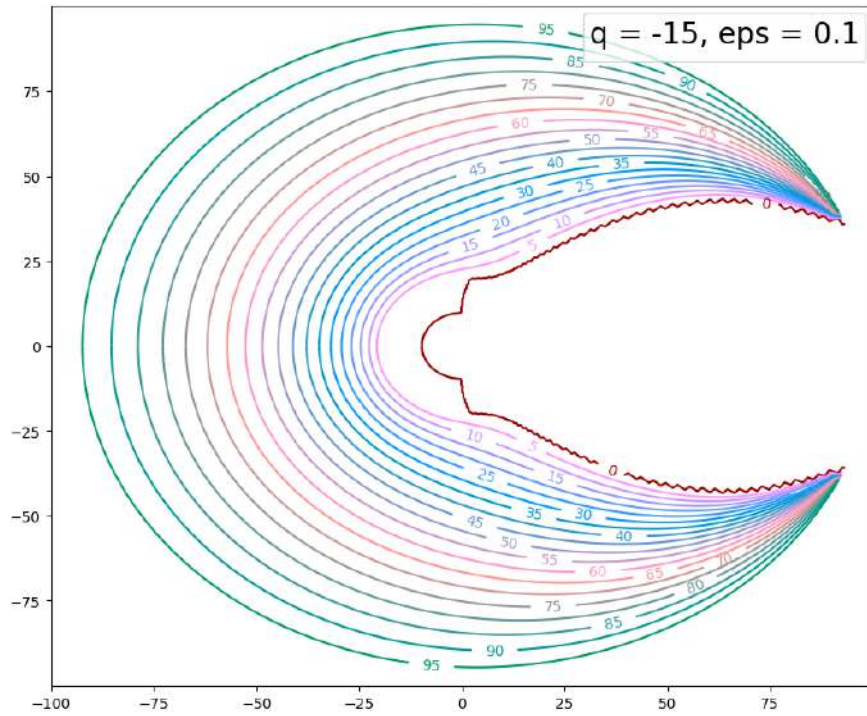
Fig. 34: $\varepsilon_2/\varepsilon_1 = 0.1$ $R_1 = 1$, $R_2 = 2$, $R_3 = 100$, $\varphi_0 = \pi/4$, $V_1 = 0$, $V_2 = 100$, $Q = -15$

The graph in Fig. 34 shows the potential distribution throughout the entire region of the investigated diode system with a field cathode, where the tip is coated with a dielectric layer, under the specified parameters.

Figures 36 show graphs of the potential distribution with respect to the variable r near the dielectric interface. It is noticeable that with an increase in the permittivity of the layer (dielectric coating of the tip) ε_1 with respect to ε_2, the field strength in the emission region $R_2 \leq r \leq R_2 + 2R_1$ increases. These calculation results correspond to known experimental facts [22].
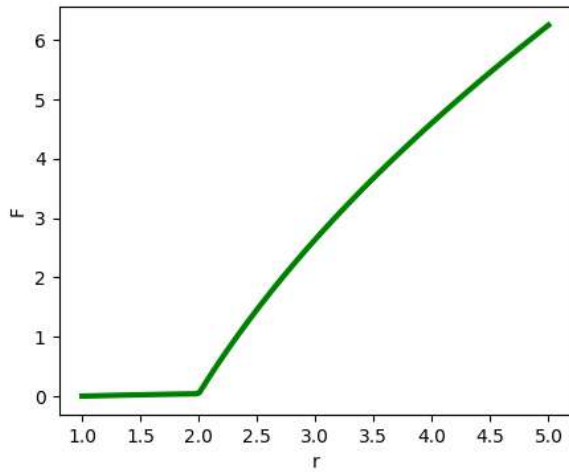
a) $\varepsilon_2/\varepsilon_1 = 0.01$
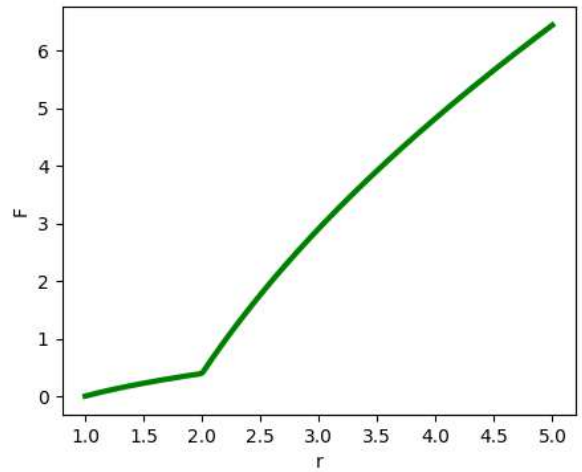
b) $\varepsilon_2/\varepsilon_1 = 0.5$
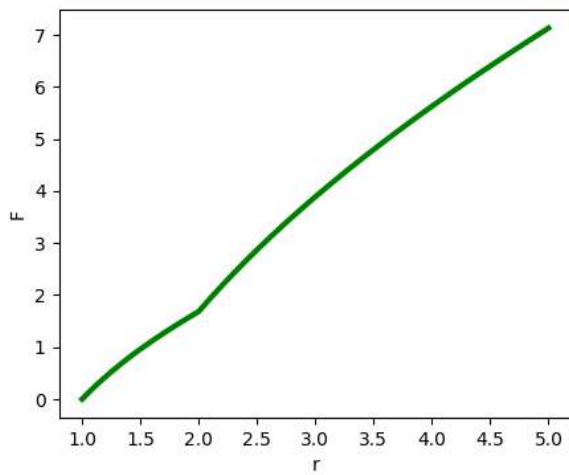
c) $\varepsilon_2/\varepsilon_1 = 0.1$
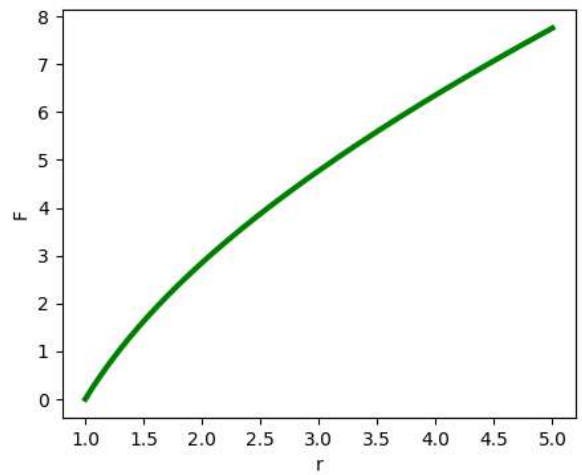
d) $\varepsilon_2/\varepsilon_1 = 1$

Fig. 35: $R_1 = 1$, $R_2 = 2$, $R_3 = 100$, $\varphi = 0$ $\varphi_0 = \pi/4$, $V_1 = 0$, $V_2 = 100$

The main results of this chapter have been published in the papers [43].

Conclusion

In this work, methods for modeling various two-dimensional emission systems based on field emitters have been proposed. One of the main objectives of studying field cathodes is to find the most convenient modeling approach that can help construct cathodes of the required sizes and shapes for specific applications. Special attention has been given to the investigation of changes in the distribution of electrostatic potential within the system and the influence of geometric parameters and the presence of dielectric layers on these changes.

The first chapter presents the following axisymmetric emission diode and triode systems in cylindrical coordinate system:
— a single field cathode of a special shape, modeled using a charged circular wire,
— a single cathode with a dielectric layer on the lateral surface.

The second chapter discusses planar symmetric emission diode systems in the Cartesian coordinate system:
— a single blade-shaped cathode, modeled using a thin charged wire. — a single blade-shaped cathode, modeled using an arbitrary number of infinitely charged wires, taking into account the influence of dielectric layers on the lateral surfaces of the diode system.

The third chapter investigates planar symmetric field multi-emitter systems in the Cartesian coordinate system: — a periodic emitter system, modeled using charged planes. — a periodic emitter system with a dielectric layer on the emitter substrate.

The fourth chapter presents the results of modeling a planar symmetric diode system with a field emitter in the Cartesian coordinate system, where the tip of the emitter is coated with a dielectric layer.

For each of the presented models, the distribution of the electrostatic potential was computed throughout the entire region of the studied system in an analytical form as a series expansion in eigenfunctions. The coefficients of the expansions were found either explicitly or through solving a system of linear algebraic equations.

Based on the derived formulas, graphs of the potential distribution were provided for various geometric parameters of the considered diode systems. Examples of system influence were demonstrated by varying the initial parameter values.

For axisymmetric systems, changing the boundaries of the region in the variables

r and z alters the shape of the cathode (Fig. 3, 4). The effect of varying the ratio of dielectric layers was also demonstrated in Fig. 7, 8.

For systems modeled in the Cartesian coordinate system, different methods were used to construct the virtual cathode, whose shape is represented by the zero equipotential: using charged filaments or charged planes. It should be noted that defining the emitter shape using charged filaments is more preferable, considering the flexibility of the model for a wide range of field cathodes of different shapes (Fig. 12–13, 15–16, 18–19, 21–22).

The solution to the problem of determining the distribution of the electrostatic potential for a blade-shaped field emitter with a given radius of curvature at the apex, represented in polar coordinates, allows for varying the shape of the field cathode itself by changing the boundary conditions and also taking into account the presence of a dielectric layer on its apex (Fig. 27–28).

The work presents graphs of the electric field strength near the apex for several of the considered systems. The electric field strength is an important emission characteristic of the model and allows for analyzing the feasibility of using a particular modeling method in the design of real vacuum electronic devices. The field strength values for circular filaments are quite high, indicating the convenience of using this method for creating relatively large cathodes in the millimeter range (Fig. 23). On the other hand, flat models have relatively weak field strength values, but their advantage lies in the ability to use such systems in nanoelectronic devices (Fig. 24–25).

Thus, each of the presented models has a set of advantages and disadvantages that should be taken into account when designing real devices. However, each of the developed models of field emission systems can be used in real devices depending on the specific technical task.

References

[1] Bugayev A.S., Vinogradova E.M., Egorov N.V., Sheshin E.P. Autoelectronic cathodes and guns – Dolgoprudny: Intellekt Publishing House, 2017 – 288 p.

[2] Vinogradova E.M., Dolgov S.L., Egorov N.V. Calculation of electrostatic potential in multi-apex and single-apex field emission systems // Bulletin of St. Petersburg University. Applied Mathematics. Informatics. Control Processes. – 2007. – Vol. 1. – pp. 29–37.

[3] Vinogradova E.M., Egorov N.V., Televny D.S. Calculation of a triode field-emission system with a modulator // Technical Physics Journal. – 2014. – Vol. 84, No. 2. – pp. 139–144.

[4] Vinogradova E.M., Egorov N.V. Mathematical modeling of an electronic gun based on a field electron cathode // Radio Engineering and Electronics. – 2004. – Vol. 49, No. 2. – pp. 251–256.

[5] Vinogradova E.M., Doronin G.G., Egorov N.V. Mathematical Simulation of a 2D Diode System with a Blade-Shaped Field Emitter // Technical Physics Journal. – 2020. – Vol. 65, No. 4. – pp. 514–517.

[6] Vinogradova E.M., Doronin G.G. Mathematical modeling of a two-dimensional periodic system of field emitters // Bulletin of St. Petersburg University. Applied Mathematics. Informatics. Control Processes. – 2020. – Vol. 16, No. 2. – pp. 121–128.

[7] Vinogradova E.M., Egorov N.V. Mathematical modeling of a diode system based on a field emitter // Technical Physics Journal. – 2011. – Vol. 81, No. 9. – pp. 1–5.

[8] Vinogradova E.M., Egorov N.V., Baranov R.Yu. Mathematical modeling of the cathode unit of a field electron gun // Bulletin of St. Petersburg University. Applied Mathematics. Informatics. Control Processes. – 2006. – Vol. 3. – pp. 3–10

[9] Vinogradova E.M., Egorov N.V., Televny D.S. Technical Physics Journal // 2014. Vol. 84, No. 2. pp. 139.

[10] Gradstein I.S., Ryzhik I.M. Tables of Integrals, Series, and Products. – Moscow: State Publishing House of Physical and Mathematical Literature, 1963. – p. 1108.

[11] Doronin G.G., Vinogradova E.M. Modeling of a triode system based on a sharp-edged field emitter // Control Processes and Stability (International Conference). – 2018. – Vol. 5, No. 1. – pp. 113–116.

[12] Doronin G.G., Vinogradova E.M. Modeling of a diode field emission system with a dielectric layer // Control Processes and Stability (International Conference). – 2019. – Vol. 6, No. 1. – pp. 73-77.

[13] Doronin G.G., Vinogradova E.M. Modeling of a field emitter in a two-dimensional diode system with dielectric layers // Control Processes and Stability. – 2020. – Vol. 7, No. 1. – pp. 90-93.

[14] Doronin G.G., Vinogradova E.M. Calculation of potential distribution in a two-dimensional diode system with a blade-shaped field cathode // Control Processes and Stability. – 2021. – Vol. 8, No. 1

[15] Doronin G.G. Mathematical modeling of emission systems based on field electron cathodes. // Saint Petersburg State University. – 2020.

[16] Egorov N.V., Sheshin E.P. Autoelectronic emission. Principles and devices: scientific edition. - Dolgoprudny: Intellekt Publishing House, 2011. - 703 p.

[17] Mirolyubov N.N., Kostenko M.V., Levinstein M.L. Methods for calculating electrostatic fields. – Moscow: State Publishing House "Vysshaya shkola". – 1963. – p. 412.

[18] Tikhonov A.N., Samarsky A.A. Equations of mathematical physics. – Moscow: Nauka Publishing House, 1977. – p. 735.

[19] M. Abramowitz, I. Stegun, Handbook of Mathematical Functions: with Formulas, Graphs, and Mathematical Tables. – Washington D.C.: Courier Corporation. – 1972. – P. 1030.

[20] Ahn Y., Kim S.J., Jeong J.-W., Park S., Kim J.-W., Go E., Lee J.-W., Kang J.-T., Yun K.N., Choi S., Kim S., Yeon J.-H., Song Y.-H. Overall control of field emission from carbon nanotube paste-emitters through macro-geometries for high-performance electron source applications // Carbon. – 2022. – Vol. 189. – P. 519–529.

[21] Al-Heeti S.A., Al-Tabbakh A.A. The effect of size distribution and degradation of carbon nanotubes on the Fowler–Nordheim plot behavior // Ultramicroscopy. – 2021. – Vol. 230. – Art. no. 113373.

[22] Al Soud A., Al Buqain R. N., Mousa M. S. Composite metallic nano emitters coated with a layer of insulator covered by Au layer // Jordan Journal of Physics. – 2020. – Vol. 13, №3. – P. 253–262.

[23] Bansode S.R., Harpale K.V., Mutadak P., Sonawane K.M., Chaskar M.G., More M.A., Sharma R.B. Morphology-dependent field emission investigations from the 2-dimensional Bi_2Se_3–RGO nanocomposites // Materials Science and Engineering B: Solid-State Materials for Advanced Technology. – 2021. – Vol. 274. – Art. no. 115450.

[24] Basu A., Swanwick M.E., Fomani A.A., Velásquez-Garcia L.F. A portable x-ray source with a nanostructured Pt-coated silicon field emission cathode for absorption imaging of low-Z materials // Journal of Physics D: Applied Physics. – 2015. – Vol. 48, №22. – Art. no. 225501.

[25] Biswas D., Kumar R., Singh G. Predicting space-charge affected field emission current from curved tips // Journal of Applied Physics. – 2021. – Vol. 130. – Art. no. 185302.

[26] Biswas, D., Rudra, R., Kumar, R. Semi-analytical theory of emission and

transport in a LAFE-based diode // 2022 Physics of Plasmas. – 2022 – Vol. 29(7). – Art. no. 073102.

[27] Biswas D., Rudra R. Shielding effects in random large area field emitters, the field enhancement factor distribution, and current calculation // 2018 Physics of Plasmas. – 2018 – Vol. 25(8). – Art. no. 083105.

[28] Biswas D., Singh G., Kumar R.Approximate universality in the electric field variation on a field-emitter tip in the presence of space charge // 2021 Physics of Plasmas. – 2021. – Vol. 28. – Art. no. 093110.

[29] Chepusov A., Komarskiy A., Korzhenevskiy S. Field electron emission properties of industrial graphite under technical vacuum conditions // Vacuum. – 2021. – Vol. 189. – Art. no. 110268.

[30] Dall'Agnol, F.F., De Assis, T.A. Close proximity electrostatic effect from small clusters of emitters // Journal of Physics Condensed Matter. – 2017 – Vol. 29, №40. – Art. no. 40LT01.

[31] Dall'Agnol, F.F., De Assis, T.A., Forbes, R.G. Electrostatic effect on the characteristic field enhancement factors when two identical emitters are in close proximity // 30th International Vacuum Nanoelectronics Conference, IVNC 2017. – 2017. – Art. no. 8051623, P. 230–231.

[32] Doronin G.G., Vinogradova E.M. The arbitrarily shaped field emitter mathematical modeling // В сборнике: 2016 Young Researchers in Vacuum Micro/Nano Electronics, VMNE-YR 2016 – Proceedings. – 2016. – Art. no. 7880402.

[33] Doronin G.G., Vinogradova E.M., Egorov N.V. The Triode System on the Basis of the Sharp-Edged Field Cathode Mathematical Modeling // 2017 Young Researchers in Vacuum Micro/Nano Electronics – VMNE-YR 2017. – 2017.

[34] Dusane P.R., Gavhane D.S., Kolhe P.S., Bankar P.K., Thombare B.R., Lole G.S., Kale B.B., More M.A., Patil S.I. Controlled decoration of palladium (Pd) nanoparticles on graphene nanosheets and its superior field emission behavior // Materials Research Bulletin. – 2021. – Vol. 140. – Art. no. 111335.

[35] Egorov N.V., Doronin G.G., Vinogradova E.M. Mathematical modeling of triode field emission system with sharp-edged cathode // 7th ITG International Vacuum Electronics Workshop (IVEW) 2020 and 13th International Vacuum Electron Sources Conference (IVeSC). – 2020. – Book of Abstracts. – P. 68.

[36] Egorov N.V., Vinogradova E.M. Mathematical model of electron gun on the field emission electron cathode basis // Vacuum. – 2000. – Vol. 57, №3. – P. 267–281.

[37] Egorov, N.V., Vinogradova, E.M. Mathematical modeling of a field emitter with a hyperbolic shape // 2020 Vestnik Sankt-Peterburgskogo Universiteta, Prikladnaya Matematika, Informatika, Protsessy Upravleniya. – Vol. 16(3) – P. 238–248.

[38] Egorov, N.V., Vinogradova, E.M. Mathematical modeling of triode system on the basis of field emitter with ellipsoid shape // 2021 Vestnik Sankt-Peterburgskogo Universiteta, Prikladnaya Matematika, Informatika, Protsessy Upravleniya – 2021. – Vol. 17. Vol. 2 – P. 131–136.

[39] Egorov, N.V., Vinogradova, E.M. Mathematical modeling of the electron beam formatting system on the basis of field emission cathode // 2005 International Conference on Physics and Control, PhysCon 2005. – Proceedings. – 2005 – Art. no. 1513995. – P. 289–292.

[40] Egorov, N.V., Vinogradova, E.M. Mathematical model of electron gun on the field emission electron cathode basis // Vacuum – 2000 – Vol. 57, №3. – P. 267-281.

[41] Egorov N.V., Vinogradova E.M. Mathematical modeling of the electron beam formatting systems on the basis of field emission cathodes with various shapes // Vacuum. – 2003. – Vol. 72, № 2. – P. 103–111.

[42] Egorov, N.V., Vinogradova, E.M. The multi-tip field emission cathode mathematical modeling // RuPAC 2012 Contributions to the Proceedings - 23rd Russian Particle Accelerator Conference. – 2012. – P. 421–423.

[43] Egorov N. V., Vinogradova E. M., Doronin G. G. Blade-like field cathode with a dielectric coating mathematical modeling. *Vestnik of Saint Petersburg University. Applied Mathematics. Computer Science. Control Processes.* – 2023. – Vol. 19. №1. – P. 65-71.

[44] Filippov S.V., Dall'Agnol F.F., de Assis T.A., Popov E.O., Kolosko A.G. Properties of blade-like field emitters // Ultramicroscopy – 2022. – Vol. 233. – Art. no. 113462.

[45] Filippov S. V., Kolosko A. G., Popov E. O., Demin G. D., Makhiboroda M. A., Djuzhev N. A., Gryazneva T. A. Korotkov S Y 2019 Investigation of the emission properties of a silicon blade-type cathode // Journal of Physics: Conference Series. – Vol. 1400, №5. – Art. no. 055011.

[46] Filippov S.V., Popov E.O., Kolosko A.G., Dall'Agnol F.F. Features of the field enhancement factor on blade-type emitters // 34th International Vacuum Nanoelectronics Conference, IVNC 2021. – 2021.

[47] Filippov S.V., Popov E.O., Kolosko A.G., Dall'Agnol F.F. Modeling basic tip forms and its field emission // 33rd International Vacuum Nanoelectronics Conference, IVNC 2020. – 2020. – Art. no. 9203096.

[48] Forbes R.G. Physical electrostatics of small field emitter arrays/clusters// Journal of Applied Physics. – 2016. – Vol. 120, №5. – no. 054302.

[49] Forbes R.G. Development of a simple quantitative test for lack of field emission orthodoxy // Proceedings of the Royal Society A: Mathematical, Physical and Engineering Sciences. – 2013. – Vol. 469, №2158. – Art. no. 20130271.

[50] Forbes, R.G. Physical electrostatics of small field emitter arrays/clusters // Journal of Applied Physics. – 2016, – Vol. 120, №5. – Art. no. 054302.

[51] Giubileo F., Grillo, A., Pelella A., Faella E., Camilli L., Sun J.B., Capista D., Passacantando M., Di Bartolomeo A. Germanium arsenide nanosheets applied as twodimensional field emitters // Journal of Physics: Conference Series. – 2021. – Vol. 2047, №1. – Art. no. 012021.

[52] Giubileo F., Faella E., Pelella A., Grillo A., Passacantando M., Di Bartolomeo A. 2D transition metal dichalcogenides nanosheets as gate modulated cold electron emitters // // IEEE Conference on Nanotechnology. – Proceedings – 2021. – P. 189–192.

[53] Harris, J.R., Jensen, K.L., Petillo, J.J., Maestas S., Tang, W., Shiffler, D.A. Practical considerations in the modeling of field emitter arrays with line charge distributions // Journal of Applied Physics. – 2017. – Vol. 121, №20. – Art. no. 203303.

[54] Harris, J.R., Jensen, K.L., Shiffler, D.A. Edge enhancement control in linear arrays of ungated field emitters // Journal of Applied Physics. – 2016 – Vol. 119, №4. – Art. no. 043301.

[55] Harris, J.R., Jensen, K.L., Shiffler, D.A. Modelling field emitter arrays using line charge distributions // Journal of Physics D: Applied Physics. – 2015 – Vol. 48, №38. – Art. no. 385203.

[56] Harris, J.R., Jensen, K.L., Shiffler, D.A., Petillo, J.J. Shielding in ungated field emitter arrays // Applied Physics Letters. – 2015 – Vol. 106, №20. – Art. no. 201603.

[57] Hongzhong Liu, Yongsheng Shi, Bangdao Chen, Xin Li, Yucheng Ding, Bingheng Lu Effect of patterned and aligned carbon nanotubes on field emission properties // Vacuum – 2011. – Vol. 86, №7. – P.934.

[58] Hansung Lee, Ki Buem Kim, Naesung Lee, Jeungchoon Goak, Jun-Young Park, Jusung Choi, Yongho Seo, Byoungyun Kong, Young Chul Choi, Choong Hu Lee, Yoon Ho Song High-current field emission of point-type carbon nanotube emitters on Ni-coated metal wires // Carbon – 2012. – Vol. 50, №6. – P.2126-2133.

[59] Huang Y.H., Lin H.C., Cheng S.L. Fabrication of vertically well-aligned NiSi2 nanoneedle arrays with enhanced field emission properties // Journal of Physics and Chemistry of Solids. – 2021. – Vol. 150. – Art. no. 109892.

[60] Jang T.H., Kim T.G., Bae M.K., Kim K., Choi J. Multi-layer thin-film deposition for high-performance X-ray field-emission characteristics //

International Journal of Modern Physics B. – 2021. – Vol. 35. – Art. no. 2140043.

[61] Jensen, K.L., Shiffler, D.A., Harris, J.R., Petillo, J.J. Schottky's conjecture, field emitters, and the point charge model // AIP Advances. – 2016 – Vol. 6, №6. – Art. no. 065005.

[62] Ji Q., Wang B., Zheng Y., Yane X., Zeng F., Lu B. Bulk graphene/multi-walled carbon nanotubes based field emitters // Journal of Alloys and Compounds. – 2022. – Vol. 897. – Art. no. 163136.

[63] Kashyap V., Kumar C., Chaudhary N., Saxena K. The role of quantum crystal radius on electron field emission properties of fractal silicon nanowire arrays // Materials Letters. – 2022. – Vol. 314. – Art. no. 131842.

[64] Kleshch, V.I., Bandurin, D.A., Orekhov, A.S., Purcell, S.T., Obraztsov, A.N. Edge field emission of large-area single layer graphene // Applied Surface Science. – 2015 – Vol. 357. – P. 1967–1974.

[65] Koh A.T.T., Hsieh J., Chua Daniel H.C. Electron emission studies of CNTs grown on Ti and Ni containing amorphous carbon nanocomposite films // Applied Surface Science. – 2009. – Vol. 256 – P. 178-182.

[66] Lawrowski R., Hausladen M., Buchner P., Schreiner R. Silicon Field Emission Electron Source with Individually Controllable Single Emitters // IEEE Transactions on Electron Devices. – 2021. – Vol. 68, №8. – Art. no. 9481184, P. 4116–4122.

[67] Lin Z., Chen H., She J., Deng S., Chen J. WO_3 nanowire field emission point electron source with high brightness and current stability // Vacuum. – 2022. – Vol. 195. – Art. no. 110660.

[68] Ludwick J., Cahay M., Hernandez N., Hall H., O'Mara J., Jensen K.L., Deane J.H.B., Forbes R.G., Back T.C. A new multiscale approach to rapidly determine the local emission current density of nanoscale metallic field emitters //Journal of Applied Physics. – 2021. – Vol. 130. – Art. no. 144302.

[69] Majumdar, J., Bhattacharjee, S. Comparative study on atomically heterogeneous surface with conical arrays of field emitters generated using plasma based low-energy ion beams
Journal of Applied Physic. – 2022. – Vol. 132, №8. – Art. no. 083304.

[70] Masur, S.M., Edgcombe, C.J., Barnes, C.H.W. On modeling the induced charge in density-functional calculations for field emitters // 2022 Journal of Vacuum Science and Technology B. – Vol. 40, №4. – Art. no. 042802.

[71] Miller, R., Lau, Y.Y., Booske, J.H. Electric field distribution on knife-edge field emitters // Applied Physics. – Letters. – 2007. – Vol. 91, №7. – Art. no. 074105.

[72] Owens C.E., Ludwick J., Ma J.Y., Headrick R.J., Williams S.M., Creichton M., Back T.C., Maruyama B., Pasquali M., McKinley G.H., Hart A.J. Pointwise Fabrication and Fluidic Shaping of Carbon Nanotube Field Emitters // 21st International Conference on Solid-State Sensors, Actuators and Microsystems, Transducers. – 2021. – P. 912–915.

[73] Park S., Gupta A.P., Yeo S.J., Jung J., Paik S.H., Mativenga M., Kim S.H., Shin J.H., Ahn J.S., Ryu J. Carbon nanotube field emitters synthesized on metal alloy substrate by PECVD for customized compact field emission devices to be used in x-ray source applications // Nanomaterials. – 2018. – Vol. 8. – Art. no. 378.

[74] Peng Y.-P., Liu C.-C., Chen K.-F., Huang C.-P., Chen C.-H. Green synthesis of nano-silver–titanium nanotube array (Ag/TNA) composite for concurrent ibuprofen degradation and hydrogen generation // Chemosphere. – 2021. – Vol. 264. – Art. no. 128407.

[75] Popov E.O., Kolosko A.G., Filippov S.V., de Assis T.A. Influence of the distribution of local field enhancement factors on the shape of the current-voltage characteristics of carbon-nanotube-based large-area emitters // Vacuum. – 2020. – Vol. 173, – Art. no. 109159.

[76] Pulagara N.V., Kaur G., Lahiri I. Enhanced field emission performance of growth?optimized CuO nanorods // Applied Physics A: Materials Science and Processing. – 2021. – Vol. 127, №11. – Art. no. 817.

[77] Qin, X.-Z., Wang, W.-L., Xu, N.-S., Li, Z.-B., Forbes, R.G. Analytical treatment of cold field electron emission from a nanowall emitter, including quantum confinement effects // Proceedings of the Royal Society A: Mathematical, Physical and Engineering Sciences. – 2010. – Vol. 467, №2128. – P. 1029–1051

[78] Ramachandran R., Biswas D. Approximate universality in the tunneling potential for curved field emitters — A line charge model approach // Journal of Applied Physics. – 2021. – Vol. 129. – Art. no. 184301.

[79] Rudra R., Biswas D. Verification of shielding effect predictions for large area field emitters // AIP Advances. – 2019. – Vol. 9, №12. – Art. no. 125207.

[80] Rughoobur, G., Ilori, O.O., Akinwande, A.I. Scanning anode field emission microscopy of a single Si emitter // Journal of Vacuum Science and Technology B. – 2022. – Vol. 40, №4. – Art. no. 042803.

[81] Sankaran K.J., Kurian J., Sundaravel B., Lin I.-N., Haenen K. Diamond-gold nanohybrids – an enhanced cathode material for field electron emitter applications // Journal of Physics D: Applied Physics. – 2021. – Vol. 54, №5. – Art. no. 053002.

[82] Shih P.-C., Rughoobur G., Cheng K., Akinwande A.I., Palacios T. Self-Align-Gated GaN Field Emitter Arrays Sharpened by a Digital Etching Process // IEEE Electron Device Letters. – 2021. – Vol. 42, №3. – Art. no. 9328289, P. 422–425.

[83] Shen Y, Xu N S, Ye P, Zhang Y, Liu F, Chen J, She J C., Deng S. Z. An analytical modeling of field electron emission for a vertical wedged ordered nanostructure // Advanced Electronic Materials. – 2021 – Vol. 3, №10. – Art. no. 1700295.

[84] Song M. Enhanced field emission properties of single-walled carbon nanotube from dip-coating catalyst // Physica B: Condensed Matter. – 2021. – Vol. 603. – Art. no. 412766.

[85] Shiffler, D.A., Tang, W., Jensen, K.L., Golby K., LaCour M., Petillo, J.J., Harris, J.R. Effective field enhancement factor and the influence of emitted

space charge // Journal of Applied Physics. – 2015. – Vol. 118, №8. – Art. no. 083302.

[86] Sun, L., Ye, Z.F., Ma, L.A., Zhang, Y.A. Improving field emission performance of patterned ZnO electron emission source by optimizing array spacing // Vacuum. – 2022. – Vol. 201. – Art. no. 111121.

[87] Sun, S., Ang, L.K. Analysis of nonuniform field emission from a sharp tip emitter of lorentzian or hyperboloid shape // Journal of Applied Physics. – 2013. – Vol. 113, №14. – Art. no. 144902.

[88] Tang, W., Shiffler, D., Cartwright, K.L. Analysis of electric field screening by the proximity of two knife-edge field emitters // Journal of Applied Physics. – 2011. – Vol. 110, №3. – Art. no. 034905.

[89] Tang, W., Shiffler, D., Golby, K., Lacour, M., Knowles, T. Field enhancement for fiber emitters in linear and rectangular arrays // Journal of Vacuum Science and Technology B: Microelectronics and Nanometer Structures. – 2014. – Vol. 32, №5. – Art. no. 052202.

[90] Tang, W., Shiffler, D., Golby, K., Lacour, M., Knowles, T. Experimental study of electric field screening by the proximity of two carbon fiber cathodes // Journal of Vacuum Science and Technology B: Nanotechnology and Microelectronics. – 2012. – Vol. 30, №6. – Art. no. 061803.

[91] Tang, W.W., Shiffler, D.A., Harris, J.R.,.Jensen.K.L., Golby K., Lacour, M., Knowles T. Field emission characteristics of a small number of carbon fiber emitters // AIP Advances. – 2016. – Vol. 6, №9. - Art. no. 095007.

[92] Tang S., Zhang Y., Zhao P., Zhan R., Chen J., Deng S. Realizing the large current field emission characteristics of single vertical few-layer graphene by constructing a lateral graphite heat dissipation interface // Nanoscale. – 2021. – Vol. 13, №10. – P. 5234–5242.

[93] Televnyy, D.S., Egorov, N.V., Vinogradova, E.M. Modeling of diode-type system based on the field emitter with dielectrics // 10th International Vacuum Electron Sources Conference, IVESC 2014 and 2nd International

Conference on Emission Electronics, ICEE 2014. – Proceedings. – 2014. – Art. no. 6892088.

[94] Televnyi D. S, Vinogradova E.M., The triode-type system on the basis of the field emitter modeling // Proceedings of XXIII Russian Particle Accelerator Conference RuPAC'2012 September, 24 - 28. – 2012. – P.410-412.

[95] Televnyi, D.S., Vinogradova, E.M. The triode-type system on the field basis of the emitter modeling // RuPAC 2012 Contributions to the Proceedings - 23rd Russian Particle Accelerator Conference. – 2012. – P. 418–420.

[96] Thombare B.R., Gavhane D.S., Lole G.S., Bankar P.K., Dusane P.R., Kolhe P.S., Khupse N.D., Choudhary R.J., Phase D.M., Devan R.S., Sonawane K.M., More M.A., Patil S.I. Cobalt ferrite decorated multiwalled carbon nanotubes as the electrode for efficient field electron emission // Physica E: Low-Dimensional Systems and Nanostructures. – 2020. – Vol. 121. – Art. no. 114131.

[97] Vinogradova E.M., Doronin G.G. Field Emitters Periodic System on Substrate with Dielectric Layer Modeling // IV Stability and Control Processes Conference in memory of Prof. Vladimir Zubov. Saint Petersburg, Russia. 5-9 October. – 2020.

[98] Vinogradova E.M., Egorov N.V. Effect of dielectrics on the field emission characterisrics in the diode system modelling // Results in Physics. – 2021. – Vol. 30. – Art. no. 104822.

[99] Vinogradova E.M., Egorov N.V., Doronin G.G. The sharp-edged field cathode mathematical modeling // 14th International Baltic Conference on Atomic Layer Deposition, BALD 2016 – Proceedings. – 2016. – Vol. 14. – P. 68–70.

[100] Vinogradova, E.M., Egorov, N.V. Effect of dielectrics on the field emission characteristics in the diode system modeling // Results in Physics. – 2021. – Vol. 30. – Art. no. 104822.

[101] Vinogradova, E.M., Egorov, N.V., Klimakov, A.A. Mathematical simulation of a diode system with a cylindrical field-emission tip // Technical Physics. – 2021. – Vol. 60, №2. – P. 176–179.

[102] Vinogradova, E.M., Egorov, N.V., Mutul, M.G., Shen, C.-C. Calculation of the electrostatic potential of the diode system based on a sharp-edged field cathode // Technical Physics. – 2010. – Vol. 55, №5. – P. 591–594.

[103] Vinogradova, E.M., Egorov, E.N., Televnyy, D.S. Mathematical modeling of field emitter array // Vacuum. – 2016. – Vol. 127. – P. 45–50.

[104] Vinogradova, E.M., Fomenko, M.G. The knife-edged field emitter mathematical modeling // RuPAC 2012 Contributions to the Proceedings - 23rd Russian Particle Accelerator Conference. – 2012. – P. 412–414.

[105] Vinogradova, E.M., Klimakov, A.A. The field cylindrical cathode mathematical modeling // 10th International Vacuum Electron Sources Conference, IVESC 2014 and 2nd International Conference on Emission Electronics, ICEE 2014 - Proceedings. – 2014 – Art. no. 6892097.

[106] Wang W. L., Qin X. H., Xu N. S., Li Z. B. Field electron emission characteristic of graphene // Journal of Applied Physics. – 2011. – Vol. 109, №4. – Art. no. 044304.

[107] Wang L., Xu Y., Cao X., Huang J., Deng S., Xu N., Chen J. Diagonal 4-in ZnO Nanowire Cold Cathode Flat-Panel X-Ray Source: Preparation and Projection Imaging Properties // IEEE Transactions on Nuclear Science. – 2021. – Vol. 68, №3. – Art. no. 9319878, P. 338–345.

[108] Watcharotone, S., Ruoff, R.S., Read, F.H. Possibilities for graphene for field emission: modeling studies using the BEM // Physics Procedia. – 2008. – Vol. 1, №1. – P. 71–75.

[109] Yadav K.K., Ankush, Kumar G., Arora A., Ghosh S., Jha M. An insight of enhanced field emission from vertically oriented $La_xNd_{1-x}B_6$ nanorods. // Materials Chemistry and Physics. – 2022. – Vol. 279. – Art. no. 125694.

[110] Yang B., Chen J., Wu X., Liu B., Liu L., Tang Y., Yan X. Enhanced field emission performance of MXene–TiO_2 composite films // Nanoscale. – 2021. – Vol. 13, №16. – P. 7622–7629.

[111] Yang H.H., Lim J., Park K.C. Field emission property of multi-cathode electron sources with vertically aligned CNT arrays // Japanese Journal of Applied Physics. – 2021. – Vol. 60(10), – Art. no. 105002.

[112] Zheng F, Pozzi G, Migunov V, Piker L, Remskar M, Beleggia M, Dunin-Borkowski R.E. Quantitative measurement of charge accumulation along a quasi-one-dimensional w5o15 nanowire during electron field emission // Nanoscale. – 2020. – Vol. 12, №19. – P. 10559–10564.

Application

This appendix provides a listing of a program that implements the numerical calculation of formulas and the construction of graphs for the problem from Chapter IV. The program is written in Python.

Program listing

```python
import numpy as np
import matplotlib.pyplot as plt
from matplotlib import colormaps as cm
import matplotlib.patches as mpatches
from matplotlib.ticker import LinearLocator


r1 = 10#int(input("r1 = "))
r2 = 20#int(input("r2 = "))
r3 = 100



eps12 = 0.1#int(input("eps2/eps1="))
q = -5
T1 = 0
T2 = 100
phi_0 = np.pi/8

N1 = 500#int(input("summa = "))
M = 500
N = 500#int(input("pazbienie = "))



# r1 = 1, r2 = 1.001, r3 = 10; q = -200;   eps = 0.1
# r1 = 1, r2 = 1.2, r3 = 10; q = -200; eps = 0.1
# r1 = 1, r2 = 2, r3 = 10; q = -100; eps = 0.1

# ############################### COEFFITIENTS
```

```python
def lmbd(i):

    lamda_i = np.pi*(i+1)/(np.log(r2/r1))

    return lamda_i

def mu(i):

    mu_i = (2*i + 1)*np.pi/(2*phi_0)

    return mu_i

def nu(i):

    nu_i = (2*i + 1)*np.pi/(2*np.log(r3/r2))

    return nu_i

def etta(i):

    etta_i = (2*i + 1)*np.pi/(2*(np.pi - phi_0))

    return etta_i

def ksi(i):

    ksi_i = (np.pi*(i+1))/np.log(r3/r2)

    return ksi_i

# ############################## SUMS

def g1sum(i,j):
```

```python
G1sum = (np.power(-1, i)) * (np.power(-1, (j+1))) * ksi(j) /
  (np.power(nu(i), 2) - np.power(ksi(j), 2))

return G1sum

def a2sum(i,j):

A2sum = (np.power((-1), i))*lmbd(j)*(np.power((-1), (j+1)))/
((np.power((lmbd(j)), 2))+(np.power((mu(i)), 2)))

return A2sum

def b2sum(i,j):

B1sum = eps12*(np.power((-1), i))*nu(j)/ ((np.power((nu(j)), 2))
+(np.power((mu(i)), 2)))

return B1sum

def c3sum(i,j):

C3sum = (np.power((-1), (i+1)))*(np.power((-1), j))*mu(j)/
((np.power((lmbd(i)), 2))+(np.power((mu(j)), 2)))

return C3sum

def d3sum(i,j):

D3sum = (np.power((-1), (i+1)))*(np.power((-1), j))*etta(j)/
  ((np.power((lmbd(i)), 2))+(np.power((etta(j)), 2)))

return D3sum
```

```python
def a4sum(i,j):


    A4sum = (np.power((-1), i))*lmbd(j)*(np.power((-1), (j+1))) /
    ((np.power((lmbd(j)), 2))+(np.power((etta(i)), 2)))


    return A4sum


def g4sum(i,j):


    G4sum = eps12*(np.power((-1), i))*ksi(j) /
      ((np.power((ksi(j)), 2))+(np.power((etta(i)), 2)))


    return G4sum


def c5sum(i,j):


    C5sum = mu(j)/ ((np.power((mu(j)), 2))+(np.power((nu(i)), 2)))


    return C5sum


def d5sum(i,j):


    pt1 = (np.power((-1),j))*etta(j)/nu(i)
    pt2 = etta(j)/(np.power((etta(j)),2) + np.power((nu(i)),2))
    pt3 = (np.power((-1),i))/(np.sinh(etta(j)*np.log(r3/r2)))
    pt4 = nu(i)/(np.power((etta(j)),2) + np.power((nu(i)),2))


    D5sum = pt1*(pt2 * pt3 - pt4)


    return D5sum


def g5sum(i,j):
```

```python
    pt1 = (np.power((-1),i))
    pt2 = ksi(j)/nu(i)
    pt3 = (np.power((-1),(j+1)))*ksi(j)/(np.power((nu(i)),2)
     - np.power((ksi(j)),2))
    pt4 = np.tanh(ksi(j)*(np.pi - phi_0))


    G5sum = pt1 * pt2 * pt3 * pt4


    return G5sum


def d4sum(i):


    pt5 = 0


    for j in range(0, M, 1):
    pt3 = np.power((-1), i) / (np.power(lmbd(j), 2)
     + np.power(etta(i), 2))
    pt1 = -np.power((-1), (j+1))
    pt2 = (np.power(-1,j+1)*eps12*((T2-T1)/
    (eps12*(np.log(r2/r1))+np.log(r3/r2)) - q*r3))
    pt4 = pt1 * pt2 * pt3
    pt5 += pt4


    return pt5


# ############################### MATRIX LEFT (1)
def an1():
    A1 = np.zeros(shape=(M+1, M+1), dtype='float')


    for n in range(0, M+1, 1):
    for j in range(0, M+1, 1):


    A1[n][j] = 0
```

```python
    return A1



def bk1():


    B1 = np.zeros(shape=(M+1, M+1), dtype='float')


    for k in range(0, M+1, 1):
        for t in range(0, M+1, 1):


            if k == t:
                B1[k][t] = (1/2)*np.log(r3/r2)
            else:
                B1[k][t] = 0


    return B1



def cm1():
    C1 = np.zeros(shape=(M+1, M+1), dtype='float')


    for n in range(0, M + 1, 1):
        for j in range(0, M + 1, 1):


            C1[n][j] = 0


    return C1


def dp1():
    D1 = np.zeros(shape=(M+1, M+1), dtype='float')


    for n in range(0, M + 1, 1):
        for j in range(0, M + 1, 1):
```

```
D1[n][j] = 0

return D1

def gt1():

G1 = np.zeros(shape=(M+1, M+1), dtype='float')
for k in range(0, M + 1, 1):
for t in range(0, M + 1, 1):
G1[k][t] = -g1sum(k,t)

return G1

# ############################### MATRIX LEFT (2)

def an2():
A2 = np.zeros(shape=(M+1, M+1), dtype='float')

for n in range(0, M + 1, 1):
for m in range(0, M + 1, 1):
A2[m][n] = a2sum(m,n)

return A2

def bk2():

B2 = np.zeros(shape=(M+1, M+1), dtype='float')

for m in range(0, M + 1, 1):
for k in range(0, M + 1, 1):
B2[m][k] = -b2sum(m,k)

return B2
```

```python
def cm2():
C2 = np.zeros(shape=(M+1, M+1), dtype='float')

for n in range(0, M + 1, 1):
for j in range(0, M + 1, 1):

if j == n:
C2[n][j] = (phi_0/2)*(np.tanh(mu(j)*np.log(r2/r1)
+eps12*np.tanh(mu(j)*np.log(r3/r2))))
else:
C2[n][j] = 0
return C2

def dp2():
D2 = np.zeros(shape=(M+1, M+1), dtype='float')

for n in range(0, M + 1, 1):
for j in range(0, M + 1, 1):

D2[n][j] = 0

return D2

def gt2():

G2 = np.zeros(shape=(M+1, M+1), dtype='float')
for n in range(0, M + 1, 1):
for j in range(0, M + 1, 1):
G2[n][j] = 0

return G2

# ############################# MATRIX LEFT (3)
```

```python
def an3():
A3 = np.zeros(shape=(M+1, M+1), dtype='float')

for n in range(0, M + 1, 1):
for m in range(0, M + 1, 1):

if n == m:
A3[n][m] = (1/2)*np.log(r2/r1)*(np.tanh(lmbd(n)*phi_0)
+np.tanh(lmbd(n)*(np.pi - phi_0)))
else:
A3[n][m] = 0
return A3

def bk3():

B3 = np.zeros(shape=(M+1, M+1), dtype='float')

for k in range(0, M + 1, 1):
for m in range(0, M + 1, 1):
B3[k][m] = 0

return B3

def cm3():
C3 = np.zeros(shape=(M+1, M+1), dtype='float')

for n in range(0, M + 1, 1):
for m in range(0, M + 1, 1):

C3[n][m] = c3sum(n,m)

return C3

def dp3():
```

```python
D3 = np.zeros(shape=(M+1, M+1), dtype='float')

for n in range(0, M + 1, 1):
for p in range(0, M + 1, 1):

D3[n][p] = d3sum(n,p)

return D3

def gt3():

G3 = np.zeros(shape=(M+1, M+1), dtype='float')
for n in range(0, M + 1, 1):
for j in range(0, M + 1, 1):
G3[n][j] = 0

return G3

# ############################# MATRIX LEFT (4)

def an4():
A4 = np.zeros(shape=(M+1, M+1), dtype='float')

for p in range(0, M + 1, 1):
for n in range(0, M + 1, 1):
A4[p][n] = a4sum(p,n)

return A4

def bk4():

B4= np.zeros(shape=(M+1, M+1), dtype='float')

for k in range(0, M + 1, 1):
```

```python
    for m in range(0, M + 1, 1):
    B4[k][m] = 0

    return B4

def cm4():
    C4 = np.zeros(shape=(M+1, M+1), dtype='float')

    for n in range(0, M + 1, 1):
    for m in range(0, M + 1, 1):

    C4[n][m] = 0

    return C4

def dp4():
    D4 = np.zeros(shape=(M+1, M+1), dtype='float')

    for n in range(0, M + 1, 1):
    for p in range(0, M + 1, 1):
    if n == p:
    D4[n][p] = ((np.pi - phi_0)/2)*(1/(np.tanh(etta(p)
    *np.log(r2/r1))+eps12*1/np.tanh(etta(p)*np.log(r3/r2))))
    else:
    D4[n][p] = 0
    return D4

def gt4():

    G4 = np.zeros(shape=(M+1, M+1), dtype='float')
    for p in range(0, M + 1, 1):
    for t in range(0, M + 1, 1):
    G4[p][t] = -g4sum(p,t)
```

```python
    return G4

# ############################### MATRIX LEFT (5)

def an5():
A5 = np.zeros(shape=(M+1, M+1), dtype='float')

for n in range(0, M + 1, 1):
for p in range(0, M + 1, 1):
A5[n][p] = 0

return A5

def bk5():

B5 = np.zeros(shape=(M+1, M+1), dtype='float')

for k in range(0, M + 1, 1):
for m in range(0, M + 1, 1):

if k == m:
B5[k][m] = (1/2)*(np.log(r3/r2))*np.tanh(nu(k)*phi_0)
else:
B5[k][m] = 0
    return B5

def cm5():
C5 = np.zeros(shape=(M+1, M+1), dtype='float')

for k in range(0, M + 1, 1):
for m in range(0, M + 1, 1):

C5[k][m] = -c5sum(k,m)
```

```python
    return C5

def dp5():
    D5 = np.zeros(shape=(M+1, M+1), dtype='float')

    for k in range(0, M + 1, 1):
        for p in range(0, M + 1, 1):

            D5[k][p] = d5sum(k,p)

    return D5

def gt5():

    G5 = np.zeros(shape=(M+1, M+1), dtype='float')
    for k in range(0, M + 1, 1):
        for t in range(0, M + 1, 1):
            G5[k][t] = g5sum(k,t)

    return G5

# ############################### MATRIX RIGHT

def dr1():

    D1 = np.zeros(shape=(M+1, 1), dtype='float')

    for k in range(0, M + 1, 1):
        pt1 = (1 / nu(k)) * (eps12 * np.log(r2 / r1)
         + (1 / nu(k)) * np.power((-1), (k)))
        pt2 = (T2-T1)/(eps12*np.log(r2/r1)
        +np.log(r3/r2)) - q*r3
        D1[k] = pt1 * pt2
```

```python
    return D1

def dr2():
    D2 = np.zeros(shape=(M+1, 1), dtype='float')

    for k in range(0, M + 1, 1):
        D2[k] = 0

    return D2

def dr3():
    D3 = np.zeros(shape=(M+1, 1), dtype='float')

    for n in range(0, M + 1, 1):
        pt1 = - np.log(r2/r1)
        pt2 = (np.power(-1, (n+1))*(1/lmbd(n))*eps12*((T2-T1)
        /(eps12*(np.log(r2/r1))+np.log(r3/r2)) - q*r3))
        pt3 = np.tanh(lmbd(n)*(np.pi - phi_0))
        D3[n] = pt1 * pt2 * pt3

    return D3

def dr4():
    D4 = np.zeros(shape=(M+1, 1), dtype='float')

    for n in range(0, M + 1, 1):

        D4[n] = 2*d4sum(n)

    return D4

def dr5():
    D5 = np.zeros(shape=(M+1, 1), dtype='float')
```

```python
    for n in range(0, M + 1, 1):

        D5[n] = 0

    return D5



    a1 = np.array(an1())
    a2 = np.array(an2())
    a3 = np.array(an3())
    a4 = np.array(an4())
    a5 = np.array(an5())


    b1 = np.array(bk1())
    b2 = np.array(bk2())
    b3 = np.array(bk3())
    b4 = np.array(bk4())
    b5 = np.array(bk5())


    c1 = np.array(cm1())
    c2 = np.array(cm2())
    c3 = np.array(cm3())
    c4 = np.array(cm4())
    c5 = np.array(cm5())


    d1 = np.array(dp1())
    d2 = np.array(dp2())
    d3 = np.array(dp3())
    d4 = np.array(dp4())
    d5 = np.array(dp5())


    g1 = np.array(gt1())
    g2 = np.array(gt2())
```

```python
g3 = np.array(gt3())
g4 = np.array(gt4())
g5 = np.array(gt5())


dr1r = np.array(dr1())
dr2r = np.array(dr2())
dr3r = np.array(dr3())
dr4r = np.array(dr4())
dr5r = np.array(dr5())


S1 = np.hstack((a1,b1,c1,d1,g1))
S2 = np.hstack((a2,b2,c2,d2,g2))
S3 = np.hstack((a3,b3,c3,d3,g3))
S4 = np.hstack((a4,b4,c4,d4,g4))
S5 = np.hstack((a5,b5,c5,d5,g5))


A1 = np.vstack((S1,S2,S3,S4,S5))


D1 = np.vstack((dr1r,dr2r,dr3r,dr4r,dr5r))

def sole():

a = A1

d = D1

x = np.linalg.solve(a, d)

return x


Q = sole()#np.array(sole())
```

```python
an = np.zeros(shape=(M + 1, 1), dtype='float')
bk = np.zeros(shape=(M + 1, 1), dtype='float')
cm = np.zeros(shape=(M + 1, 1), dtype='float')
dp = np.zeros(shape=(M + 1, 1), dtype='float')
gt = np.zeros(shape=(M + 1, 1), dtype='float')


an = Q[0:M, 0]
bk = Q[M + 1: 2*M + 1, 0]
cm = Q[2*M + 2: 3*M + 2, 0]
dp = Q[3*M + 3: 4*M + 3, 0]
gt = Q[4*M + 4: 5*M + 4, 0]




# ############### UNKNOWN


# ############# MAIN

def u1(r, phi):

t11 = q*eps12*r3*np.log(r/r1) + T1
t_n = 0
t_m = 0



for n in range(0, N1, 1):
t_n += an[n]*(np.exp(-lmbd(n)*(phi_0 - (phi))))
*((1+np.exp(-2*lmbd(n)*(phi)))/
(1+np.exp(-2*lmbd(n)*phi_0)))*np.sin(lmbd(n)*np.log(r/r1))

for m in range(0, N1, 1):
```

```python
        t_m += cm[m]*(np.power((r/r2), mu(m)))*
        ((1-np.power((r/r1), -2*mu(m))))/
        (1-np.power((r1/r2), 2*mu(m))))*np.cos(mu(m)*(phi))


    full = t11 + t_n + t_m


    return full




def u2(r, phi):

    t22 = q*r3*np.log(r/r2) + q*r3*np.log(r2/r1)*eps12 + T1
    t_k = 0
    t_m = 0


    for k in range(0, N1, 1):
        t_k += bk[k]*(np.exp(-nu(k)*(phi_0 - (phi))))
        *((1+np.exp(-2*nu(k)*(phi)))/
        (1+np.exp(-2*nu(k)*phi_0)))*np.sin(nu(k)*np.log(r/r2))

    for m in range(0, N1, 1):
        t_m += cm[m]*(np.power((r/r2), -mu(m)))
        *((1 + np.power((r/r3), 2*mu(m)))/
        (1 + np.power((r2/r3), 2*mu(m))))*np.cos(mu(m)*(phi))


    full = t22 + t_k + t_m


    return full




def u3(r, phi):

    t33 = T1 + eps12*((T2-T1)*np.log(r/r1))/(eps12*np.log(r2/r1)
```

```python
+np.log(r3/r2))
t_n = 0
t_p = 0


for n in range(0, N1, 1):
    t_n += (an[n] + (np.power(-1, (n+1))*(2/lmbd(n))*(eps12)
    *((T2-T1)/(eps12*(np.log(r2/r1))+np.log(r3/r2)) - q*r3)))*
    (np.exp(-lmbd(n)*((phi)-phi_0)))*
    ((1+np.exp(-2*lmbd(n)*(np.pi-(phi))))/(1+np.exp(-2*lmbd(n)
    *(np.pi-phi_0))))*np.sin(lmbd(n)*np.log(r/r1))


for p in range(0, N1, 1):
    t_p += dp[p]*np.power((r/r2), etta(p))*
    ((1-np.power((r/r1), -2*etta(p)))/
    (1-np.power((r1/r2), 2*etta(p))))
    *np.cos(etta(p)*(np.pi - (phi)))
full = t33 + t_n + t_p


return full

def u4(r, phi):

    t44 = T2 + ((T2-T1)*np.log(r/r3))/
    (eps12*np.log(r2/r1)+np.log(r3/r2))
    t_t = 0
    t_p = 0

    for t in range(0, N1, 1):
        t_t += gt[t]*(np.exp(-ksi(t)*((phi) - phi_0)))*
        ((1+np.exp(-2*ksi(t)*(np.pi - (phi))))/
        (1+np.exp(-2*ksi(t)*(np.pi - phi_0))))*
        np.sin(ksi(t)*np.log(r/r2))
```

```python
for p in range(0, N1, 1):
t_p += dp[p]*np.power((r/r2), (-etta(p)))*
((1-np.power((r/r3), (2*etta(p))))/
(1-np.power((r2/r3), (2*etta(p)))))
*np.cos(etta(p)*(np.pi - (phi)))


full = t44 + t_t + t_p


return full




def potential(r, phi):


U = 0


if  r < r1:
U = 0
if 0 <= (abs(phi)) <= phi_0 and r1 <= r <= r2:
U = u1(r, abs(phi))
if  0 <= (abs(phi)) <= phi_0 and r2 < r <= r3:
U = u2(r, abs(phi))
if phi_0 <=(abs(phi)) < np.pi + 1 and r1 <= r <= r2:
U = u3(r, abs(phi))
if phi_0 <= (abs(phi)) < np.pi + 1 and r2 < r <= r3:
U = u4(r, abs(phi))


return U

x_arr = np.zeros(shape=(N, N))
y_arr = np.zeros(shape=(N, N))
r_arr = np.zeros(shape=(N, N))
phi_arr = np.zeros(shape=(N, N))
```

```python
F_arr = np.zeros(shape=(N, N))


with open("polar.txt", "w") as file:
for k in range(0, N, 1):
for i in range(0, N, 1):


phi = -np.pi + 2 * np.pi * i / (N - 1)
r = r1  + (2*r2 - r1)* k / (N - 1)


x = (r*np.cos(phi))
y = (r*np.sin(phi))


F = float(potential(r, phi))


if F < 0:
F = 0


r_arr[k][i] = r
phi_arr[k][i] = phi
x_arr[k][i] = x
y_arr[k][i] = y
F_arr[k][i] = F


plt.contour(x, y, F, colors='black')


file.write(str(gt) + " ")
#file.write(str(x) + " ")
#file.write(str(y) + " ")
#file.write(str(F) + "\n")
file.write("\n")
file.close
```

```python
fig, ax = plt.subplots()


lev_line = [0, 5, 10, 15, 20, 25, 30, 35, 40, 45,
50, 55, 60, 65, 70, 75, 80, 85, 90, 95, 100]
lev_line = [0,1,2,3,4,5,6,7,8,9,10]
c = ('#990000', '#FF99FF', '#CC99FF', '#9999FF', '#6699FF',
'#3399FF', '#0099FF', '#0099CC', '#3399CC', '#6699CC',
'#9999CC', '#CC99CC','#FF99CC', '#FF9999', '#CC9999',
 '#999999', '#669999','#339999', '#009999',
 '#009966', '#339966', '#669966','#999966', '#CC9966')
contours = ax.contour(x_arr, y_arr, F_arr,
levels= lev_line, colors = c)
ax.clabel(contours)
ax.legend(title = 'q = -5, eps = 0.1',    # заголовок
title_fontsize = '20'    # размер шрифта заголовка
)


#plt.plot(r_arr, F_arr)
plt.show()


fig, ax = plt.subplots(subplot_kw={"projection": "3d"})

surf = ax.plot_surface(x_arr, y_arr, F_arr,
 cmap='coolwarm', linewidth=0, antialiased=False)
fig.colorbar(surf, shrink=0.5, aspect=0.5)


plt.show()
```